Chem Soc Rev

REVIEW ARTICLE

View Article Online
View Journal | View Issue



Cite this: *Chem. Soc. Rev.*, 2015, 44, 6330

Received 10th February 2015

DOI: 10.1039/c5cs00133a

www.rsc.org/chemsocrev

# Bio-inspired synthesis of metal nanomaterials and applications

Jiale Huang,†[a] Liqin Lin,†[b] Daohua Sun,[a] Huimei Chen,[c] Dapeng Yang*[b] and Qingbiao Li*[abc]

This critical review focuses on recent advances in the bio-inspired synthesis of metal nanomaterials (MNMs) using microorganisms, viruses, plants, proteins and DNA molecules as well as their applications in various fields. Prospects in the design of bio-inspired MNMs for novel applications are also discussed.

## 1. Introduction

### 1.1 Definition of bio-inspired synthesis

A number of fascinating advances, technologies and possibilities have emerged in recent years in the burgeoning field of nanotechnology.[1–5] As building blocks, nanomaterials (NMs) can play a vital role in nanotechnology due to their remarkably different properties as compared to their bulk counterparts.[6] Metal nanomaterials (MNMs) including common nanoparticles (NPs), nanoclusters (NCs, $<2$ nm), nanowires (NWs) and related nanostructures have received tremendous attention owing to their unique catalytic, electrical, magnetic and thermal properties.[2,7] "Top-down" and "bottom-up" approaches in nanotechnology[8] are also generally applicable to the fabrication of MNMs. However, in contrast to "top-down" approaches, "bottom-up" protocols enable a comparatively flexible and inexpensive preparation, being consequently more intensively investigated in recent years.[8,9]

MNMs have long existed in natural environments. Some metal ions might be adsorbed and further reduced to elemental metals by microorganisms, plants, biomass, *etc.* Inspired by the biological paradigm for the formation of MNMs, bio-inspired syntheses have emerged as innovative and alternatively attractive synthetic protocols for MNMs. Seminal reports on bio-inspired synthesis date back to the late 90s when Ag and Au NPs were prepared from *Pseudomonas stutzeri* AG259[10] and alfalfa

[a] *Department of Chemical and Biochemical Engineering, College of Chemistry and Chemical Engineering, and National Laboratory for Green Chemical Productions of Alcohols, Ethers, and Esters, Xiamen University, Xiamen, P. R. China. E-mail: kelqb@xmu.edu.cn; Fax: +86 592 2184822; Tel: +86 592 2184822*
[b] *College of Chemistry and Life Science, Quanzhou Normal University, Quanzhou, P. R. China. E-mail: yangdp@qztc.edu.cn*
[c] *Environmental Science Research Center, College of the Environment & Ecology, Xiamen University, Xiamen 361005, P. R. China*
† The two authors contribute equally to this work.

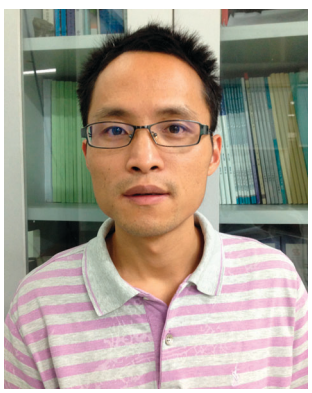

**Jiale Huang**

*Dr Jiale Huang received his PhD degree in industrial catalysis from Xiamen University. Then he worked as assistant professor in 2009 at the College of Chemistry and Chemical Engineering of Xiamen University and was promoted to associate professor in 2012. And he worked as Visiting Fellow in the University of Bristol from 2007 to 2008 and Visiting Scholar in the Hong Kong University of Science & Technology from 2013 to 2015. His current research focuses on bio-inspired synthesis of metal nanostructures and their applications. He has coauthored over 80 papers in refereed journals.*

**Liqin Lin**

*Dr Liqin Lin received her PhD degree in environmental engineering at the College of Environment and Ecology of Xiamen University in 2013. Currently, she is an assistant professor at the College of Chemistry & Life Science of Quanzhou Normal University. Her research focuses on the design and synthesis of metal nanomaterials and their applications in catalysis and biological sensors. She has coauthored over 10 papers in refereed journals.*

plant biomass,[11] respectively. Along with microorganisms and plants, viruses,[12] proteins[13] and DNA[14] have also become potentially useful candidates for bio-inspired synthesis of MNMs. Herein, based on these biological candidates, bio-inspired synthesis encompasses a combined application of biological concepts, mechanisms and functions for the design and development of innovative bio-derived (nano)materials with a number of applications.[15–18] Such combined application could be applicable to the synthesis or assembly of a wide range of inorganic NMs.[19–25]

### 1.2 Scope of the present review

Based on the scale of bio-inspired candidates, bio-inspired syntheses can be divided into two different types, namely synthesis using (1) biomatrices with sizes ranging from nanometers and microns to macroscale, *e.g.*, microorganisms, live plants and viruses ((a) in Fig. 1) and (2) water soluble DNA, proteins or those biomolecules secreted or extracted from microorganisms and plants ((b) in Fig. 1). Biomatrices can bridge the gap between bulk materials and MNMs. As-synthesized MNMs may not be immobilized onto some support prior to application. Such matrices can consequently play the same role as supports ((a) in Fig. 1). As far as the synthesis with those soluble biomolecules is concerned, the resulting MNMs may be immobilized onto some support for further applications ((b) in Fig. 1). Herein, broadly speaking, supports include not only common catalytic supports but also substrates able to support bio-inspired MNMs.

The complex interaction between bio-inspired candidates, metal ions and MNMs has been the subject of intensive research efforts from chemical, biotechnological or chemical engineering communities in the past decade. The design of simple and useful bio-supported MNMs as well as interfacing bio-MNMs with diverse supports has attracted some attention for different applications in recent years. The present contribution has been

**Daohua Sun**

*Dr Daohua Sun received her PhD degree in environmental science at College of Ocean and Environment of Xiamen University in 2007, and is currently an associate professor at the College of Chemistry and Chemical Engineering of Xiamen University. She worked as Visiting Fellow in Brown University from 2009 to 2010. Her research expertise is in synthesis and application of functional nanomaterials for catalysis and environmental technologies. She has coauthored more than 80 papers in refereed journals.*

**Huimei Chen**

*Ms Huimei Chen is currently a PhD student at the College of Environment and Ecology of Xiamen University under the supervision of Professor Qingbiao Li. She had been a visiting PhD student in the Hong Kong University of Science & Technology from February to May in 2015. Her current research focuses on bio-inspired synthesis of metal nanostructures and their catalytic applications.*

**Dapeng Yang**

*Prof. Dapeng Yang received his master's degree in Biology from the Shandong University of Technology and PhD degree in Materials Science and Engineering from Shanghai Jiao Tong University. Currently, he is a Professor at Quanzhou Normal University. His research interests mainly include biomineralization (mollusk shell), biotemplated material synthesis and applications (catalysis and biomedicine). He has coauthored over 30 papers in refereed journals.*

**Qingbiao Li**

*Prof. Qingbiao Li received his bachelor's, master's and PhD degrees in chemical engineering in Tianjin University. Currently, he is distinguished professor at Xiamen University and president at Quanzhou Normal University. His research focuses on biosorption and bioaccumulation of heavy/noble metals, new technology to treat organic/toxic wastewater, bio-inspired synthesis of noble metal nanoparticles and their catalytic applications, and cleaner technology in the chemical industry, which has been supported by NSFC, and 863 and 973 Programs of China. He has coauthored over 120 papers in refereed journals and has been one of Editorial Board members of Chin. J. Chem. Eng.*

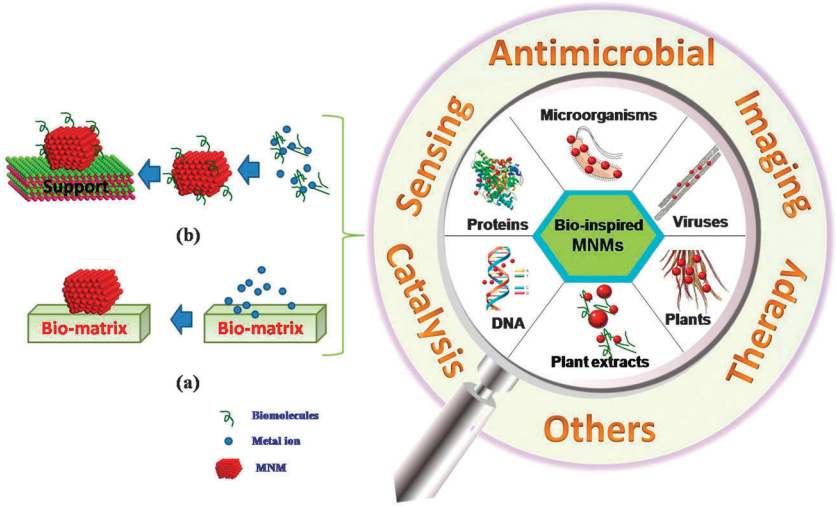


Fig. 1 Schematic representation of bio-inspired synthesis of MNMs using microorganisms, viruses, plants, proteins and DNA molecules. (a) Reduction of metal ions with biomatrices; (b) reduction of metal ions with water-soluble biomolecules.

aimed at providing an overview of recent progress related to the bio-inspired synthesis of MNMs (mainly noble metals) from microorganisms, plants, microbial or plant biomass, viruses, proteins and DNA. The chemistry of the bio-metal-ions-MNM interfaces as well as applied interfaces of bio-MNMs or bio-MNMs-support is critically reviewed in this work. Furthermore, prospects in the field of bio-inspired synthesis of MNMs have also been discussed. Recent overviews have touched upon these topics[26,27] but not limited to MNMs. Readers are also kindly referred to related reviews exclusively focused on the synthesis of NMs using plant extracts.[28–32]

## 2. General mechanism of bio-inspired synthesis of MNMs

The basic mechanism of bio-inspired synthesis of MNMs differs from that of bio-inspired candidates. Microorganisms are ubiquitously present on earth. Live microorganisms host a significant array of metabolic reactions required for functions including nutrient processing, growth, and energy release.[33] The metabolic process of live microorganisms might be involved in the bioreduction of metal ions to reduce the toxicity of metal ions. Through the transport system, microbes can intracellularly accumulate metals ions. Metal ions can be reduced by various reducing species present inside microbes (*i.e.* on cell walls, *etc.*)[34] as well as extracellularly reduced by different metabolites.[35,36] In contrast to live microorganisms, dead entities are not dependent on metabolic processes. Metal ions are bound by microbial cells which then provide preferential nucleation sites for MNM growth on their surface. Various functional groups including thiol, hydroxyl, carboxyl, imidazole, amino, guanidine and imino groups have been demonstrated to have high affinity to bind metal ions.[37] Upon reduction of metal ions (with microbial cells themselves or auxiliary reductants), MNMs are formed through nucleation and surface growth. As-synthesized MNMs can be entrapped or confined by the surface, often exhibiting an excellent stability.

Similar to microorganisms, viruses usually provide binding sites for metal ions and nucleation sites for MNM formation in the presence (and even absence) of additional reducing agents. Though there are many coating protein molecules in wild-type (WT) viruses, some active groups embedded inside the viral matrices are not accessible to metal ions.[12] Certain essential procedures should be therefore adopted to condition WT viruses prior to their use for the synthesis of MNMs (*i.e.* surface modification) to promote the metallization of viruses by increasing their low affinity for metal precursors.[12,39] The capsids of viruses can be modified by various strategies including charge and genetic modifications to provide uniform and precisely spaced binding sites for metal ions.[38] In some cases, auxiliary reductants are also required for the virus-templated synthesis of MNMs.

Inspired by the bioremediation of heavy metals by plants,[40] live plants have emerged as an alternative candidate in MNM biosynthesis.[41] However, the general mechanism for the bio-inspired synthesis of MNMs by live plants has not been fully understood.[41,42] Water-soluble biomolecules from microbial or plant biomass generally play dual roles as reducing and protecting agents in bio-inspired syntheses.[43–45] Functional groups (*e.g.* hydroxyl groups) play reductive roles in the formation of MNMs while the strong interaction between biomolecules and MNMs leads to an excellent stablity of as-synthesized MNMs.[44,45]

For the protein-templated synthesis of MNMs, there are a significant number of chemical functional groups (such as –COOH, –SH, $–NH_2$ and –OH) on proteins providing different sites to bind a variety of metal ions.[46] Upon addition of metal ions into an aqueous protein solution, the protein molecules are able to rapidly bind and entrap metal ions.[13] The interactions between metal ions and functional groups can lead to conformational changes of proteins in aqueous solution. As a result, the hydrophobic residues of proteins can be exposed to outside aqueous phases which, due to changes in solution

 

conditions (*i.e.* temperature, pH as well as the introduction of reducing agents), favour the transformation of entrapped metal into MNMs. Furthermore, a self-assembly process often occurs under the influence of hydrophobic interactions and multiple nanoscale forces.[47] The structure and morphology of resulting MNMs is consequently dependent on protein/metal ions ratio, temperature, amount of reducing agents, *etc.*[48] In addition, denatured protein molecules are also responsible for directing crystal growth and subsequent capping of the resulting MNMs.[49]

DNA has unique advantages in the formation of ordered nanostructures and nano-assemblies. The building-up process can be divided into two strategies, namely (1) *in situ* reduction and growth and (2) electrostatic interaction or molecular hybridization. The first strategy generally entails a two-step metal precursor binding to the DNA template followed by *in situ* reduction into MNMs with DNA directing NP growth. NCs, spherical NPs and one-dimensional (1D) MNMs can be prepared using this strategy. Comparatively, DNA is used to direct the assembly of pre-synthesized NPs into desired nanostructures through electrostatic interaction or molecular hybridization in the second approach. The assembly can be tuned by varying the number of DNA strands on each metal NP, the base sequence as well as the length and structure of DNA. This strategy can be implemented in the synthesis of various assemblies including dimers, trimers and polymeric structures. Modern DNA self-assembly techniques including DNA-tile or DNA-origami approach can facilitate the design of more complicated assemblies such as 2-dimensional (2D) or 3-dimensional (3D) nanostuctures.

# 3. Chemistry of bio-inspired synthesis for MNMs

## 3.1 Microorganism-mediated synthesis

Microorganisms can be essentially classified as prokaryotic and eukaryotic. Bacteria and fungi represent prokaryotic and eukaryotic microorganisms as main bio-inspired candidates for the synthesis of MNMs. Live microorganisms not only exhibit complicated biological activity but also possess a complicated hierarchical structure. An increasing number of insights into metal resistance in the bioreduction process mediated by microorganisms have been recently achieved but have not been well addressed in currently available reviews. Metal NPs can be found in the periplasmic space, on the cell wall and outside the cells. It is believed that various enzymes take an active part in the bioreduction process of transporting electrons from certain electron donors to metal electron acceptors for different microorganisms,.[50,51] The roles of enzymes as well as MNM formation have been extensively studied in recent years.

Dead entities are comparably not dependent on metabolic processes with respect to living microorganisms. As previously mentioned, the surface structure in non-enzymatic alternatives provided an excellent biotemplating medium to grow MNMs. Cell-free extracts from microorganisms have also been utilized to prepare MNMs. Without microbial cells, the extracts are more flexible for shape/size control, downstream processing of MNMs and design of bio-microreactors. The synthesis of MNMs through enzymatic and non-enzymatic reduction corresponding to living and dead microorganisms, respectively, as well as cell-free extracts from microorganisms will be critically reviewed in the next sections.

### 3.1.1 Enzymatic reduction

*3.1.1.1 Metal resistance.* As noble metal ions are toxic to microorganisms, metal resistance in the microbial reduction of these metal ions should be considered. Both Ag(I) ions and Ag NPs are well known toxic elements to live microorganisms. However, Klaus *et al.*[10] employed *Pseudomonas stutzeri* AG259 in the preparation of Ag NPs. Ag-resistance can involve the formation and accumulation of Ag precipitates outside the cytoplasmic membrane, possibly accompanied by metal efflux and metal binding.[10] Mukherjee *et al.*[52] later reported the use of eukaryotic microorganisms *Verticillium* fungus (*Verticillium* sp.) in the intracellular synthesis of metal NPs. They showed that the toxic effects of Ag(I) could be minimized by reducing Ag(I) ions to elemental Ag NPs within the cells, which were alive and could further reproduce after reduction.[52] Ag NPs were also prepared *via* $AgNO_3$ reduction with *Lactobacillus* strains.[34] While the exact Ag-resistant mechanism was not elucidated in this work, further studies related to the extracellular formation mechanism of Ag NPs by Ag-resistant *Morganella* sp. demonstrated by three homologous genes silE, silP and silS were closely associated with Ag-resistance.[35] Several Ag-specific proteins were found to be secreted outside the cell during the growth and were suggested as being responsible for the reduction of Ag(I) ions and formation of Ag NPs in the extracellular microenvironment.[35] Interestingly, Ramanathan *et al.*[53] further proved that a kinetically controllable growth of Ag-resistant *Morganella psychrotolerans* could allow the fine-tuning of anisotropic Ag NPs. The silE protein-based Ag-binding machinery of bacteria was activated due to the exposure to Ag(I) ions, leading to the cellular uptake of Ag(I) ions.[53] Very recently, Lin *et al.*[54] also investigated the biosynthesis of Ag NPs upon reduction of Ag(I) ions by the periplasmic nitrate reductase *c*-type cytochrome subunit NapC in a Ag-resistant *Escherichia coli* (*E. coli*) under anaerobic conditions. Results showed that *c*-type cytochromes such as NapC located in the periplasm could reduce Ag(I) ions to Ag NPs (Fig. 2).[54]

Compared to Ag(I) ions, Au(III) ions are less toxic to microorganisms. For some microorganisms, Au(III) ions can be reduced to obtain Au NPs. Das *et al.*[55] demonstrated a comprehensive study on the characterization of bioreduction process of Au(III) ions in the fungus *Rhizopus oryzae* (*R. oryzae*) to form Au NPs. Growth of *R. oryzae* in the presence of sublethal Au(III) concentrations (130 μM) induced stress response proteins which were correlated with the biosynthesis of Au NPs.[55] At Au(III) concentrations of $>250$ μM, the cellular ultrastructure was damaged due to Au toxicity and the biosynthesis of Au NPs was drastically suppressed. Au-specific genetic responses were further identified as two cytoplasmic proteins of $\sim$45 and $\sim$42 kDa likely responsible for the biosynthesis of Au NPs at Au(III) concentrations of $<130$ μM. An $\sim$80 kDa protein was comparatively proposed to serve as a capping agent for Au NPs and stabilized Au NP bioconjugates through electrostatic repulsion.[55]

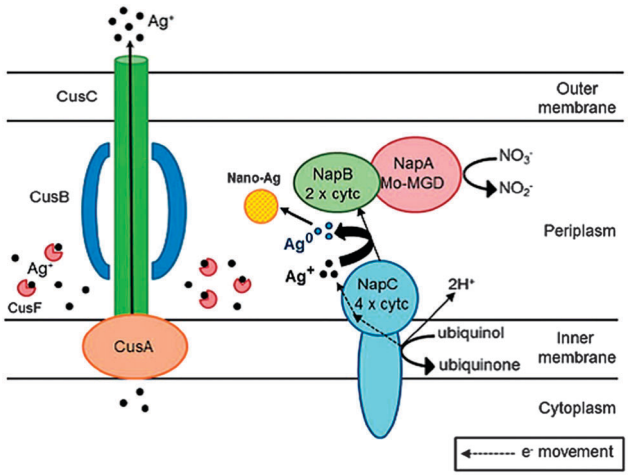


Fig. 2 A proposed model of biosynthesis of nano-Ag by periplasmic c-type cytochrome NapC in the Ag-resistant *E. coli* strain 116AR. Reprinted with permission from ref. 54. Copyright © 2014, Royal Society of Chemistry.

Very recently, Rösken *et al.*[56] examined the time-dependent growth of *in vivo* Au NPs in cyanobacteria *Anabaena* sp., when exposed to Au(III) ions at 0.8 mM. All microorganisms seemed to be dead after 8 days due to the incorporation of Au NPs. However, in some cases, Au(III) ions could not be completely reduced by microorganisms. Instead, the complete reduction of Au(III) ions required the input of electron donors as demonstrated in the rapid preparation of Au NPs by *Shewanella algae* (*S. algae*) ATCC 51181 using $H_2$ as electron donor (Au NPs formed in the periplasmic space).[57,58]

The microbial reduction of Pd(II) and Pt(IV) ions was reported to be conducted in the presence of an electron donor[59–62] as in the recent reduction of Pd(II) ions by *Desulfovibrio desulfuricans* (*D. desulfuricans*) NCIMB 8307 in the presence of formate or hydrogen as the electron donor.[59] Pd NPs were unable to be generated by bacteria without the addition of an electron donor. Similarly, Pt NPs could be prepared using *D. desulfuricans* NCIMB 8307 and $H_2$ as electron donors.[60] Using sodium lactate as an electron donor, Pt NPs could also be prepared from *S. algae* ATCC 51181[61] and *E. coli* MC4100[62] (using $H_2$ as the electron donor). Recently, Yates *et al.*[63] demonstrated that Pd NPs primarily formed outside the *Geobacter sulfurreducens* cells could reduce the toxicity of metal ions and allow the recovery of Pd NPs without cell destruction. However, the resistance of the related microorganisms against Pd(II) and Pt(IV) ions was little discussed; therefore it is unclear whether Ag or Au resistance is applicable to that of Pd(II) and Pt(IV) ions.

As far as the resistance against other metals is concerned, a few reports are available for the microbial reduction. A recent demonstration pointed to the synthesis of stable Cu NPs by Ag-resistant *Morganella morganii* (*M. morganii*) RP42.[64] The authors claimed that Cu(II) ions were uptaken by *M. morganii* using the same/similar proteins involved in Ag(I) ion uptake from previous studies.[53] The resulting Cu NPs were then released into the media using the bacterial efflux system.[64]

*3.1.1.2 Identification of enzymes and formation of MNMs.* Besides the metal resistance summarized above, enzymes play vital roles in the microbial reduction of metal ions. Although some pioneering studies were conducted,[10,34,52,65] the identification of enzymes involved and understanding of their roles in microbial reduction remains a significant challenge. Table 1 summarizes some examples of enzymes involved in the microbial reduction of metal ions.

Intracellular synthesis of MNMs was generally achieved using bacteria. Nair *et al.*[34] prepared Au NPs through reduction of $HAuCl_4$ with *Lactobacillus* strains, in one of the earliest reports on microbial synthesis. Au(III) ions were believed to be reduced by sugars and enzymes on cell walls.[34] However, no experimental evidence was provided. Ahmad *et al.*[66] subsequently demonstrated the use of single-spore bacteria (*Thermomonospora* sp.) for the reduction of Au(III) ions to Au NPs at 50 °C. The results pointed to proteins (molecular weight 80–10 000) playing an important role in the reduction of Au(III) ions at 50 °C, also favorable for the survival of the thermophilic bacteria.[66] The reduction of Pd(II) ions to produce Pd NPs with *D. desulfuricans* ATCC 29577 was conducted in the presence of sodium pyruvate, formate or $H_2$ as an electron donor.[67] Hydrogenase and cytochrome C3 were claimed to be potentially involved in the reduction of Pd(II) ions.[67]

Table 1 Examples of enzymes involved in the microbial reduction of metal ions

| Microorganisms | MNMs | Size | Enzymes |
|---|---|---|---|
| Bacteria | | | |
| *D. desulfuricans* ATCC 29577[67] | Pd NPs | —[a] | Hydrogenase and cytochrome C3 |
| *M. psychrotolerans*[53] | Ag nanoplates | Edge length of 100–150 nm | Ag reductase |
| *S. maltophilia*[68] | Ag NPs | ~93 nm | Chromium reductase |
| *Shewanella oneidensis*[69] | Ag NPs | 24.4 ± 0.8 nm | c-Type cytochromes |
| *E. coli*[54] | Ag NPs | 5–70 nm, average size: 26.9 nm | Nitrate reductase |
| Fungi | | | |
| *F. oxysporum*[70] | Ag NPs | 20–40 nm | NADH-dependent reductases |
| *R. oryzae*[55] | Au NPs | ~15 nm | Cytoplasmic proteins |
| *L. edodes*[71] | Au NPs | 5–50 nm | Laccase, tyrosinase, and Mn-peroxidase |
| *F. oxysporum*[72] | Ag NPs | 10–20 nm | Nitrate reductase |
| *Thermomonospora* sp.[73] | Au NPs | 2–6 nm, average size: 3 nm | Sulfite reductase |
| *F. oxysporum* IRAN 31C[74] | Ag NPs | Average size: 50 nm | Nitrate reductase |

[a] Not mentioned in the corresponding reference.

 

Intracellular synthesis of metal NPs using fungi was first demonstrated by Mukherjee *et al.*[52,65] A comprehensive study was conducted on the intracellular biomineralization mechanism of Au by zygomycete fungi *R. oryzae.*[55] The authors showed that the majority of Au(III) was transported into the cytoplasmic region where reduction to Au NPs took place facilitated by cytoplasmic proteins (*i.e.* metal reductases). The accumulation of spherical Au NPs inside the mycelial cells of *L. edodes* was also recently reported.[71] The results of enzyme assays showed that the intracellular phenol-oxidizing enzymes (laccases, tyrosinases, and Mn-peroxidases) were involved in Au(III) reduction to give electrostatically stabilized colloidal solutions.[71]

Extracellular synthesis of metal NPs using fungi were also first reported by Mukherjee *et al.*[70] for the particular example of Au NPs which could be extracellularly synthesized by *Fusarium oxysporum* (*F. oxysporum*). Results also showed that *F. oxysporum* was able to release a large number of coenzyme (NADH)-based proteins to reduce Au(III).[70] Reductases were a class of characteristic enzymes of *F. oxysporum*, while intracellular or extracellular reduction of Au(III) could not be achieved by other strains such as *F. moniliforme*. Protein-bound Au NPs through the amino groups from cysteinyl acid residues and lysine residues provided Au NPs with long-term stability. These studies proved that the use of fungi has the added advantages of simplicity in processing and handling of biomass for extracellular synthesis.[70] Based on the same reduction mechanism, extracellular biosynthesis of Ag,[75] Au–Ag[76] and other NPs with *F. oxysporum* was further investigated at the National Chemical Laboratory of India. In recent years, the synthesis of MNMs using cell-free extracts from microorganisms also confirmed the reductive ability of some enzymes, which will be separately discussed.

Studies of MNM formation and size control clearly demonstrated that cell walls of microorganisms usually provide binding sites for metal ions and preferential nucleation sites for the synthesis of MNMs in the presence of enzymes. In the intracellular synthesis of metal NPs, electrostatic interactions between Au(III) or Ag(I) ions and the charged groups (such as lysine residues) of enzymes within the cell wall of fungus *Verticillium* sp. can lead to entrapping of metal ions on the cell surface, where enzymes facilitated the reduction of metal ions to NPs.[52,65] Similarly, Au(III) ions initially bound by the cell surface of *R. oryzae* could be reduced to intermediate Au(I)–protein complexes and eventually to Au NPs.[55] Bacterial cells were able to provide enzymes as reducing agents (with cells as nucleation sites to favor crystal growth) in the reduction of Pd(II) ions by *D. desulfuricans* NCIMB 8307 using formate or hydrogen as electron donors.[59] Very recently, a time-dependent study on Au NP growth using X-ray powder diffraction (XRD) and transmission electron microscopy (TEM) pointed out that the formation of Au NPs started at the heterocyst polysaccharide layer (HEP) of heterocysts (HCs).[56] At longer times, the vegetative cells (VCs) were the most important area of synthesis.[56] Even after one day, the number of Au NPs inside the HCs as well as inside HEP was inferior as compared to that in VCs.[56]

Microorganisms used for the extracellular synthesis of metal NPs need to be extensively screened.[77] Metal NPs were in most cases simultaneously produced intracellularly and extracellularly, with the associated challenges in controlling their particle size. Furthermore, microorganisms possess a hierarchical cell structure, which is essentially detrimental for the production of metal NPs with a narrow particle size distribution. Adjusting the synthetic conditions can potentially facilitate particle size control in MNM synthesis. As an example, the formation rate of intracellular Au NPs using two types of fungi (*V. luteoalbum* and Isolate 6-3) could be influenced by changes in pH value, reaction temperature, Au(III) concentration and reduction reaction time, affecting the size of Au NPs.[78,79] A genetic approach to size control was recently proposed by Ng *et al.*,[69] comparing the particle size of the extracellular NPs from WT *Shewanella oneidensis* and its mutant. Results showed that the mutant lacking outer membrane c-type cytochromes produced significantly smaller NPs with respect to WT.[69]

**3.1.2 Non-enzymatic reduction.** The non-enzymatic reduction of metal ions to NPs based on dead cells has also received some attention in recent years. This approach is independent on the metabolic process of microorganisms[80–83] and consequently different from enzymatic reduction. The protocol essentially entails a simple adsorption and reduction of metal ions on cell surfaces, which result in completely extracellular metal NPs. Reported examples include the formation of Au NPs using *Shewanella oneidensis* through a fast biosorption but slow reduction process in the presence of an electron donor.[84] The reduction was claimed to be non-enzymatic as microorganism cells were killed at high Au precursor concentrations.[84] A similar study could yield Au NPs using dried yeast *Pichia pastoris* (*P. pastoris*) in the absence of electron donors.[37] The cell surface also exhibited high affinity for Au(III) species in aqueous solution. Au(III) ions were rapidly absorbed and slowly reduced to Au(0) by $-NH_2$, –OH and other functional groups on the surface. As a result, as-synthesized Au NPs were tightly bound to the cell surface. In a separate study, the adsorption and reduction of Pd(II) ions by *P. pastoris* cells was also investigated.[85] Analogously to Au(III) ions, biosorption of Pd(II) ions was also rapid. However, Pd(II) reduction was comparatively very slow and incomplete, in good agreement with previous reports for the reduction of Pt(IV) ions with *Bacillus megatherium* D01 biomass.[86] The adsorption ability of the cells for Pd(II) ions was greatly enhanced after pretreatment with aqueous HCl, aqueous NaOH and methylation of amino groups. Nevertheless, even slower reduction rates were observed by pretreated *P. pastoris* cells as compared to untreated cells for the reduction of the Pd(II) ions.[85]

Such observed slow reduction rates have also been one of the most important issues in the synthesis of Ag NPs. In this regard, various methodologies have been proposed to accelerate the reduction of Ag(I) ions (*i.e.* adjusting the pH of the reaction solution).[87] Wang *et al.*[88] synthesized stable Ag NPs with narrow size distribution using dried *Aeromonas* sp. SH10 cells in the presence of hydroxyl ions. $[Ag(NH_3)_2]^+$ ions first reacted with $OH^-$ to form $Ag_2O$ species, and subsequently non-enzymatically reduced by the cells to Ag NPs on the surface of the $Ag_2O$ particles. Sun *et al.*[89] demonstrated that Ag NPs prepared by the bioreduction method exhibited a superior thermal and chemical stability

as compared to those synthesized *via* sodium citrate reduction. Results indicated that Ag NPs remained stable even after heat treatment at 100 °C for 6 h. The stability of the Ag NPs was significantly influenced by hydrogen ions and the electrolyte with multivalent cations, while it was little affected by the presence of hydroxide anions.[89]

The biosorption and bioreduction of metal ions has been extensively studied by Lin *et al.*[82,86,90,91] at Xiamen University, China. *S. cerevisiae* was demonstrated to have a remarkable affinity for Au(III) ions due to the presence of oxygen-containing functional groups (hydroxyl and carboxylate ion groups) on the cell wall.[90] Reduction of Au(III) ions to zero-valent Au was mainly affected by the free aldehyde group of the reducing sugars.[90] Using infrared spectrometry studies, polypeptides were proposed to be potentially activated by the intervention of Au(III) ions *via* the molecular reconformation and profoundly affected the course of Au(0) nucleation and crystal growth.[91] In the case of Pt(IV) ions bound by proteins on cell walls, polypeptide chains might change from β-folded to α-helical forms, with α-helical being potentially more advantageous than β-folded to prevent Pt NPs from aggregation.[86] The secondary constructions of proteins (*e.g.* α-helical, β-folded, *etc.*) and pores of the net-like structural polysaccharides on peptidoglycan layers of cell walls may play important roles in stabilizing Pt NPs and promoting the formation of uniform particles.[86]

As a matter of fact, microbial biomass has been used to remove heavy metal ions from wastewater for a long time. The biosorption process is not simply the adsorption of metal ions onto the microbial biomass and may be accompanied by the reduction of metal ions.[50] For example, an interesting demonstration was reported by Salvadori *et al.*,[92] who showed that the dead biomass of *Rhodotorula mucilaginosa* may be considered to be a fast and low-cost bioprocess for the formation of Cu NPs in which the biomass acted as a nano-adsorbent of Cu(II) ions in wastewater.

**3.1.3 Reduction with cell-free extracts from microorganisms.** Besides microorganisms, cell-free extracts from microorganisms have been used in the synthesis of MNMs. The use of cell-free extracts confers the advantage of flexible shape control of MNMs. For example, He *et al.*[93] used the cell-free extract of *Rhodobacter capsulatus* for the preparation of Au NWs. At higher Au(III) concentration conditions, quasi-spherical Au NPs easily cascaded to form curly Au NWs with wide diameter and length distributions.[93] Wadhwani *et al.*[94] showed that polyhedral Au NPs could be produced by mixing cell suspensions of *Acinetobacter* sp. SW 30 with $HAuCl_4$ solutions. Lee *et al.*[95] reported the use of recombinant *E. coli* cell extracts, a hydrogel polymer and a microdroplet based microfluidic device to fabricate a mass amount of artificial cellular bioreactors with uniform sizes and shapes as reactors to synthesize diverse metal NPs (Fig. 3). The hydrogels were able to protect the encapsulated cell extracts from the surrounding environment and maintained the functionality of cellular components in cellular bioreactor applications.

The identification of active biomolecules and MNMs formation understanding under reduction with cell-free extracts is comparatively simpler to those of processes in the presence of

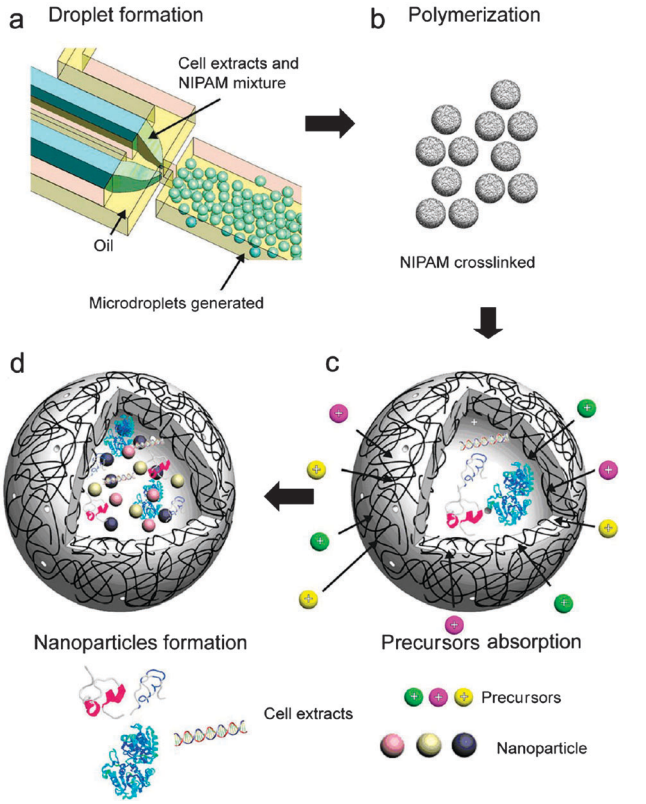


Fig. 3 Schematic representation of the microdroplet-generation model using a microfluidic device. (a) Microdroplets are produced with the mixture of cell extracts and NIPAM monomers in a microfluidic device. (b) Polymerized NIPAM monomers serve as an artificial membrane. (c) Different types of precursor solutions are dispersed in the artificial cellular bioreactors. (d) The precursors are transferred into the cells, and NPs are subsequently formed in the artificial cellular bioreactors. Reprinted with permission from ref. 95. Copyright © 2014, American Chemical Society.

microbial cells. Velmurugan *et al.*[96] studied the use of nitrate-reducing *Bacillus subtilis* EWP-46 cell-free extracts for the preparation of Ag NPs. Nitrate reductase enzymes with a molecular weight of 43 kDa might be responsible for the formation of Ag NPs. Talekar *et al.*[72] demonstrated that NADH-dependent nitrate reductases from *F. oxysporum* cell extracts were directly immobilized as cross-linked enzyme aggregates (CLEAs) and investigated for the synthesis of Ag NPs from silver nitrate.

**3.1.4 Microorganism-mediated surfactant-directed synthesis.** Microbial reduction emerged as a novel and viable alternative to chemical and physical methods for synthesis of metal NPs in recent years. Generally, metal ions was adsorbed and reduced by the microbial surface, resulting in very small NPs that gradually grew over the microorganisms. However, the shape of MNMs cannot be effectively controlled under microbial reduction. Inspired by the seed-mediated, surfactant-directed synthesis of MNMs,[97] Wang *et al.*[98,99] developed a microorganism-mediated, surfactant-directed (MSD) synthesis to fabricate AuNW/microorganism and Au-nanohorn/microorganism composites using *P. pastoris* cells. Such nanohorns are difficult to synthesize by pure chemical reduction. Yang *et al.*[100] expanded the MSD approach to synthesize hierarchically branched AuNWs by

using *E. coli* cells. Au nanohorns could be also synthesized using the MSD approach with *E. coli* cells and cetyltrimethylammonium chloride (CTAC).[101]

The interesting phenomenon of microbially induced aggregation of Au nanostructures around *E. coli* cells in the presence of cetyltrimethylammonium bromide (CTAB) and ascorbic acid (AA) was also observed. A microorganism-mediated CTAB-directed approach could be used to rapidly recover Au from aqueous solutions.[102] The work provided a new concept in which Au recovery could be strengthened through engineering Au nanostructures, thereby opening a new avenue to enhance the efficiency of recovery of precious metals.[102] Huang *et al.*[103] further investigated the effect of surfactants on recovery rate and morphology of recovered Au. Results showed that the carbon chain length had a minimum effect on the recovery rate and morphology in the presence of $Br^-$. In contrast, the recovery rate of Au was much lower in the presence of $Cl^-$ due to the formation of horn-like nanostructures. Interestingly, the recovered Au together with cell residues could be used as a surface-enhanced Raman scattering (SERS) substrate.[103]

As far as the role of microorganisms in the MSD approach is concerned, the microbial surface was demonstrated to provide biosorption of Au ions and preferential nucleation sites for Au nuclei.[98–100,102] $CTA^+$ was selectively adsorbed onto specific crystal facets to enable preferential growth of other facets.[98,100] The resulting anisotropic particles tended to connect together to form AuNWs due to the shape-directing effect of $Br^-$.[98,100,104] In the case of CTAC, further anisotropic growth of the branch-like nanostructures led to film-like nanostructures part of the growing AuNHs.[99,101]

Binary metal ions can be simultaneously adsorbed by microorganisms, which may provide nuclei for the growth of bimetallic nanostructures.[105] Very recently, Chen *et al.*[106] described a MSD proof of concept approach to synthesize novel AuPd bimetallic nanoflowers (NFs) consisting of 1D pedicels and 3D horns in the presence of CTAC (Fig. 4). The authors justified the advantage of the MSD approach to obtain bimetallic nanostructures in one pot protocol at room temperature. Furthermore, the problem of metal leaching that occurs in the galvanic replacement reaction for synthesizing bimetallic nanostructures can be circumvented. In addition, the bimetallic nanostructures could form application-oriented nano-composites with microorganisms which, for example, could be directly used as active catalysts in the selective hydrogenation of 1,3-butadiene. Results also showed that all obtained materials were alloys with Pd-enriched surfaces. The diameters of horns increased while those of pedicels decreased with the increase of Pd precursor feeding concentration.[106] The presence of the Pd precursor was vital for the formation of the nanowire part of the NF structure. Such NFs have not been reported, partially due to synthetic difficulties under pure chemical reduction methods. Therefore, the work opened up a new avenue for the shape control of novel bimetallic NMs.

### 3.2 Virus-templated synthesis

A variety of viruses have emerged as promising candidates in the bio-inspired synthesis of MNMs in the past decade. Some viruses have the advantages of unique dimensions and structures, well-spaced functionalities, high chemical stability and high yields, which stimulated research interest in the synthesis

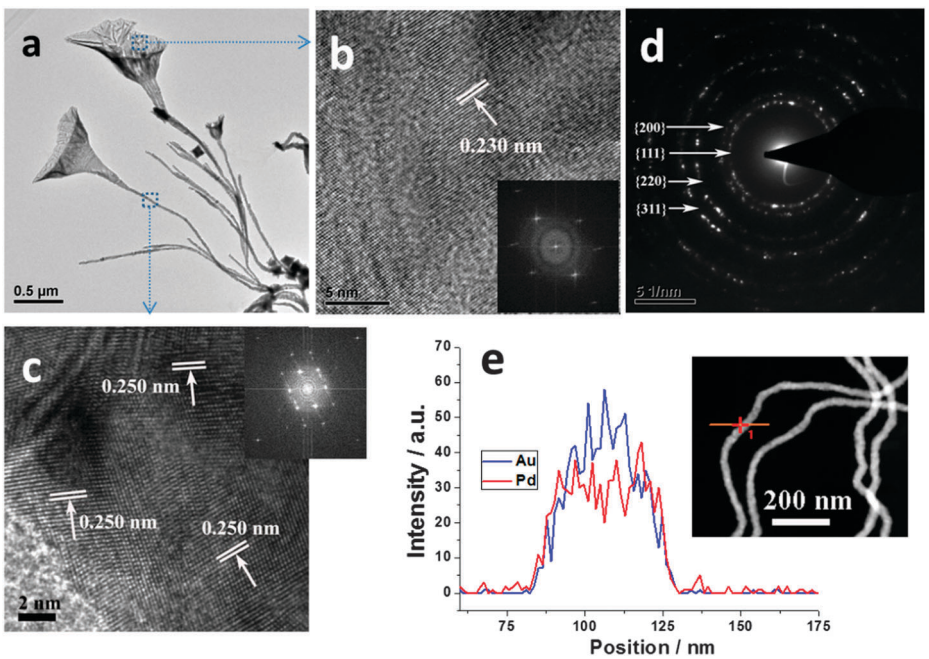


Fig. 4 (a) TEM image of AuPd NFs, (b) HRTEM image of blossom, (c) HRTEM image of pedicel, (d) SAED pattern of AuPd NFs, and (e) EDX line profiles of an individual AuPd nanowire (pedicel) corresponding to the framed part (dash) in (a). The insets indicate the corresponding fast Fourier transform (FFT) pattern. Reprinted with permission from ref. 106. Copyright © 2014, Royal Society of Chemistry.

of virus-templated MNMs. Structurally, most viruses consist of two parts:[107] (i) the genetic material from either deoxyribonucleic acid (DNA) or ribonucleic acid (RNA); (ii) the capsid comprising of a number of identically coated protein molecules. Generally, the average size of viruses is about one-hundredth that of bacteria.[107] Importantly, the capsids of viruses can be conveniently modified by various strategies to provide uniform and precisely spaced binding sites for metal ions. At present, viruses for the synthesis of MNMs included tubular (*e.g.* Tobacco Mosaic Virus (TMV)),[108] filamentous (*e.g.* M13),[109] icosahedral (*e.g.* Cowpea Mosaic Virus (CPMV),[110] *fd* bacteriophages[111]) and elongated icosahedral viruses (*e.g.* T4 bacteriophages[112]) as detailed in Table 2.

Wild type (WT) genetically modified and chemically modified viruses have also been employed to synthesize MNMs. As shown in Table 3, TMV, M13 virus, *fd* virus, CPMV and T4 virus are the main strains used for templated synthesis of MNMs. Generally, as-synthesized MNMs are metal clusters or spherical NPs ranging from 1 nm to more than a dozen nanometers in size. Pure metal NWs could be obtained only in some exceptional cases though metal–virus NWs could be prepared using tubular or filamentous viruses. Mild reductants including dimethylamine borane complexes (DMAB),[119] sodium cyanoborohydride ($NaBH_3CN$),[39] hydrazine hydrate ($N_2H_5OH$),[12] hydroxylamine ($NH_2OH$),[118] hydroxylamine hydrochloride ($NH_2OH{\cdot}HCl$),[125] sodium hypophosphite hydrate ($NaH_2PO_2$), and strong reductants such as $NaBH_4$[109] as well as UV irradiation[12] have been employed to reduce metal precursors during virus-templated synthesis of MNMs.

**3.2.1 Metallization with wild-type viruses.** Viruses usually provide binding sites for metal ions and nucleation sites for MNMs formation with or without the need of additional reducing agents. Various strategies have been considered for WT viruses pretreatment to improve their metallization potential for the synthesis of MNMs. A proposed strategy deals with the activation of viral surfaces for enhanced nucleation. Knez *et al.*[127] first reported the metallization of TMV plant viruses through a facile Ni deposition inside the TMV channels mediated by Pd(II).[12] In contrast, the high affinity of Ag(I) ions to the most external aminoacid of TMV followed by reduction with formaldehyde led to the exclusive formation of Ag NPs on the exterior surface of TMV. In this case, Ag(I) played a role as own activator for NP formation. Upon pretreatment of TMV with Pd(II) or Pt(II), Kern's group reported a TMV-templated synthesis of 3 nm Ni and Co NWs *via* faster electroless deposition in the central channel in the absence of phosphate buffer.[116,128] Similarly, Aljabali *et al.*[114] employed WT icosahedral CPMV as a template for the electroless deposition of monodisperse metallic Co, Ni, Fe, Pt, Co–Pt and Ni–Fe NPs at room temperature with reduced Pd as nucleation sites.[114]

Unmodified CPMV empty virus-like particles were also demonstrated to simply encapsulate Co or iron oxide within the capsid interior.[129] Similar metallization was observed in the case of the T4 bacteriophage with the elongated icosahedron.[112,115] Balci *et al.*[117] also demonstrated an electroless synthesis of 3 nm wide CoFe alloy NWs (Fig. 5) inside 4 nm channels of TMV on the basis of pre-adsorption of Pd(II) ions. They believed that the formation of a Pd catalyst and autocatalytic deposition of the alloy from reduction of metal precursors with $BH_3$ was responsible for the formation of the CoFe alloy NWs.

Furthermore, nonspecific electrostatic interactions may give rise to some effective binding sites for the growth of MNMs. For example, Avery *et al.*[109] showed that metal–M13 NWs can be prepared through the electrostatic interactions between cationic metal complexes and the negatively charged (carboxylate groups) pVIII region of WT M13 bacteriophage, followed by borohydride reduction. In contrast to anionic metal complexes (from $K_2PtCl_6$ or $HAuCl_4$), the negatively charged pVIII surface could promote the coating of metal NPs.

**3.2.2 Promoted metallization by surface modification of viruses.** Charge modification and genetic modification have been used to strengthen the binding of metal precursors onto viruses. As far as charge modification is essential for the enhanced metallization, Dujardin *et al.*[12] replaced aminoacid residues glutamate 95 (Glu95) and aspartate 109 (Asp109) in TMV mutant E95Q/D109N with the corresponding amides through site-directed oligonucleotide mutagenesis. Metal–virus tubular nanocomposites could be obtained under a controllable organization of metals (Pt, Au and Ag) NPs on the external surface or within the 4 nm central channel of TMV by chemically controlling the surface charge of the virus.[12] Aljabali *et al.*[126] adopted a surface charge modification approach of lysine groups on the surface of WT CPMV to promote the templated metallization using succinamate. The obtained Co–CPMV NPs are monodisperse with a diameter of 31.2 ± 0.5 nm. The use of polyelectrolyte-modified CPMV was also reported for the templated synthesis of narrowly dispersed Au NPs.[125] Cationic poly(allylamine) hydrochloride (PAH) was electrostatically bound to the external surface

Table 2 Characteristic dimension of some viruses for bio-inspired synthesis

| Virus | Characteristic dimension | Subunits |
|---|---|---|
| Tobacco mosaic virus (TMV) | 300 nm-long hollow cylinder with an outer diameter of 18 nm and a 4 nm-wide inner cavity[12] | 2130 identical coat protein molecules following the right-handed helix of an associated RNA strand[12] |
| M13 virus | ~6.5 nm diameter, 880 nm length[113] | ~2700 major coat proteins (p8) helically wrapped around its single-stranded DNA, with minor coat proteins (p3, p6, p7, and p9) at each end[113] |
| *fd* bacteriophages | The same to M13 virus[111] | The same to M13 virus[111] |
| Cowpea mosaic virus (CPMV) | Icosahedron, ~28 nm diameter. | 60 asymmetric units (with a small, 24 kDa, and a large, 41 kDa, subunit)[114] |
| T4 | Elongated icosahedron, ~60 nm diameter[112,115] | A regular pattern of four kinds of coat proteins: gp23*, gp24*, highly antigenic outer capsid, and small outer capsid.[112] |

 

Table 3 Synthesis of MNMs with viruses

| Virus | Activator or modifier | Reductant | pH | MNMs | Size/diameter | Metalized viral diameter |
|---|---|---|---|---|---|---|
| E95Q/D109N mutant of TMV[12] | Amides | $N_2H_5OH$ | 7 | Pt NPs | 2.5–5 nm | —[b] |
| | | $N_2H_5OH$ | 3 | Au NPs | 8.6 ± 3 nm | |
| | | UV irradiation | 2.3 | Ag NPs | <5 nm (channel)<br>10–15 nm (outer) | |
| WT TMV[116] | Pd(II) | Pd(II) | 6–8 | Ni NWs | ~3 nm | —[b] |
| | Pt(II) | Pt(II) | | Co NWs | ~3 nm | |
| WT TMV[117] | Pd(II) | Pd(II) | 6–8 | CoFe NWs | ~3 nm | —[b] |
| 6His mutant of TMV[118] | Genetic modification | $NH_2OH$ | 5 | Au NWs (annealed) | ~40 nm | —[b] |
| TMV1cys[39] | Cysteine | DMAB, $NaBH_3CN$ | —[a] | Pd NPs | 5–15 nm (DMAB)<br>4–6 nm | —[b] |
| TMV1cys[119] | Cysteine | DMAB | —[a] | Pd NPs | 11.4 nm | —[b] |
| TMV1cys[120] | Cysteine | DMAB | —[a] | AuPd NPs | <5 nm | —[b] |
| TMV1cys[38] | Cysteine | No | —[a] | Pd NPs | 1–2 nm | —[b] |
| TMV1cys[121] | Cysteine | No | —[a] | Ag NPs | 2 nm | —[b] |
| TMV2cys[122] | Cysteine | DMAB | —[a] | Au NPs | 2.9 ± 1.4 nm | —[b] |
| | | | | Ag NPs | 5.8 ± 2.7 nm | |
| | | | | Pd NPs | <5 nm | |
| TMV2cys[123] | Cysteine | No | —[a] | Pd NPs | 1–8 nm | 33.4 ± 1.1 nm |
| M13 virus[113] | Peptide | Tetraglutamate | —[a] | Au NPs | ~5 nm | —[a] |
| M13 virus[109] | No | $NaBH_4$ | —[a] | Rh NPs | ~5 nm | —[a] |
| M13 virus[124] | No | AA | —[a] | Au NWs<br>AuPt NWs | 10–50 nm | —[a] |
| *fd* virus[111] | No | DMAB | | Pd NPs | 2–3 nm | 20 ± 3 nm |
| WT CPMV[114] | Pd(II) | DMAB | —[a] | Co NPs | 2–3 nm | 32.0 ± 0.5 nm |
| | | $NaH_2PO_2$ | | Fe NPs | | 31.0 ± 0.3 nm |
| | | DMAB | | Ni NPs | | 32.4 ± 0.4 nm |
| | | $NaH_2PO_2$ | | Pt NPs | | 32.6 ± 0.5 nm |
| | | | | NiFe NPs | | 31.4 ± 0.5 nm |
| | | | | CoPt NPs | | 34.4 ± 0.3 nm |
| WT CPMV[125] | Polyelectrolyte | $NH_2OH{\cdot}HCl$ | —[a] | Au NPs | 10–18 nm | ~67 nm |
| WT CPMV[126] | Succinamate | $NaBH_4$ | —[a] | Co NPs | ~2 nm | 31.2 ± 0.5 nm |
| T4 virus[115] | No | DMAB | —[a] | Pt NPs | 3–4 nm | —[a] |
| T4 virus[112] | No | DMAB | 8.5–9 | Pt, Rh, Pd, Fe, Co, and Ni NPs | 2.0–4.5 nm | —[a] |

[a] Not mentioned in the corresponding reference. [b] Diameter of ~20 nm.

of the virus capsid. As a result, the adsorption of anionic Au complexes can be promoted, which facilitated their reduction to form a metallic Au coating under mild conditions. Templated Au NPs could also be further modified with thiol reagents or assembled into large, hexagonally packed, tessellated-spheres after reaction with PAH-modified CPMV.

Genetic modification was also used to intensify metal precursor binding in viruses. TMV1cys and TMV2cys were obtained by the insertion of one and two cysteine residues into the amino-terminus of the coat protein on the outer surface of TMV, respectively.[122,130] Culver's group in Maryland University demonstrated an improved metal coating density on TMV2cys compared with WT TMV. The additional sulfhydryl groups on TMV2cys enhanced ion uptake of the virus and provided a significant portion of the potential metal loading onto the TMV surface.[122,131,132] For example, TMV1cys and TMV2cys efficiently enhanced the biosorption of metal ions and the corresponding formation of Ag, Au and PdAu alloy NPs.[122] Yi's group extensively investigated virus-templated growth of Pd NPs with TMV1cys and their catalytic applications. Manocchi *et al.*[39,133,134] also reported a size controllable growth of Pd NPs based on surfaced assembled TMV biotemplates and TMV solution by grazing incidence small-angle X-ray scattering (GISAXS). Thermal stability studies of Pd NPs on TMV showed that an improved stability of TMV-templated Pd NPs in comparison to Pd NPs formed on the solid substrate surface. The degradation temperature of Pd NPs increased from 214 °C on Au chips to 279 °C for Pd particles formed on TMV. Due to the presence of genetically displayed thiol functionalities, the self-assembly of TMV1cys on Au surfaces was more consistent and uniform as compared to WTTMVs, which results in the formation of high-density Pd NPs on TMV1cys.[39]

Recently, Yang *et al.*[121] demonstrated TMV1cys to be a sacrificial biomediator in the synthesis of Ag NPs with a tunable average size ranging from 1.9 to 9.5 nm. Under the highly alkaline conditions (pH > 10) of Tollens' reagent, TMV may thus disassemble into reducing peptides or proteins (amino acids serine, aspartic acid, tyrosine and cysteine) for coordination and reduction of Ag(I) ions.

WT viruses can also be modified by peptides to increase binding sites for metal ions. Belcher's group in the Massachusetts Institute of Technology conducted considerable work on virus-templated MNMs with M13 virus. Nam *et al.*[113] incorporated Au-binding peptides into the filament coat of $Co_3O_4$/M13 virus composites to prepare hybrid Au–$Co_3O_4$ wires that improved battery capacity at room temperature. The combination of virus-templated synthesis at the peptide level and methods for controlling 2D assembly of viruses on polyelectrolyte

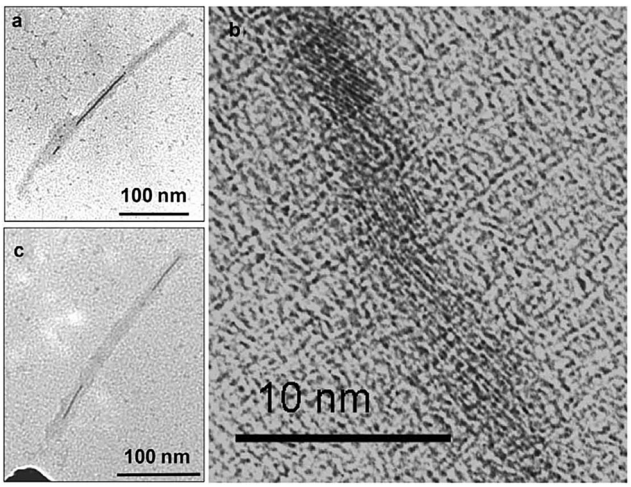


Fig. 5 (a) TEM micrograph of CoFe alloy NWs within the channel of a TMV particle (dark gray). The black line in the center corresponds to an alloy wire of ~3 nm in diameter and approximately 100 nm in length. In the lower part of the same virion a second small nanowire (~10 nm long) is located. Another short virion (~100 nm long) is attached to the lower portion of the metallized virion. (b) High-resolution TEM image of a CoFe nanowire inside TMV. Crystal planes of various orientation and spacing are visible, all compatible with various orientations of CoFe. The image was calibrated by imaging Au particles at the same magnification. (c) TEM image of two short CoFe(Ni) wires located in a single virion cavity. The dark nodule at the bottom part stems from bulk deposition of the alloy. Reprinted with permission from ref. 117. Copyright © 2012, Institute of Physics.

multilayers can provide a systematic platform to integrate these NMs to form thin, flexible lithium ion batteries.[113] Aljabali *et al.*[135] used peptide–CPMV conjugates to produce *ca.* 32 nm monodisperse NPs coated with Co–Pt and Fe–Pt, which are not easy to synthesize using other methods. Recently, Wnęk *et al.*[118] engineered the TMV coat protein by incorporating a highly selective His-tag (HHHHHH, 6His) metal-binding peptide that would be readily accessible on the outer surface of assembled protein disks or rods. They demonstrated the use of such genetically engineered TMV coat protein gene as a bio-template for the fabrication of Au NWs through thermal annealing.

In addition, coating viruses with oxides may enhance the affinity for metal ion adsorption and the stability of viral templates. For instance, silica coatings on TMV1cys[136] promotes the formation of MNMs on TMV. A pretreatment of TMV with aniline was used to generate a uniform silica attractive surface for the growth of silica layer of $>20$ nm in thickness. These silica shells not only enhanced the stability of TMV, but also promoted the deposition of various metal NPs through conventional silica mineralization chemistries.

**3.2.3 Assembly and size control of virus-templated MNMs.** Virus-templated synthesis gives rise to different assembled structures and various MNMs. The assembled structures of MNMs on external surfaces or inside the channels of individual virus have primarily attracted much attention in recent years. The overall structures depended on geometrical shapes of viruses. For example, tubular TMV was used to assemble metal–TMV NWs or in the synthesis of metal NWs templated by external surface and interior channels, respectively. Knez and coworkers[128] demonstrated for the first time that specific spatial selectivity for metal clusters-deposited TMVs could be modulated by a careful selection of metal ion, pH and duration of treatment. Metal (Pt, Au and Ag) NPs could be simply deposited on the external surface of TMV to obtain metal–virus tubular nanocomposites.[12] Tunable Au–TMV NWs consisting of TMV and densely packed Au NPs through adjustable addition–reduction cycles were also demonstrated.[137] Ethanol addition after the first addition–reduction cycle and wrapping of the Au–TMV nanohybrids with poly-L-lysine were adopted to ensure high homogeneity and stability in the nanowire suspension.[137] Recently, Khan *et al.*[138] also proved a simple, fast and high-yield binding of citrate-coated Au NPs to deprotonated WT TMV. The deprotonation overcome predominant electrostatic repulsion so that attractive van der Waals forces dominated.[138] In contrast to metal–virus NWs templated at the external surface of TMV, Ni and Co NWs could be synthesized inside TMV's internal channels in the absence of phosphate buffers reported by Knez and coworkers.[128]

Similar to tubular TMV, filamentous M13 virus can be employed to fabricate metal–virus NWs. Metal–M13 NWs can be prepared through nonspecific electrostatic interactions between cationic aqueous metal complexes and the anionic carboxylate groups of the pVIII region of WT M13 bacteriophages.[109] However, pure metal NWs cannot be simply obtained using M13 viruses lacking tubular channels. To promote the growth of crystalline CoPt and FePt NWs, nucleation of CoPt and FePt particles on genetically modified M13 viruses were achieved by means of a chemical reduction of metal precursor salts, with assemblies annealed at 350 °C to remove the virus template.[139] Later, a combination of M13 viral templates and CTAB could lead to stable, high-yield and tunable Au NWs and core–shell Au–Pt NWs using genetically modified M13 templates with specific Au binding peptides.[124] As discussed in Section 3.1.4, $CTA^+$ and $Br^-$ are both vital for the formation of 1D metal nanostructures. In the absence of CTAB, only metal NPs could be obtained.

Three CPMV mutants through cysteine modification were employed as scaffolds to bind charge-stabilized Au NPs (2 and 5 nm) through Au–sulfur bond formation to produce patterns of tunable inter-particle distances.[110] Recently, Fontana *et al.*[140] demonstrated a self-assembly strategy to create 3D icosahedral plasmonic Au–CPMV NPs with precisely spatial and orientational order mediated by a genetically engineered CPMV, which led to superstructures with new electromagnetic properties. Au–CPMV NPs exhibited sensitive magnetic response to the positioning of each Au particle.

The size and loading density control of virus-templated MNMs should also be considered. Manocchi *et al.*[133] showed that the amount of Pd NPs formed on TMV1cys templates could be tuned by simply adjusting Pd precursor concentrations. Higher Pd precursor concentration led to Pd NPs with higher density on TMV. They also carried out a comprehensive study on the effect of Pd precursor concentration, type of reductant and concentration and metallization time on the size of Pd NPs. Results showed that sodium hypophosphite concentration was

a key parameter affecting NP sizes. Other common reductants such as $NaBH_4$ resulted in polydisperse Pd NPs with no size-reductant concentration relationship and inconsistent particle formation.[39] Pd NPs growth quickly occurred under the investigated conditions and the particles reached their final size after 1 min of incubation.[39] In the case of CPMV, Aljabali *et al.*[114] demonstrated that variations in the type of reducing agent did not have any significant effects on the size of $Pd^0$–CPMV particles. However, in the case of metallization with cobalt, the thickness of the metallic coating was dependent on the incubation time in a eletroless deposition solution.[114]

Yang *et al.*[141] reported a tunable assembly of TMV on Au chips on which electroless deposition of Pd NPs could be achieved. By varying the concentration of TMV solutions for surface assembly or the Au surface area on patterned silicon chips, the surface density and spatial location of Pd–TMV could be controlled which further correlated well with Pd loadings and catalytic activities. Patterned assembly of metal-coated TMV without particular surface modification of silicon substrates can also be achieved[142] and even a rapid microfluidic fabrication of hybrid Pd–TMV–PEG microparticles with Pd–TMV directly embedded in polymeric hydrogels for catalytic dichromate reduction.[143] A similar example of an interesting replica molding approach has been illustrated in Fig. 6 for the encapsulation of spontaneously formed Pd–TMV1cys composites into Pd–TMV–PEG 3D microstructures with controllable Pd NP size, internal Pd–TMV density, internal Pd loading density and external microparticle size.[38] Pd NPs ranged from 1 to 2 nm in size and Pd–TMV–PEG materials could be used as efficient, stable and recyclable catalysts for dichromate reduction. TMV templates provided an alternative and efficient system containing catalytically active and accessible Pd NPs supported on stable microparticles.[143] Based on the previous work on assembly of WT TMV into long nanofibres *via* aniline polymerization,[144] Zhou *et al.*[111] demonstrated that PANI–Pd–TMV and PANI–Cu–TMV NWs could be synthesized by coating WT TMV with polyaniline.

M13 phages and Au NPs were recently modified with antigens (tagpeptides) and antibodies, respectively, to specifically interact with each other.[145] As a result, M13 phages and Au NPs in the hydrogels formed lyotropic liquid crystals and well-ordered network structures through time-dependent cross-linking processes, respectively, leading to highly regular structures and enhanced macroscopic mechanical properties.[145] Courchesne *et al.*[146] explored the layer-by-layer (LBL) assembly of a M13 bacteriophage-based template for the organization of Au NPs into nanoporous networks (Fig. 7). The results proved that Au NPs needed to be incorporated into the bacteriophage films during the LBL process in order to remain well-dispersed as well as to preserve the resonance peak location. Otherwise, Au NPs incorporated after LBL-assembly resulted in aggregation with significantly red-shifted and broadened spectra.

### 3.3 Plant-mediated synthesis

Intracellular or extracellular synthesis of MNMs by microorganisms had been extensively studied. However, downstream processing of intracellular MNMs is difficult while screening

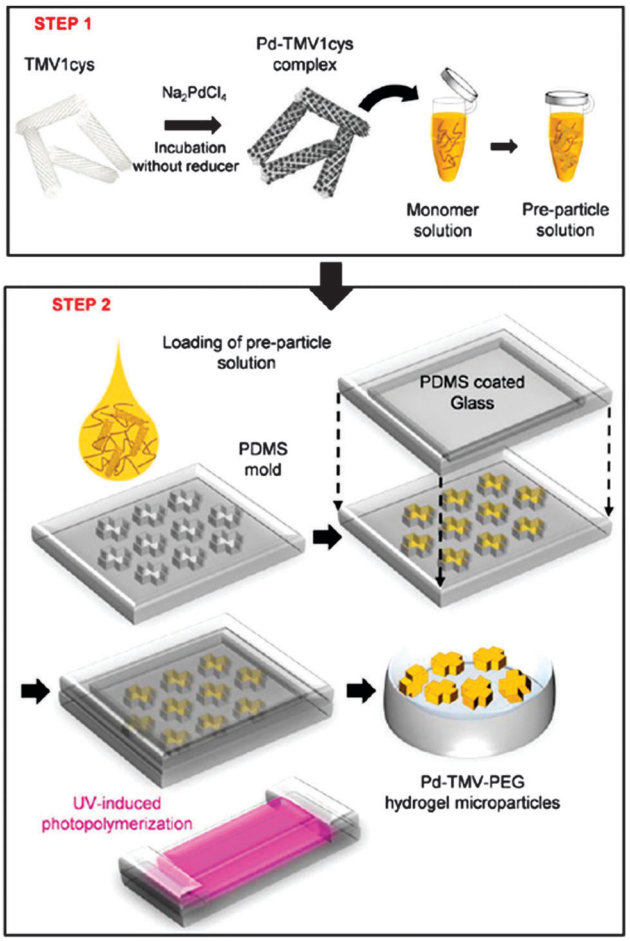


Fig. 6 Synthesis of Pd–TMV encapsulated PEG-based microparticles by replica molding (RM). (Step 1: spontaneous formation of Pd NPs without reducing agent. Step 2: fabrication of PEG-based microparticle *via* replica molding technique.) Reprinted with permission from ref. 38. Copyright © 2014, American Chemical Society.

microorganisms for extracellular synthesis is very laborious.[77] In contrast, plants have attracted significant attention as simple and effective alternative scaffolds for the extracellular synthesis of MNMs. Live plants, plant biomass and biomolecules extracted from plants or plant biomass have all been employed in the synthesis of MNMs.

**3.3.1 Biomineralization using live plants.** The first demonstration of plant-mediated synthesis was reported in 1999 by Gardea-Torresdey *et al.*,[11] who described the synthesis of Au NPs by bio-precipitation from Au(III) solutions with alfalfa biomass. Au and Ag NPs were formed using live alfalfa plants.[41,147] Some examples of similar biomineralization strategies in recent years are listed in Table 4. Spherical metal NPs (Au, Ag, Pd, Pt and AuAg) with a wide range of size distributions could be synthesized using live plants in most cases. For example, Bali *et al.*[148] reported that *M. sativa* and *B. juncea* plants were able to accumulate and translocate Pt from aqueous substrates. Pt NPs (*ca.* 3–100 nm in size) were evenly distributed across all tissue systems including epidermal, cortical and vascular within the roots of both plant species. The synthesis of AuAg NPs with

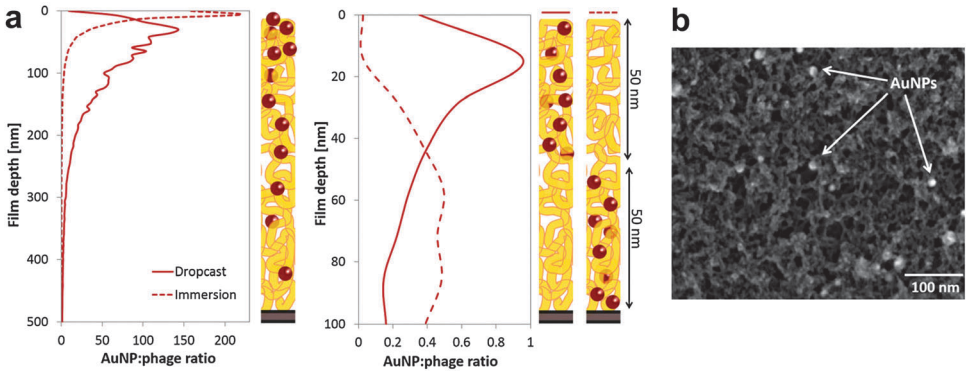


Fig. 7 Tight spatial distribution control of the bacteriophage-mediated incorporation of Au NPs. (a) XPS depth profiling analysis of the Au distribution as a function of the film depth, converted to NP to phage ratio for different film architectures. The top panel shows the distribution for NPs infiltrated post-assembly, while the bottom panel shows films that were assembled with phage–NP complexes. (b) SEM image of a phage film infiltrated with Au NPs, and coated with titania. Bright circles are imaged Au NPs dispersed within the nanowire mesh. Reprinted with permission from ref. 146. Copyright © 2014 Wiley-VCH Verlag GmbH & Co. KGaA, Weinheim.

Table 4 Examples of biomineralization with live plants

| Plants | MNMs | Shape | Size (nm) |
|---|---|---|---|
| *Sesbania*[150] | Au NPs | Spherical | 6–20 |
| *Brassica juncea*[151] | Ag NPs | Spherical | 2–35 |
| *Medicago sativa*, *Brassica juncea*[148] | Pt NPs | Triangular, spherical | 3–100 |
| *Brassica juncea*[149] | Au, AuAg NPs | Spherical | $<50$ |
| *Arabidopsis*[42] | Pd NPs | Spherical | $\sim32$ |
| *Populus deltoides*[152] | Au NPs | Spherical | 20–40 |
| *Arabidopsis thaliana* L.[153] | Au NPs | Spherical, irregular | 5–100 |

*B. juncea* plant was reported by Anderson *et al.*[149] Very recently, Parker *et al.*[42] demonstrated the ability of *Arabidopsis* to produce Pd NPs in a relatively simple way without any requirement for toxic chemicals or energy intensive processes.

The mechanism of metal uptake and transport into the plant cells has been studied.[152] Sharma *et al.*[150] also demonstrated that biomatrix-embedded Au NPs resulted from the reduction of Au(III) ions in the root cells and symplastic transportation of Au NPs to the aerial parts or shoots. The proposed sequence of Au transformation in *Arabidopsis thaliana* L. ((1) uptake of the ionic Au followed by (2) subsequent reduction of Au *in planta* to create NPs) was found to be a plausible route for Au NP formation.[153] The environment around *Arabidopsis thaliana* L. may affect the uptake or deposition of metallic ions. Parameters such as the concentration of metal ions, the influence of other metallic ions, *etc.* have been taken into consideration to evaluate the possibilities of MNM syntheses. Haverkamp *et al.*[151] demonstrated Ag NPs could be deposited on *Brassica juncea* if Ag precursor concentrations ($AgNO_3$, $Na_3Ag(S_2O_3)_2$, and $Ag(NH_3)_2NO_3$ solutions) were below a limit of *ca.* 0.35 wt% Ag on a dry plant basis. Higher levels of Ag would lead to the concentration of metallic salts within the plant instead of metallic deposition. *In vivo* effects of Cu and Ag on the synthesis of Au NPs in *Brassica juncea* plants were also studied[149] with results showing the formation of discrete Au NPs in shoots in the absence of Cu and Ag. The presence of Cu and Ag reduced the size of Au NPs while also limiting the concentration of Au(0) species in plant tissues. In the controlled experiment, AuAg alloy NPs were observed in the presence of Ag(I) ions in spite of an equal concentration of Cu ions in the soil had little effect on the synthesized Au and/or Ag structures (and did not alloy with Au and/or Ag).

**3.3.2 Synthesis of MNMs using plant extracts.** Metal NPs embeded in plant matrices are generally difficult to harvest for further applications. Plant biomass and extracts can be a comparatively better option to whole plants. Nevertheless, the use of plant biomass poses the difficulty in purification of as-synthesized metal NPs prior to their applications. Soluble biomolecules from plants or plant biomass have been consequently preferred for extracellular biosynthesis of metal NPs in the past decade.[154,155] Compared to microbial reduction, the biosynthesis of metal NPs with plant extracts possesses higher reduction rates of metal precursors and facile shape control for metal NPs.[155–158] Plant-mediated syntheses can take advantage of existing plant resources and achieve the extracellular synthesis of MNMs. The tedious screening and cultivation process of microorganisms can also be circumvented.

Following the first demonstration on plant-mediated synthesis of Au NPs,[11] some researchers in the National Chemical Laboratory of India conducted extensive work on plant-mediated synthesis of MNMs with plant extracts, *i.e.* broths of geranium leaves,[159,160] neem leaves,[161] lemongrass,[43,162] tamarind leaves,[163] *Emblica officinalis* fruit[164] and *Aloe vera* leaves.[165] It is worth mentioning that triangular Au NPs could be prepared by plant-mediated synthesis with a higher yield compared to those obtained *via*

chemical methods.[43,166] Plant-mediated synthesis of Au nanoplates has become one of the major interests in the area of biosynthesis.[150,167–179] Interestingly, Zhan *et al.*[180] adopted *Cacumen Platycladi* (*C. Platycladi*) extracts as a weak reducing and capping agent to easily synthesize Au nanoplates in high yields under kinetic control without other chemical reagents, as shown in Fig. 8. The reduction rate could be easily controlled through modulating the experimental factors such as addition modes/rates of feeding solutions, temperature and pH based on a syringe–pump apparatus. A two-step size- and shape-separation of biosynthesized Au NPs by density gradient centrifugation and subsequent agarose gel electrophoresis, respectively, was also recently reported.[181] In the second step, Au nanoplates could be well separated from spherical Au.

Ag NFs with 3D structures were synthesized by *Canarium album* foliar broths at room temperature by an one-pot synthetic protocol assisted by trisodium citrate.[182] Further exploration of the formation mechanism of Ag NFs showed that both biomolecules and trisodium citrate played very important roles in shaping 3D Ag NFs, different from previous Ag nanoplates.[183] The preferential adsorption of citrate ions on Ag(111) faces resulted in the preferential growth of other crystal faces while the protective components in the foliar broth could cause the formation of the cracking and stacking up of the petals.[182] Combining plant-mediated synthesis and microwave irradiation has been proved to be an ideal approach to the rapid synthesis of MNMs. WA simple and rapid biological approach was recently disclosed to synthesize water-soluble and highly roughened "meatball"-like Au NPs using green tea extract under microwave irradiation.[184] The synthesized Au meatball-like NPs possess excellent monodispersity and uniform size (250 nm in diameter). Furthermore, reduction of aqueous metal precursors with plant extracts can be combined under a continuous-flow tubular reactor to produce well-defined MNMs. The first example was reported by Huang *et al.*,[185] who described the continuous-flow biosynthesis of Ag NPs using *Cinnamomum camphora* (*C. camphora*) leaf extract. Liu *et al.*[186] further investigated the effect of process parameters on size distribution of Ag NPs and simulated the profile evolution of velocity, biomass concentration and temperature in the tubular microreactors by Computational Fluid Dynamics (CFD). Recently, they implemented reactive kinetics coupled with population balance model (PBM) and CFD to simulate the formation of Ag NPs in a microtubular reactor.[187] The model and its applicability in

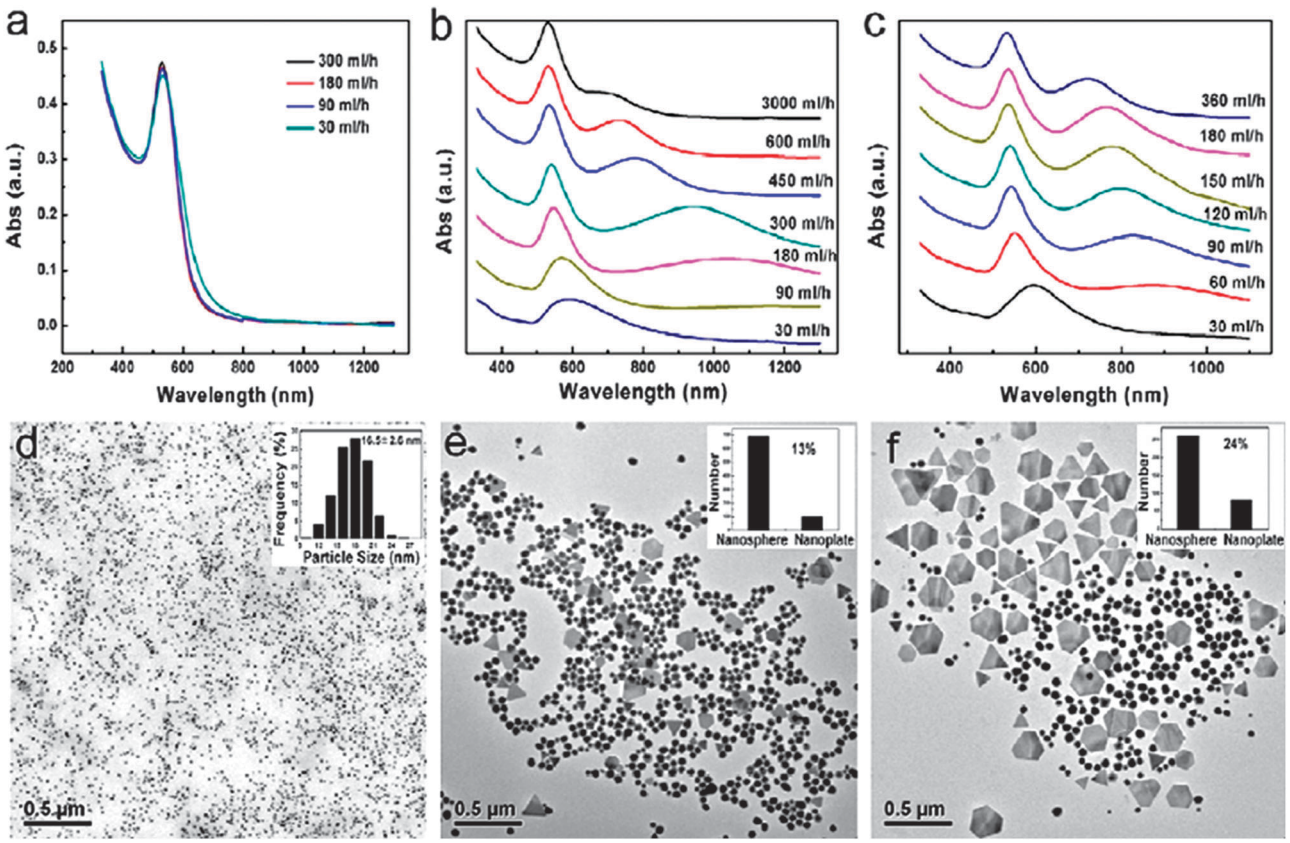


Fig. 8 (a–c) UV-vis-NIR spectra of Au sols prepared by addition modes (a) A, (b) B, and (c) C. (d–f) Representative TEM images of the Au NPs prepared by (d) mode A at an addition rate of 300 mL $h^{-1}$, (e) mode B at an addition rate of 450 mL $h^{-1}$, and (f) mode C at an addition rate of 90 mL $h^{-1}$. The reaction temperature and pH for all samples were 90 °C and 3.41, respectively. Three different mixing modes were adopted: mode A, involving the addition of Au precursor to *C. Platycladi* extract; mode B, involving an inverted addition of the extract to the Au precursor; and mode C, involving the simultaneous injection of the two feed solutions (*C. Platycladi* extract and Au precursor) with equal addition rates. Reprinted with permission from ref. 180. Copyright © 2012, American Chemical Society.

predicting formation and particle size distribution of Ag NPs in the continuous-flow tubular system were subsequently validated. The continuous-flow biosynthesis with plant extracts could also be extended from Ag NPs to bimetallic AuAg NPs.[188]

Besides monometallic NPs, bimetallic NPs could also be simply synthesized by plant-mediated synthesis. Spherical AuPd bimetallic NPs (~7 nm size) have been synthesized by simultaneous reduction of Au(III) and Pd(II) precursors using a *C. Platycladi* leaf extract at 90 °C.[189] Scanning TEM (STEM)-EDX mapping, XRD and UV-Vis characterizations confirmed the alloy structures and *ca.* 10 nm AgPd bimetallic alloy NPs could be successfully synthesized using the same plant leaf extract at three different ratios of 3 : 1, 1 : 1 and 1 : 3 using $AgNO_3$ and $Pd(NO_3)_2$ precursors at the same temperature.[190] ~10 nm AuAg alloy NPs could also be prepared using a similar method.[191] According to the reduction rates of Au and Ag ions characterized by atomic absorption spectrophotometry (AAS), 90 °C was a suitable temperature for the one-pot synthesis of AuAg alloy NPs using *C. Platycladi* leaf extracts. Furthermore, FTIR spectra confirmed the presence of N–H, (NH)C=O, and –OH groups in the plant extract which served as reducing parts, whereas the peptides or proteins prevented the alloy NPs from aggregation. A further combination of plant extract and the addition of a mild reductant (ascorbic acid, AA) could generate novel bimetallic NPs. For instance, ~40 nm flower-shaped AuPd alloy NPs were attained just to allow interation between AA and Au(III) and Pd(II) solutions for 20 s before adding *C. Platycladi* leaf extract at room temperature (Fig. 9).[192] Through careful time-resolved TEM studies, the flower-shaped NPs evolved from small decahedral particles and tended to be stable only after a reaction time of 20 min. However, prior to the addition of *C. Platycladi* leaf extract, Au(III) precursor solution was first reduced by AA to produce Au seeds, and then Pd(II) precursor solution was slowly dropped into the solution, resulting in flower-like Au@Pd NPs with the average size of 47.8 nm.[193] The slow formation rate of the Pd clusters was vital to facilitate the formation of fine flower-like core–shell Au@Pd NPs during the synthesis. Lu *et al.*[190] reported a facile and green synthesis of AgPd alloy bimetallic NPs using *C. Platycladi* extract. The alloy nature of AgPd alloy bimetallic NPs has been obviously confirmed by EDX elemental analysis. Regardless of the initial mole ratio of Ag/Pd, the Ag and Pd were homogeneously distributed over the entire NPs.

Size control of MNMs has also been investigated. The size of MNMs could be easily modulated by changing the reaction parameters, such as metal precursor concentration, plant extract concentration and reaction temperature.[44,45,194] Generally, higher plant extract concentration can lead to smaller metal NPs, given the same metal precursor concentration.[44,45,194] And higher reaction temperature can give rise to metal NPs with narrower size distribution.[44] As an alternative to size control, spherical Au NPs with different sizes and Au nanoplates with different edge lengths could be well fractionated to obtain monodisperse Au NPs through the two-step size- and shape-separation.[181]

**3.3.3 Elucidation of complicated bioreductive mechanism.** One of the focuses in the biosynthesis of metal NPs with plant extract is to understand the bioreductive mechanism that is very challenging due to complicated components in plant extract. In an attempt to explore the mechanism, a research group in Xiamen University has conducted a comprehensive study on the identification of active components in some plant extracts.[130,170,171,173–175] Firstly, the contents of flavonoids, polysaccharides, reducing sugars and proteins *etc.* in the extract before and after the reaction were measured. Secondly, simulated solutions of the active components by mixing several known chemical substances were prepared to verify the outcome of the synthesis. Thirdly, the main active compounds were isolated and validated.[45,154,194–197] Results showed that flavonoid and reducing sugar were the main reductive and

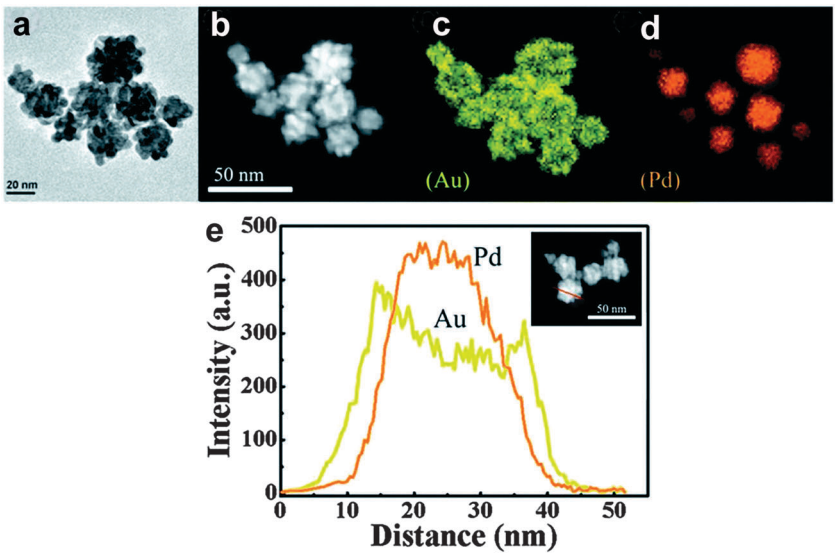


Fig. 9 (a) TEM image and (b) high-magnification STEM image of the flower-shaped AuPd NPs with an initial AuPd ratio of 1 : 1; energy dispersive X-ray (EDX) elemental maps of (c) Au and (d) Pd concentrations in the NPs and (e) the distribution of the Au and Pd components along the cross-sectional line profiles of a single AuPd NP. Reprinted with permission from ref. 192. Copyright © 2014, Royal Society of Chemistry.

protective components in *C. Platycladi* leaf and alfalfa extract to biosynthesize Au and Ni NPs, respectively.[194,197] For the first time from the standpoint of statistics, Zhou *et al.*[154] confirmed an electrostatic force or ionic bond-based interaction between the chloroauric ions and the involved bioconstituents, manifested the importance of flavonoid and reducing sugar to reduce metallic ions and illustrated a significant linear relationship between the anti-oxidant activity of the foliar broths and their capability to reduce Au(III) into Au(0). But for *Artocarpus heterophyllus* Lam leaf extract, Jiang *et al.*[195] reported reducing sugars (F2), flavones (F17), and polyphenols (F13) were the major biomolecules involved in the biosynthesis of Au NPs. The main active components of the leaf extract were further separated by AB-8 resin. Interestingly, the spherical Au NPs were preferentially formed by separating the main content of reducing sugar, monodisperse flower-like Au NPs by polyphenols, and triangular/hexagonal Au NPs (yield of 39.6%) by flavones. That is, shape control of MNMs was achieved during the synthesis by the isolated active components. Moreover, Lu *et al.*[196] investigated only geniposide in *Gardenia jasminoides* Ellis extract had the shape-directing capacity to fabricate Ag NWs, but it barely showed any reducing and capping capacity. Rutin, gallic acid and chlorogenic acid possesses both reducing and capping capacity, and gallic acid exhibited the strongest reducing capacity to produce Ag NPs.

Further, to quantitatively understand the nucleation and growth kinetics during the formation of Au NPs, Zhou *et al.*[198] established a model-assisted dynamic spectroscopic approach using *in situ* UV-vis spectroscopy. As shown in Fig. 10, temporal evolution of the SPR absorbance (the Abs–$t$ plot) was found to be sigmoidal with an evident nucleation stage and a crystal growth stage. Results revealed the growth of Au NPs *via* a zeroth-order reaction with respect to the concentration of the Au atoms. With the reaction proceeding, the growth rate became a first-order reaction and then a second-order reaction.[198] Furthermore, a Reduction–Crystallization (R–C) model (1) which deals with the two major events of such a physicochemical process were proposed. As shown below, $A_t$ and $A_{max}$ denote the absorbance of the sample at time $t$ and the end of the reaction, respectively, $k_1$ the apparent overall nucleation rate constant which is inversely proportional to the induction stage of the sigmoidal Abs–$t$ plots, and $k_2$ the apparent overall growth rate constant which is positively proportional to the maximum crystal growth rate.[198]

$$A_t = A_{max} \cdot \left(1 - \frac{k_2 + k_1}{k_2 + k_1 e^{(k_1+k_2)t}}\right) \quad (1)$$

The R–C model provides the quantitative kinetic information underlying the qualitative morphologies of nanocrystals. The above results demonstrated that the nucleation stage for

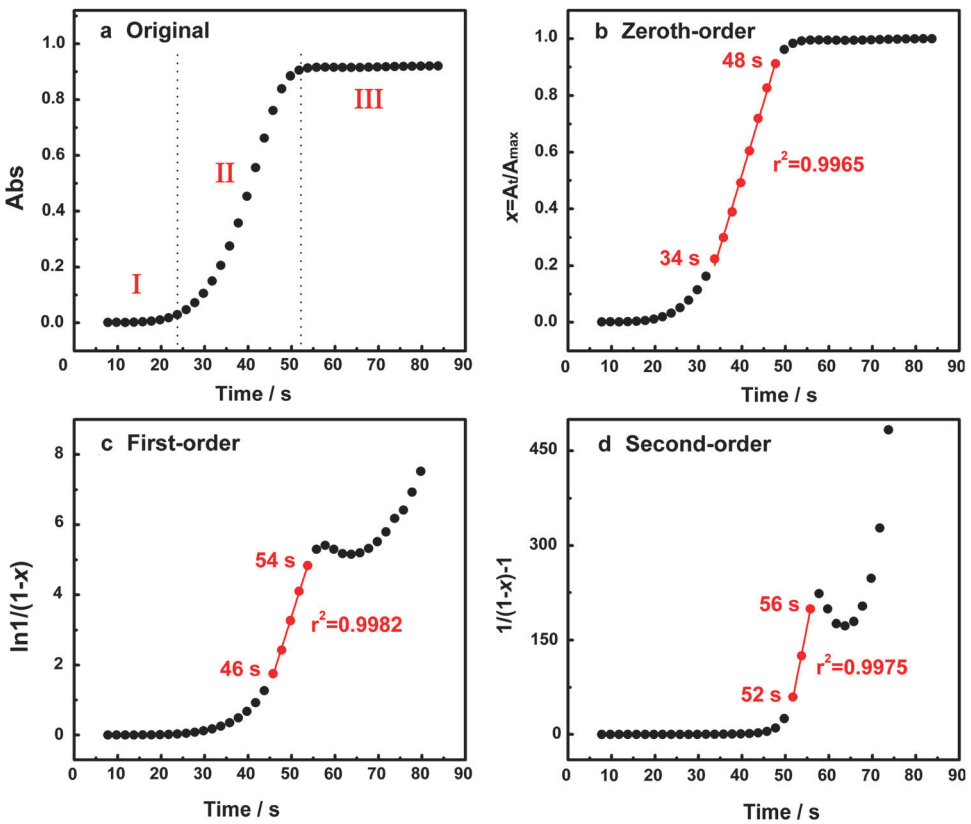


Fig. 10 (a) Typical sigmoidal Abs–$t$ profile and its responding $x$–$t$ profiles obtained by treating the Abs–$t$ profile with (b) zeroth-order, (c) first-order and (d) second-order rate laws for Au NPs synthesized by L-ascorbic acid reduction. Reprinted with permission from ref. 198. Copyright © 2013, Academic Press Inc. Elsevier Science.

Au NPs consisted of two steps, *i.e.*, (I) formation of Au NCs of several nanometers, and (II) formation of twinned crystal seeds out of those NCs, which indicated that formation of flaky Au NPs was a kinetic-controlled process favored by slow reduction of Au precursors.[198]

Furthermore, the sigmoidal Abs–*t* kinetic data were also fitted with the classical JMAK model (2) which was originally developed for the phase transformation process.[199] The results showed that the relationship between JMAK model parameters could be correlated to the crystallization behaviors and the dimensionality of the Au NPs.[199] The rate parameter $k$ mainly depends on the nucleation rate, and the Avrami exponent $n$ could be used as an efficient indicator to evaluate the extent of heterogeneous nucleation and to characterize the geometric dimension of Au NPs.[199]

$$x = 1 - e^{-kt^n} \quad (2)$$

### 3.4 Protein-templated synthesis

In nature, biological systems have evolved a full line of synthetic routes to inorganic minerals in the nanoscale *via* a biomineralization process.[18,200] Two prominent examples are the compositions and structures of mollusk shell and diatom, which are made up of $CaCO_3$ and Si NMs with hierarchical architectures. Nowadays, it is well known that these intricate nanostructures are formed with the main involvement of proteins,[201] which play a key role in tuning the size, morphology and polymorph of inorganic minerals *in vivo*.[17] Proteins have been the subject of particular attention due to their nanoscale dimensions, distinctive molecular structures and functionalities, and their ability to adjust the size of inorganic crystals during nucleation and growth. Therefore, the use of proteins to direct the ''bottom up'' synthesis of inorganic NMs *in vitro* has become a logical approach to creating novel nanocomposites.[202]

Compared with other bio-templates, the complicated proteins possess abundant binding sites that can potentially bind and further reduce metal ions, thus providing excellent scaffolds for the template-driven formation of MNMs.[27] In fact, protein is one of the best bio-templates for directing the synthesis of MNMs.[202] Firstly, the reaction conditions are normally much milder than some traditional chemical synthesis pathways. Room temperature, aqueous solutions, neutral pH and use of benign reducers (some reactions even without reducers) are some basic characters, which make the whole process inherently ''green''. Secondly, the size, morphology, component and crystal structure of MNMs can be exquisitely controlled by choosing the different kinds of proteins and/or variable experimental conditions. This is significant because these characteristics often take effect on the properties of the resulting products. Thirdly, the surfaces of the end-products are usually surrounded by a layer of protein molecules, which contain a plethora of chemical functional groups. This is very convenient to conjugate the targeting agents and drug molecules for the following biological/medical applications. Additionally, the protein-capped MNMs show rather strong stability under a wide range of salt concentrations, in phosphate and MES buffer. Last, the protein template is relatively cheap and can be easily obtained (*via* naturally extracted or protein engineering), which enables the whole preparation process in a large scale. Herein, due to space limitation, this section mostly focuses on the protein-directed synthesis of MNMs in the last 5 years.

To date, a variety of proteins have been used as templates for the synthesis of MNMs.[202] According to the shape differences, they can be generally divided into two types-spherical and filamentous proteins. In general, the metal NPs (including clusters), nanoplates or microspheres can be obtained by using the spherical proteins. On the other hand, the metal NPs, NWs or nanotubes will be prepared by using the filamentous proteins. Herein, for the spherical proteins-based MNMs synthesis, we mainly discuss two most popular templates – ferritin and bovine serum protein (BSA). For filamentous proteins-based MNM synthesis, collagen and silk as templates will be primarily discussed.

#### 3.4.1 Spherical proteins

*(a) Ferritin.* Ferritin is a well-studied family of protein that plays an important role in iron homeostasis and storage. Structurally, ferritin is composed of 24 subunits of two types, the heavy chain (H-ferritin) and light chain (L-chain), self-assembled into a hollow cage-like architecture with an external diameter of 12 nm and an 8 nm diameter cavity.[203] Physiologically, an iron oxide core comprising up to *ca.* 4500 atoms of iron is located in the cavity of ferritin. At the subunit junctions, some channels are formed for the purpose of transport of iron and other metal ions into and out of protein shell. The superior stability of the ferritin cage architecture over a wide range of pH (3–10) and temperatures (up to 80–100 °C) makes it become an excellent nanoreactor,[204] in which, many metal ions can be mineralized.[205] Moreover, it is thought that the outside protein cages could enhance the solubility and chemical stability of MNMs. Mann and Wong were the first to explore apo-ferritin as the template for the synthesis of inorganic NMs.[206]

Following their work, a variety of metal–protein hybrids have been successfully prepared by using apo-Ft (demineralized ferritin, the iron oxide core is removed) as scaffold, such as Co, Ni, Cr, Au, Ag, Pt NPs *etc.*[27] For apo-Ft templated synthesis, the usual synthesis route is the introduction of a certain amount of metal ions into its aqueous solution, followed by the addition of reducer (sodium borohydride or ascorbic acid). Herein, it is worth noting that the concentrations of metal ions and reducers have a significant impact on the uniformity and shape of protein–MNMs. A high concentration of metal ions is thought to denature the protein template, which further give rise to the heavy aggregation during diffusion of metal ions, leading to the resulting products with broad sizes and irregular shapes. For example, Sun *et al.*[207] synthesized the paired Au cluster within the apo-Ft nanoreactor, where ferrous ion is oxidized by the ferroxidase center of H-ferritin. The ferroxidase center is composed of 6 amino acid residues. One histidine (His), one aspartic acid (Asp), one glutamine (Gln), and three glutamic acids (Glu). Among them, His residue is utilized as ''points of control'' to grow Au clusters. To further control the

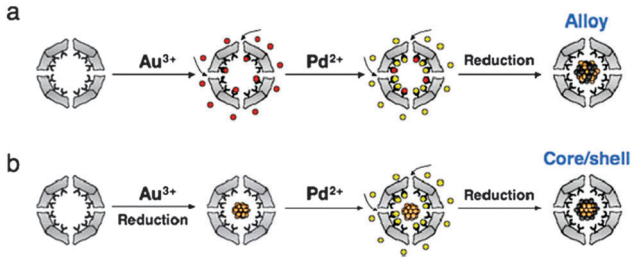


Fig. 11 Schematic illustrations of the two different synthesis methods of Au/Pd NPs in apo-Fr solution. (a) The synthesis of Au/Pd alloy structure; (b) the synthesis of Au@Pd core–shell structure. Au(III), Au(0), Pd(II) and Pd(0) atoms are colored red, orange, yellow and brown, respectively. Reprinted with permission from ref. 209. Copyright © 2014, Royal Society of Chemistry.

formation process of Au clusters, NaOH was used to allow the reaction to be processed slowly and in a controlled manner. Since every apo-Fr has two H-ferritin subunits, a pair of Au cluster can be assembled in each part. The molar ratio of Au ions to apo-Fr determines the size of the resulting Au clusters. With increasing Au(III)/apo-Fr ratio, the sizes of Au clusters increased. In addition, the preparation of Pt cluster by using apo-Fr was reported by the same group.[208] In theory, Ag and Cu clusters can also be obtained through judiciously tuning the reaction conditions.

Besides the synthesis of mono-metal clusters, the bimetallic clusters or NPs can also be prepared by using apo-Fr as the template. For example, Suzuki *et al.*[209] reported the preparation of bimetallic Au/Pd core–shell and alloy AuPd NPs by using two completely different strategies in apo-Fr aqueous solution, as shown in Fig. 11. Because of the different coordination properties of Pd(II) and Au(III) ions to apo-Fr, for the synthesis of Au@Pd core–shell NPs, the Au core is first prepared as a monometallic NP in apo-Fr, followed by introduction and reduction of Pd ions to form the shell. The Au/Pd alloy NPs were obtained by mixing aqueous solutions of $KAuCl_4$ and $K_2PdCl_4$, subsequent co-reduction by $NaBH_4$. In theory, a series of bimetallic even tri-metallic NPs could be prepared by adopting these methods. However, due to the spatial limitation of the local microenvironment in the cavity, the sizes of ferritin-templated MNMs are most strictly constrained to below 8 nm. To extend the vessel's limitation, next, we will introduce another kind of popular template protein-bovine serum albumin (BSA), which will greatly expand the MNM sizes and morphology range.

*(b) Bovine serum albumin.* Bovine serum albumin (also known as BSA or ''Fraction V'') is a globular protein derived from cows. The surname-''Fraction V'' refers to albumin being the fifth fraction of the original Edwin Cohn purification methodology that made use of differential solubility characteristics of plasma proteins.[210] It is often employed as a protein concentration standard in lab experiments. A mature BSA protein contains 583 amino acid residues and a corresponding molecular weight of 66 463 Da. The isoelectric point of BSA in water at 25 °C is 4.7. Of all the amino acids residues, 35 cysteine units form a total of 17 disulfides, which results in nine loops. Cysteine units are responsible for the tertiary structure of the protein. It is worth noting that a free sulfhydryl group is located at the cysteine residue on the position 34 of the amino acid sequence. 35 threonine and 32 serine unites bearing hydroxyl groups can act as milder reducer, which is similar to the case of polyvinyl pyrrolidone (PVP) widely used in the synthesis of NMs. In addition, several amino acid residues such as sulfur-, oxygen-, and nitrogen-bearing groups might also provide the electrons required for metal ions reduction. In its native state, BSA presents a heart-shape and consists of three homologous domains (I, II and III), each domain is made up of a sequence of large-small-large loops forming a triplet. The secondary structure of BSA consists of 67% helix, 10% turn, and 23% extended chain. Under the influence of external factors, such as temperature, pH as well as metal ions, the secondary structure of BSA often undergoes structural changes and transforms into its unfolded or tertiary configuration. The unfolded or denatured BSA can not only serve as an excellent capping/stabilizing agent, but is also very efficient in controlling the crystal growth and morphology.

Up to now, BSA has become one of the most popular protein templates for synthesis of MNMs,[211] which can be attributed to the following several reasons: the readily available and relatively cheap features for large-scale production, the outstanding foaming behavior for the simultaneous binding of cationic and anionic metal complexes as well as the superior stabilizing and modifying abilities for further biological/biomedical application. Owing to the existence of large numbers of reactive functional groups, BSA itself can work as a reducer and a stabilizer for the synthesis of MNMs with different sizes and morphologies. As many research reported, BSA had no reducing ability at room temperature.[48] It is necessary to resort to other ways such as an elevated temperature, a pH change or a physical means (*e.g.*, photo-irradiation or microwave heating) in the presence of additional initiators to trigger the reducing nature of BSA. Meanwhile, it is well known that the major driving force for protein denaturation is entropy, and a rise in temperature would increase the entropic effect. Moreover, the temperature should affect the reduction rate of metal ions as well as the rates for the nucleation and growth of the MNMs. Currently, a variety of MNMs with distinct shapes and sizes have been widely explored by using BSA as the template. For example, Xie *et al.*[212] synthesized the single-crystalline Au nanoplates (0.6–3 μm in size along their longest edge and ~19 nm in thickness) in aqueous solution of BSA at physiological temperature, where BSA provided the dual functions of metal ions reduction and directing the anisotropic growth of Au nanocrystals. The environmental factors such as temperature and pH had a significant influence on the conformation change, reduction and capping ability of BSA and hence the reduction kinetics, the nucleation and the crystalline growth of Au NPs. At physiological temperature, BSA remains its native configuration. Between 40 and 50 °C, the reversible changes in its configuration occur, whereas they become irreversible between 50 and 60 °C. Above 60 °C, unfolding of BSA with β-aggregation begins, which ultimately leads to gel formation around 70 °C.[213] At room temperature, they found that no particles were formed after 2 days of

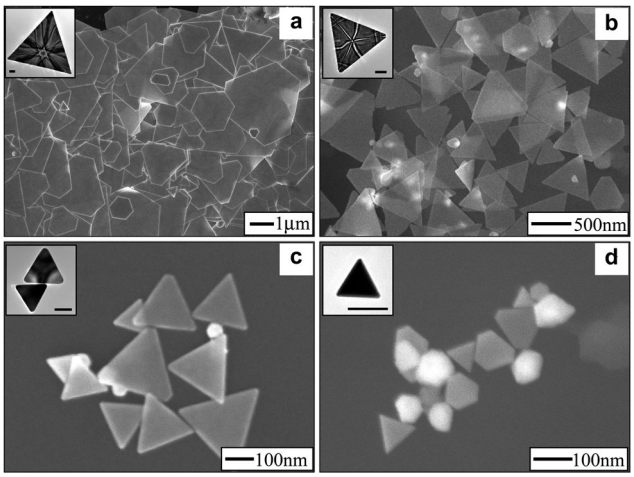


Fig. 12 (a–d) Representative SEM images of Au nanoplates synthesized in BSA solution with different Ag(I) concentrations of 0, 1, 5 and 10 μM, respectively. Insets are the high magnification TEM images. All scale bars are 100 nm. Reprinted with permission from ref. 212. Copyright © 2007, American Chemical Society.

reaction, revealing that BSA had no obvious reducing ability. However, increasing the reaction temperature over 37 °C, a color change rapidly took place, indicating the enhanced reduction capacity of BSA at high temperature. In view of this, a mild temperature was preferable for the formation of high-yield Au nanoplates (80%). In contrast, no Au nanoplates were formed at a high temperature (100 °C). To tune the sizes of Au nanoplates, the addition of different amounts of Ag ions could lead to the different lateral sizes ranging from a few μm to tens of nm, as shown in Fig. 12.[212]

pH value also had an essential influence on the morphology of the resulting products. At neutral and alkaline pH, the spherical Au NPs were exclusively obtained; at acidic pH, the planar Au NPs were formed. It is thought that BSA undergoes five isomeric conformations with changes of pH value. It is present in the normal form at neutral pH, and changes its conformation to the basic form at alkaline pH, which involves the unfolding of domain I and domain III. The unfolding is expected to facilitate the reduction of metal ions and the attachment of BSA chains to the NPs surface, thus producing uniform NPs with smaller diameter.

Considering these effects of temperature, pH value as well as ionic species to sizes and morphologies of MNMs, Au *et al.*[48] designed an optimum experimental parameters to prepare Au microplates covered by a dense array of BSA bumps. To obtain uniform Au microplates, an elevated temperature in the range of 55–65 °C, an acidic solution with pH ≈ 3, and the presence of NaCl with certain concentration (0.14 M) are indispensable. The formation mechanism of Au microplates can be tentatively proposed as following: in the presence of heat and/or $HAuCl_4$, a structural change occurred in BSA: the protein structure is unfolded and the disulfide bonds are broken with the appearance of many sulfhydryl groups. Meanwhile, the reducing hydroxyl groups in both serine and threonine residues are also exposed to the outside. Note that both sulfhydryl and hydroxyl groups are useful for the synthesis and growth of Au microplates. The hydroxyl groups work as the reducing agent and sulfhydryl groups can provide additional reaction sites for attaching the denatured BSA onto the surface of Au and thus stabilizing the final products.

In addition, the ratio of BSA and metal ions concentrations is also critical for controlling the crystal sizes. Due to their ultrasmall sizes, good biocompatibility, and high fluorescence properties, there has been a great deal of research work on the synthesis of metal NCs, especially Au and Ag by using proteins.[214] In a pioneering work completed by Xie *et al.*,[13] BSA is first used as template to synthesize the highly fluorescent Au clusters *via* a biomineralization mechanism. BSA sequestered and interacted with inorganic ions, followed by providing scaffolds for mineral formation though chemical function groups. To a fixed Au precursor concentration (5 mM), a low concentration of BSA (below 2.5 mg $mL^{-1}$) gave rise to the larger NPs without fluorescence; in contrast, a high concentration of BSA (10–25 mg $mL^{-1}$) formed the stable Au clusters with strong fluorescence. Therefore, the high concentration of BSA can sequester Au ions and entrap them, and further limit the further growth of Au clusters. The addition of NaOH (pH reaches up 12) and the 21 Tyr residues on BSA are responsible for the reduction of the Au precursor. Accompanied by this work, a series of metal clusters such as Ag, Pt, Cu as well as their alloy were continuously reported,[215–218] and the formation mechanisms were also discussed in detail.

On the other hand, in the presence of external reducers such as sodium borohydride, hydrazine hydrate and ascorbic acid, BSA is often used as a stabilizer and shape-directing agent for the MNM synthesis. For example, our group synthesized a series of noble metals (Au, Ag and Pt) microspheres structure in the aqueous phase at room temperature by using hydrazine hydrate or ascorbic acid as[219–225] reducers (Fig. 13). These as-prepared noble metal microspheres (*ca.* 300 nm in diameter) have unique core–shell structures with small metal NPs assembly inside and a layer of BSA molecules outside. The basic synthesis process is briefly described as follows: a certain amount of metal ions precursor (10 mM) was added into the BSA aqueous solution (5 mg $mL^{-1}$) at room temperature with vigorous magnetic stirring. After that, a certain amount of reducer was rapidly added into the mixture solution. Finally, the mixture was left to react for several hours. The resulting product is a composite microsphere structure, which is composed of many metal NP assembly ("supraspheres") and a layer of BSA coating. In light of their structures, the formation mechanism can be tentatively deduced as following: when the metal ions are added into the BSA aqueous solution, a configuration change rapidly appeared owing to the interaction of metal ions and BSA. BSA possessing plenty of functional groups such as –COOH, $–NH_2$ and –SH can provide multiple binding sites for the interaction with metal ions. When the reducers were added into the mixture solution, burst nucleation occurred and a lot of small metal NPs were formed. Under the influence of denatured BSA and NPs aggregation, a self-assembly process occurred, leading to the formation of microspheres. However, the detailed mechanism is worthy of further investigation.

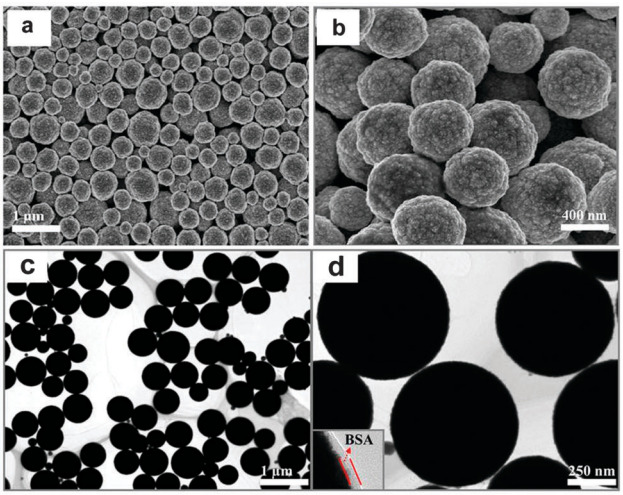


Fig. 13 SEM and TEM images of BSA-templated synthesis of 3D Ag microspheres (a) Au microspheres (b) Pt microspheres (c and d). Reprinted with permission from ref. 221, 222 and 225. Copyright © 2012–2014, American Chemical Society.

Metal porous structures have attracted intensive research interest because of their high surface area and enhanced performances. In addition to 3D noble metal microspheres, some porous structures such as mesoflowers and macroporous film can also be obtained by using BSA as the template. For example, Zhuang *et al.*[226] synthesized porous Ag, Pt and Pt–Ag alloy mesoflowers in BSA aqueous solution. To obtain these flower-like structures, the Ag mesoflowers composed of multilayer Ag nanosheets needs be first prepared using BSA as the capping agent and ascorbic acid as the reductant at 80 °C. Subsequently, the as-prepared Ag mesoflowers were further used as the sacrificial template for the preparation of Pt and its alloy structures *via* the galvanic replacement reaction. The prepared Pt mesoflowers exhibited a predominant enhancement in electrocatalytic activity toward electrical oxidation of methanol, which can be attributed to their 3D porous structure and small crystal sizes.

Recently, the synthesis of the 3D macroporous Au film by using BSA was reported by Hou *et al.*[227] The synthesis is based on a bottom-up biomineralization approach. First, BSA and metals ions are mixed at room temperature to form a mixed solution. Then, ascorbic acid was rapidly added into solution to reduce metal ions. At this point, the nucleation began to grow and some primary clusters arose. They quickly turned into small NPs and self-assembled into supraspheres. Lastly, calcination was carried out under high temperature to remove proteins so that a macroporous Au film was formed. Similarly, other macroporous metal or oxides can be also synthesized in this way.[228] These macroporous structures may have promising potential applications in catalysis, sensing, biofuel cells and tissue engineering.

**3.4.2 Filament proteins.** Apart from the globular proteins, the other type of protein assemblies – filamentous proteins provides another powerful platform for the capturing, interaction, reduction of metal ions and subsequent crystal growth of MNMs. There is a multitude of different filamentous proteins in nature, such as collagen, silks, wool, elastins, actins, keratins, myosins, flagellins *etc.* These proteins can self-assemble to form superstructures, which act as an intriguing template for the mineralization of MNMs.[11] Although many filamentous proteins are used as templates for the preparation of mental NMs, in the review we will focus on the collagen and silk proteins as they are the most extensively investigated, readily abundant and highly commercial values.

*(a) Collagen.* Collagen is one of the long, fibrous structural proteins whose structures and functions are quite different from those of globular proteins, as mentioned earlier. Collagen is one of the most important and abundant structural proteins in the extracellular matrix (ECM) of mammals. It forms more than 30% of the human body, and over 90% is type 1 collagen. Each collagen molecule is composed of three polypeptide chains with triple-stranded helical structure with a helical diameter *ca.* 1.4 nm and a length of 300 nm. The collagen molecules in the skin aggregate through fibrillogenesis into microfibrils, which consist of four to eight collagen molecules, and further into fibrils. These collagen fibrils organize into collagen fibers.

Like BSA, type 1 collagen has no reducing ability at room temperature. It still requires an extra introduction of chemical reductants (citrate or sodium borohydride) or physical methods (heat treatment, γ-ray and UV irradiation) to trigger the reduction of metal ions. For example, Alarcon *et al.*[229] synthesized spherical 3.5 nm Ag NPs in type 1 collagen solution at room temperature with the help of UVA irradiation. The photochemical preparation of metal NPs leads to the generation of peroxyl radicals, which could attack the collagen promoting oxidation and metal ion reduction. Collagen is used as a capping and stabilizing agent. However, although collagen itself contains an abundance of functional groups (including –OH, –COOH, $-CONH_2$ and $-NH_2$), they still are weak to stabilize and immobilize the metal NPs. To resolve this problem, a combined procedure is adopted. That is to graft some natural plant polyphenols onto the surfaces of collagen fiber to improve the stabilization and immobilization ability for metal NPs. Plant polyphenols having a high reactivity with collage of skins and specific affinity to many metal ions, is regarded as the unique bridge molecule to connect between collage and metal ions. For example, Wu *et al.*[230] grafted epigallocatechin-3-gallate (EGCG) onto the collage fiber to synthesize Pd NPs (Fig. 14). The hydroxyl-rich groups possess high adsorption ability for Pd(II) ions through the formation of a high-stable five member chelating ring. Thus, the well-dispersed and stable Pd(0) NPs can be *in situ* generated on the surface of EGCG-grafted collage fiber after $NaBH_4$ reduction of these anchored Pd ions. The process is schematically illustrated in Fig. 9. Likewise, Ag and Pd NPs were synthesized by using bayberry tannin grafted collagen fiber.[231]

Silk is a kind of protein fiber on a large scale and has been widely used in clothing manufacture. Silk fiber is produced by silkworms and spiders. As a natural protein-based fiber, *Bombyx mori* (*B. mori*) silk is mainly composed of an outer layer of sericin protein (*ca.* 30 kDa) and a core of fibroin protein

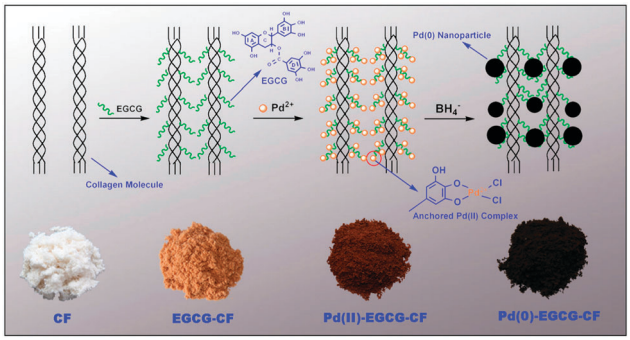


Fig. 14 Schematic illustration of the Pd NPs formation on EGCG-grafted collagen molecules. Reprinted with permission from ref. 230. Copyright © 2010, Academic Press Inc. Elsevier Science.

(*ca.* 350 kDa). Utilizing sericin proteins as both the reductant and stabilizer, Zhang *et al.*[232] fabricated luminescent silk and fabric. The reaction was carried out at 80 °C through mixing an aqueous solution of $HAuCl_4$ (0.143 mM) and silk (10 mg), followed by the addition of NaOH. Both the high temperature and the introduction of NaOH are necessary, which will greatly enhance the reducing ability of silk proteins. The resulting golden silk possesses outstanding optical properties, including a relatively long-wavelength fluorescence, a high quantum yield, a long fluorescence lifetime and high photostability. Moreover, it also shows better mechanical properties than the pristine silk, as well as a better UV light inhibiting ability. Based on the biomineralization mechanism of metal ions and proteins, one believes that many other luminescent metals-silk NCs can also be prepared using a similar strategy.

The pristine silk is insoluble in aqueous solution. In order to prepare the alternative material morphologies (*e.g.* film, fibers with nanoscale diameters, hydrogels and capsules), a particular solvent is necessary to dissolve and denature the proteins. Once the silk proteins are dissolved, it can be processed into a variety of morphologies and structures with metal NPs through some physical or chemical methods. For example, Cohen-Karni *et al.*[233] utilized electrospinning technology to create a 3D silk nanofiber matrix, incorporating Au NPs on and within silk nanofibers (Fig. 15). Doping the metal NPs can significantly improve the mechanical properties of silk. Some functional silk nanofibers can be obtained by mixing the soluble silk proteins and metal NPs in this way. Silk fibroin is also used as a template to produce Ag NPs *in situ* under light at room temperature. In the whole reaction system, silk fibroin provides multifunctions, serving as a reducing, dispersing and stabilizing agent. Similarly, the authors thought that Tyr residues in the silk fibroin are responsible for the reduction of Ag(I) into Ag NPs *in situ*.

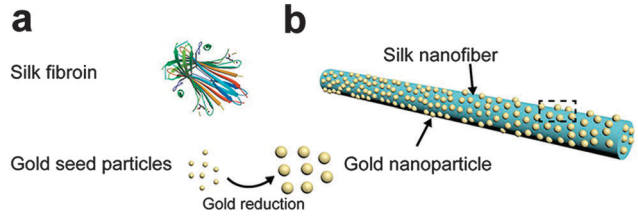


Fig. 15 Synthesis and fabrication of Au NPs-doped SNF. (a) The building blocks: silk fibroin and Au seed NPs. (b) A SNF doped with Au NPs (SNFAu) on the surface and throughout the fiber cross section. Reprinted with permission from ref. 233. Copyright © 2012, American Chemical Society.

### 3.5 DNA-templated synthesis

DNA is a well-known biopolymer with many unique features. Firstly, DNA sequences can hybridize with each other to form linear and branched double-stranded (ds) helical structures, which is predictable and programmable. Secondly, DNA possesses a strong affinity for a lot of metals such as Au, Ag, Pd and so on. These features make DNA an ideal building block for the templated synthesis of MNMs with defined shapes and sizes and endow it with great potential in materials sciences and nanotechnology. Nowadays, there are a lot of reports on the metallization of DNA. Herein, some examples in the construction of DNA-templated MNMs are discussed in this section.

#### 3.5.1 Methodologies for DNA metallization

*(a) Metallization by electrostatic interaction.* According to the conformation of DNA, there are a lot of phosphate backbones, which are negatively charged. This property was exploited to assemble some low-dimensional metal nanostructures based on the electrostatic interaction between the phosphate backbones of DNA and a cationic head-group on the functionalized metal NPs, thus forming interconnected metal NPs onto DNA. The metal NPs was pre-synthesized by chemical reduction reaction and functioned by the capping agent with cationic head-group through ligand exchange reactions. Simply mixing the metal NPs and DNA, and then incubating at room temperature for a period of time can lead to their nano-assembly. For example, several desirable architectures including the linear, ribbonlike and branched DNA–Au NPs assemblies could be constructed through electrostatic binding of ligand stabilized Au NPs to the λ-DNA backbone.[234] Another example was the fabrication of DNA-templated conductive Au NWs made of Au NP chains.[235] Aniline-capped Au NPs were assembled along the immobilized and stretched DNAs through the electrostatic interaction between the positively charged amine groups of the Au NPs and the negatively charged phosphate groups of the DNA (Fig. 16).[235] The as-synthesized Au chain DNA showed an Ohmic behavior at room temperature with the conductivity of two orders of magnitude smaller than the bulk Au.[235]

*(b) Metallization by in situ reduction and growth.* Different from the metallization of DNA by electrostatic interaction, there was another method to prepare the DNA–metal complex, in which the metallic precursor was *in situ* reduced to metal atoms on the DNA. The process usually consists of two steps. Firstly, the metallic precursor was mixed with DNA and the combined solution was incubated for a period of time to ensure that metal ions were thoroughly bound to the DNA. Afterwards, the reducing agent (*e.g.* $NaBH_4$, DMAB or AA) was introduced and the metal NPs could be formed onto the DNA. This facile method can be successfully utilized to synthesize monometallic NPs

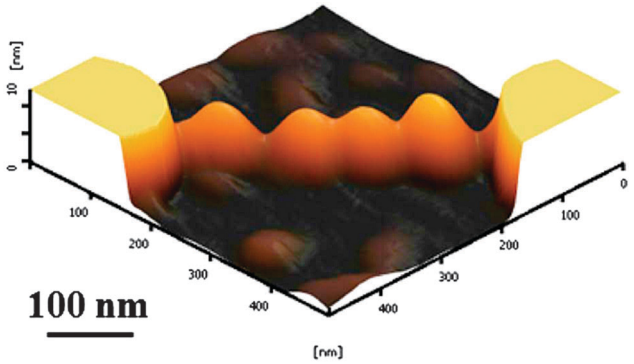


Fig. 16 AFM image of Au NP chain between the two electrodes. Reprinted with permission from ref. 235. Copyright © 2010, Institute of Electrical and Electronics Engineers.

such as Au, Ag, Pd and Pt NPs, or bimetallic NPs. Some examples are illustrated in Table 5.

Apart from spherical NPs, wire-like, rod-like and nanoring structure can be constructed by the *in situ* reduction and growth onto the DNA templates. The structure of DNA was of great importance in the synthesis of desired DNA–metal nanostructures. For instance, wire-like Ag NPs (17 ± 3 nm) with an average particle gap of about 1.7 nm on a ds-DNA template could be fabricated by mixing a proper amount of DNA with $AgNO_3$ solution and then placing the mixture under the UV-light at a wavelength of 260 nm for 3 h.[245] This Ag–DNA wire-like complex can act as a potential SERS substrate in which DNA played dual roles, not only in the formation of the Ag-NPs but also for the remarkably enhancement of the SERS signals.[245] Very recently, DNA with the toroidal morphology was used as template to deposit Au nanorings with an outer diameter of 105 ± 17 nm and inner diameter of 26 ± 14 nm through the slow photochemical reduction of Au precursor.[246]

In recent years, metal NCs (<2 nm) have become a hot research topic due to their fluorescence response pattern to a specific analyte. The previous studies indicated that the properties of NCs are highly dependent on the nature of the template molecules used for the NC synthesis, which is especially prominent for the DNA-based metal NCs.[247] There are already a lot of reports about the synthesis of DNA-based metal NCs and their application as a fluorescence sensor.[237–240] Almost all of DNA-based metal NCs were prepared through this *in situ* reduction and growth onto the DNA template. Different types of DNA, reducing agent and ratio between DNA to metal precursor were adopted in the studies. Thomas *et al.*[237] synthesized blue fluorescent Au NCs on the poly-cytosine DNAs by using citrate as a reducing agent. Park *et al.*[238] reported the fabrication of Ag NCs on the branched double-stranded DNAs. Results showed that the concentration and molar ratio of Ag and DNA had a great influence on the fluorescence efficiency. The brightest Ag NCs with the photoluminescence quantum efficiency of 19.8% were obtained when the molar ratio of Ag and X-DNA was about 7. Sengupta and coworkers[248] studied the specific influence of bases and base sequence on formation and stabilization of Ag NCs. The results indicated that thymine-rich oligonucleotides directed formation of Ag NCs that showed only blue/green-emission, whereas cytosine-rich oligonucleotides formed both red- and blue/green-emitting Ag NCs.

*(c) Metallization by molecular hybridization.* Well-defined and controlled assemblies of metal NPs have important applications in the fields of medical science, electronics, optics and catalysis. The assembly of multiple NPs has gained much attention because plasmonic coupling between metal particles results in the enhancement of electric fields, which is greatly dependent on the inter-particle spacing. It is well known that there is specific complementary binding of adenine with thymine and cytosine with guanine leading to the formation of helical duplex structure of double-stranded DNA, therefore making DNA a wonderful ligand or template in the assembly of metal NPs. As a result, the metallization can be effectively tuned by varying the number of DNA strands on metal NPs, the base sequence and the length and structure of DNA.

In a typical synthesis, one end of DNA was usually modified with a functional group suitable for binding with a metal surface. For example, thiol-modified DNA was usually employed to functionalize the Au or Ag NPs since there was strong interaction between the NPs and the mercapto-group of DNA. The assembly of multiple NPs to form dimer, trimer and multimer can be conducted through the complementary strand hybridization. Mirkin's group[249] first reported the construction of a macroscopic network *via* complementary DNA hybridization in which two sets of non-complementary alkanethiol group terminated DNA were utilized to functionalize citrate-stabilized Au NPs. Then linker DNA was introduced and the NPs could self-assemble

Table 5 Some examples about the metallization of DNA

| DNA | Metal NPs | Reducing agent | Morphology | Size/nm |
|---|---|---|---|---|
| G-quadruplex, I-motif, duplex[236] | Ag | $NaBH_4$ | Spherical | 2.1, 2.3, 2.9 |
| Poly-cytosine[237] | Au | Citrate | NCs | <1 |
| Branched DNA[238] | Ag | $NaBH_4$ | NCs | — |
| 5′-CCCTTAATCCCC-3′[239] | Au/Ag | $NaBH_4$ | NCs | ~2.45 |
| DNA duplexes[240] | Cu | Ascorbic acid | NCs | 1.69 |
| DNA hydrogel[241] | Au | $NaBH_4$ | Spherical | 2.8 |
| ss-DNA[242] | PtAu | $N_2H_4H_2O$ | Spherical | — |
| λ-DNA/calf thymus DNA[243] | Pd | DMAB/$NaBH_4$ | Network of NWs | 5–45 |
| DNA origami[244] | Au | $NH_2OH$ | Rod-like | 40(length) |
| ds-DNA[245] | Ag | UV | Wire-like | 17 (Ag) |
| Toroidal[246] | Au | UV | Nanoring | 40(thickness) |

into aggregates based on the molecular hybridization.[249] Afterwards, it was reported that Pt NPs could be decorated with a discrete number of DNA molecules and the Pt–DNA could be separated by gel electrophoresis. Interestingly, the Pt NPs can be assembled into dimer, trimer, core–satellite heteronanostructures *via* complementary binding with DNA-conjugated Au NPs.[250]

The DNA-origami approach, as a new technology, has particularly received high attention in recent years and was widely applied as a template to assemble metal NPs since it can facilitate more stable and precise assembly of NPs on it. One of the typical examples was reported by Ding *et al.*[251] Using triangular DNA origami as a template, six Au NPs covered by the corresponding thiolated complementary DNA strands can be assembled on the template through three DNA complementary hybridizations, generating linear chain of different-sized Au NPs with well-controlled orientation and spacing less than 10 nm. Pal *et al.*[252] employed a similar triangular-shaped DNA origami structure to assemble DNA–Ag-NPs through a two-step procedure. Firstly, triangular-shaped DNA origami displaying capture strands at predetermined locations was prepared. Then Ag NPs functionalized with chimeric phosphorothioated DNA was hybridized with capture strands on the DNA origami. After the assembly, discrete and well-ordered Ag nanoarchitectures with precisely tunable inter-particle distances from 94 to 29 nm as well as a trimeric architecture were constructed with high yield.

### 3.5.2 Assembly and size control of DNA-templated MNMs

*(a) One-dimensional structures.* 1D structures including NWs and chain-like structures can be constructed through a DNA-templated synthesis. DNA-templated synthesis of metal NWs can be conducted not only in the solution but also on the solid surface. For the solution synthesis, it can be directly fabricated through the self-assembly of NPs on the long DNA template. Rapid self-assembly of Au NPs into NWs on double-stranded DNA was proposed by mixing a proper concentration of DNA with Au salt and irradiating the mixture with UV light.[253] However, the length of as-prepared NWs through such a solution procedure was usually shorter than the origin DNA template since various multivalent cationic molecules/complexes could cause the transition of DNA conformation.[253] For example, the interaction between Pd(II) and DNA lead to the bending of the DNA base planes.[254] In order to generate the highly ordered and aligned NWs, DNA was immobilized on a solid substrate and then metalized through electroless deposition. An excellent example was the molecular combing technology to arrange λ-DNA into a stretch and parallel style on a mica surface.[255] Specifically, the metal ions quickly absorbed onto negatively charged DNA backbones through the electrostatic interaction and followed by the chemical reduction of the absorbed metal ions.[255] Parallel and uniform Pd NWs with an average diameter of about 30 nm can be produced.[255] Similarly, 3 nm tall Cu NWs could be fabricated by aligning the λ-DNA on a silicon surface and treating it with aqueous $Cu(NO_3)_2$, which was further reduced by AA.[256] Alternatively, the DNA-templated Au NWs with controllable interval could also be fabricated using surface-patterning techniques.[257] Another basic one-dimensional self-assembly structure was chain-like structure, which was usually constructed through the hybridization of complementary oligonucleotide strands functionalized on the surface of metal NPs. As an example, Barrow *et al.*[258] showed the synthesis of one-dimensional linear chains containing 1–6 Au NPs with inter-particle spacing of about 1 nm *via* DNA assembly.

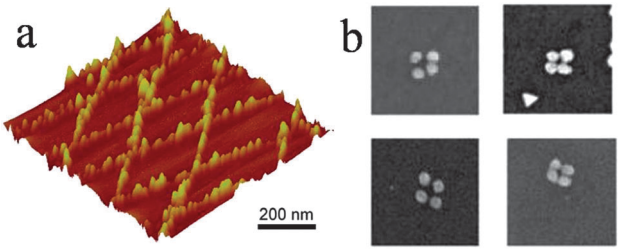


Fig. 17 (a) AFM image of 2D array of Pd NWs (b) SEM images of four Au NPs assembling on per origami. Reprinted with permission from ref. 255 and 260. Copyright © 2003 and 2014, American Chemical Society, respectively.

*(b) Two-dimensional structures.* With the development of DNA nanotechnology, 2D and 3D DNA pattern such as DNA origami can be constructed, therefore promoting the fabrication of DNA–metal complex with more complicated structure. For example, 2D array of Pd NWs could be successfully fabricated by the metallization of a 2D-aligned DNA sample (Fig. 17a).[255] As another example, a circuit-like DNA origami structure was employed as a template and conductive Au and Cu nanostructures on Si surfaces can be fabricated through the multiple Pd seeding step.[259] Moreover, the rectangular origami was utilized as a template to build the Au–DNA 2D structure.[260] Functionalized Au NPs were attached onto each corner of the modified DNA origami template, leading to the formation of various tetramer structures (Fig. 17b). The as-synthesized tetramer exhibited a significant Raman signal enhancement after attaching the Raman-active molecules to the metal NPs.[260]

*(c) Three-dimensional structures.* Compared to 1D and 2D structures, the preparation of highly symmetric 3D DNA–metal complex is more challenging. For example, Au NPs could be assembled into 3D architectures including stacked rings, single spirals, double spirals, and nested spirals through the interaction between NPs and DNA (Fig. 18).[261] Conjugation of Au NP with a single DNA strand incorporated Au NPs into a planar DNA tile array, with the tendency to form the DNA tube because of the systematic steric and electrostatic repulsion effects.[261] The size of Au NPs was demonstrated to have a great influence on the tube conformation.[261] Recently, 3D asymmetric tetramer was constructed by organizing four identical Au NPs on a rigid DNA origami template.[262] The chiral structural symmetry and the strong plasmonic resonant coupling between the Au NPs could give rise to the pronounced circular dichroism.[262]

*(d) Size control of DNA-templated metal NPs.* For the size control of DNA-templated metal NPs, the reducing agent, the ratio between the metal precursor and DNA, and the conformation of DNA was demonstrated to play a vital role. Hatakeyama *et al.*[263]

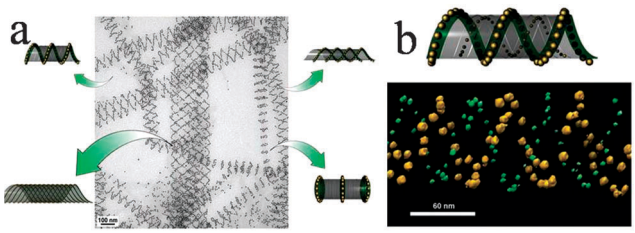


Fig. 18 (a) TEM image of different of various 3D architectures tube conformations. (b) Schematic side and top views of the binary particle tube architectures (top panels); the corresponding electron tomographic image (bottom panels). Reprinted with permission from ref. 261. Copyright © 2009, American Association for the Advancement of Science.



synthesized DNA–Pd nanostructures by using λ-DNA as the template. The effect of the Pd(II) concentration and reducing agent on the morphology of Pd NPs was studied. The result indicated that the increase of Pd(II) concentration resulted in the formation of larger NPs when using $NaBH_4$ as the reducing agent. And the size distribution of Pd NPs synthesized by using $NaBH_4$ was broader than those by using ascorbic acids. Kundu *et al.*[253] found that the eventual diameter of the particles in the range of 10–50 nm can be tuned by controlling the ratio between DNA and Au salt. Zheng *et al.*[236] investigated the influence of DNA structure and Ag(I)/base ratios on the size of as-prepared Ag NPs. Results illustrated that lowering the Ag(I)/base ratio gave rise to the decrease in the size of Ag NPs. The formation of Ag NPs was also affected by the DNA structure. When using G-quadruplex and duplex DNA as a template, Ag NPs measuring 1.6 nm can be prepared, which was compared to Ag NPs of 3.9 nm synthesized by I-motif DNA. Rotaru and coworkers[264] described a method for selective metallization of the double-strand of DNA with Cu NPs. They demonstrated that no Cu NPs were formed when using single-stranded DNA as a template at the low concentration of $CuSO_4$. Conversely, double-stranded DNA can be used as an effective template for the synthesis of Cu NPs. It was interesting that the size of NPs could be controlled by the use of a double-stranded DNA template with a selected length. The average height of Cu NPs formed in the presence of DNA6/DNA7 duplex was 2.1 ± 0.6 nm, whereas the average height of Cu NPs on the longer DNA8/DNA9 was 5.2 ± 1.9 nm. Kim *et al.*[265] demonstrated the synthesis of Au NCs by dithiothreitol and monothiol DNA. The size of Au NCs could be well tuned by balancing the concentrations of dithiothreitol and monothiol DNA. Increase in the amount of dithiothreitol led to the formation of larger NPs.

# 4. Interfaces of bio-metal systems for some applications

As discussed above, novel MNMs with interesting shape and assembly structure could be facilely synthesized with the assistance of the bio-inspired candidates. Furthermore, it can take advantage of readily available and green resources of bio-inspired candidates. Therefore, it has become a viable alternative to the traditional chemical and physical methods of synthesis of MNMs. Meanwhile, bio-inspired MNMs have been of great interest for applications in catalysis, sensing, antimicrobials, therapy, imaging and many others.

## 4.1 Catalysis

MNMs are attractive for the development of efficient catalysts owing to their large surface-to-volume ratio. The fabrication of green nanocatalysts that addresses energy and environmental concerns can be facilely achieved by the bio-inspired synthesis. Conventionally, micronized or nanosized supports that are usually needed to immobilize metal NPs to bridge the gap between bulk supports and NPs, make NPs highly dispersed and reduce the metal amount. Basically, there are two types of bio-inspired nanocatalysts, *i.e.* bio-supported metal catalyst and bio-MNM-support catalyst. For the former, the bio-inspired candidates are simultaneously employed as supports to immobilize bio-inspired MNMs *in situ*. For the latter, well-dispersed bio-inspired MNMs are immobilized onto some conventional supports (*e.g.* metal oxides). Although considerable progress has been made in the above bio-inspired synthesis, catalytic applications of bio-inspired MNMs, especially metal NPs, have been received much attention only in recent years.

### 4.1.1 Bio-supported metal catalysts

*(a) Microorganism-supported metal catalysts.* As far as enzymatic reduction was concerned, isolation of intracellular NPs for catalytic applications was difficult and microorganisms used for production of extracellular NPs only have to be extensively screened.[10,266] In the case of non-enzymatic reduction, though only extracellular NPs can be formed, they tightly adhere to microorganisms and are also hard to isolate from the cell surface. Hence, it is not easy to load microbially biosynthesized NPs onto conventional catalytic supports. However, from the viewpoint of bio-metal composites, dual functions of microorganisms as reductive scaffolds for NPs and supports for catalytic applications could circumvent the isolation of NPs from the microorganisms. Some earlier reports were demonstrated by Macaskie *et al.*, who showed the use of bacteria-supported Pd catalysts in the dechlorination of polychlorinated biphenyls,[267–272] reduction of Cr(VI),[67,273] hydrogenation of itaconic acid[274] and 2-butyne-1,4-diol.[275] Such Pd catalysts for the dechlorination of polychlorinated biphenyls were superior to those commercialized.[276] Furthermore, such catalysts can be extended to the realm of carbon–carbon bond formation (such as Suzuki–Miyaura and Mizoroki–Heck reactions).[277] Results showed that the properties of similar Pd catalysts for the Suzuki–Miyaura cross-coupling and hydrogenation reactions were affected by the ratio of biomass to Pd.[278] In addition, the stable and recyclable Pd-NP/*E. coli* catalysts could be developed for the deracemization of racemic amines[279] while Pd catalysts for the abatement of halogenated contaminants could be prepared by fermentative bacterial strains without extra hydrogen as the electron donor.[280]

Recently, the Pd-NP/*P.pastoris* catalysts exhibited higher stability for the reduction of 4-nitrophenol (4-NP), based on the pretreatment of the cells with aqueous HCl, aqueous NaOH and methylation of amino groups.[85] The enhanced stability can

be attributed to smaller Pd NPs, better dispersion of the Pd NPs, and stronger binding forces of the pretreated *P. pastoris*.[85] Similarly, the environmentally benign Au-NP/*P. pastoris* catalysts for the reduction of 4-NP were facilely achieved by biosorption and subsequent bioreduction.[37] Compared with the two other catalysts prepared by introducing an extraneous reductant, the Au-NP/*P. pastoris* composites exhibited superior and durable activity.

Due to the synergistic effects of bimetals, microbial biosynthesis of bimetallic nanocatalysts has been studied in recent years,[281–284] *e.g.* PdFe,[284] AuPd,[281–283] AgAu,[76,285] *etc.* As far as the biosynthesis of AuPd NPs was concerned, Hosseinkhani *et al.* adopted a two-step method to synthesize bimetallic AuPd NPs supported over *Cupriavidus necator* H16 with formate as the electron donor which showed a much better catalytic activity for the reduction of 4-NP than Au and Pd NPs.[283] Furthermore, AuPd NPs were supported on *S. oneidensis* bacteria, which could efficiently catalyze the degradation of diclofenac and trichloroethylene (TCE)[281,286,287] and Suzuki coupling reaction.[288] In addition, core–shell Au/Pd NPs on *E. coli* could be synthesized using microbially premade Pd seeds and the resulting AuPd/*E. coli* composites showed excellent benzaldehyde selectivity in solvent-free oxidation of benzyl alcohol without a base at low temperature, outperforming a commercial Pd catalyst.[282,287]

*(b) Virus-supported metal catalysts.* Like microorganisms, viruses can bridge the gap between MNMs and supports for catalytic applications. Yang *et al.*[119,141,289] thoroughly investigated the TMV1cys-templated Pd nanocatalysts *via* selective surface assembly on Au chips for dichromate reduction. Results showed that the average size of the Pd NPs was about 11 nm and changed slightly after the dichromate reduction. In contrast to the Pd-loaded chips in the absence of TMV, the Pd–TMV chips showed high durability for the catalytic reaction.[289] They also showed that the catalytic activity of the chips correlated well with the surface density of Pd–TMV and the surface area of the chips.[141] Their recent study showed that the reaction kinetics of dichromate reduction can be represented by the Langmuir–Hinshelwood model, which involves competing surface adsorption of dichromate and formic acid on the active Pd surface to start the surface reaction.[119] Dichromate was shown to have substantially stronger adsorption onto the Pd nanocatalyst surface than formic acid. The Pd catalyzed dichromate reduction with formic acid as the electron donor is a size sensitive reaction, where larger Pd particle size tends to have higher catalytic activity per Pd surface area. Meanwhile, TMV-templated Pd nanocatalysts with lower loading density showed higher catalytic efficiency (per Pd surface area).[119]

Also, the Pd–TMV nanocatalysts could be applied to the ligand-free Suzuki coupling reaction toward value-added chemical synthesis.[290] A moderately high temperature clearly facilitated the Pd–TMV catalyzed Suzuki reaction. Reaction condition studies demonstrated that the solvent ratio played an important role in the selectivity of the Suzuki reaction, and that a higher water/acetonitrile ratio significantly facilitated the cross-coupling pathway.[290]

Through a virus-templated approach, active metal components can be integrated with metal oxides on the scaffold of viruses to obtain nanocatalysts. For example, Au–$Co_3O_4$ NWs could be fabricated by the genetically modified M13 virus and used as building blocks for lithium ion battery electrodes.[113] M13 viruses were also used as biological templates to co-assemble Au and $IrO_2$ to enhance electron mobility in the NWs for an electrochromic anode material.[291] The Au string structure beneath the $IrO_2$ layer led to much higher electrochromic switching speed (35 ms for oxidation and 25 ms for reduction) than $IrO_2$ NWs without Au NPs (340 ms and 177 ms for the oxidation and reduction, respectively) at a similar color contrast.[291] Magnetically separable Rh/$Fe_3O_4$/M13 catalysts for hydrogenation was another example.[109] Also, active metal–virus can be embedded in the polymer matrix. Interestingly, Yang *et al.*[38] showed that the robust 3D Pd–TMV–PEG microstructures with Pd–TMV1cys as building blocks exhibited excellent catalytic performance for dichromate reduction, *i.e.*, 6-fold higher activity than commercial Pd/C catalysts per Pd mass. Furthermore, the reaction rate was linearly proportional to the Pd loading density inside the Pd–TMV–PEG hydrogel microparticles.[38]

As discussed above, metal–virus composites with metal NPs can act as active catalysts. However, the other morphologies except NPs have been little reported through virus-templated synthesis. Lee *et al.*[124] demonstrated that CTAB-directed, virus-templated Au NWs and Au–Pt core–shell NWs exhibited excellent catalytic activity for CO oxidation and ethanol oxidation, respectively. It should be noted that the Au NWs and Au–Pt core–shell NWs are different from the previous metal–virus composite NWs.

*(c) Plant-supported metal catalysts.* Some examples of plant-supported metal catalysts have been reported in the past ten years. The first report was presented by Sharma *et al.*,[150] who demonstrated *in situ* catalytic role of the Au-NP-rich biomatrix towards reduction of aqueous 4-nitrophenol (4-NP), exemplifying a plant-cell-immobilized stable catalyst. Afterwards, Jia *et al.*[292] reported the biosynthesis of Pd NPs supported by the biomass of *Gardenia jasminoides Ellis* that can serve as long lifetime nanocatalysts for *p*-nitrotoluene hydrogenation. Antioxidants including geniposide, chlorogenic acid, crocins and crocetin in water crude extract were identified as reducing and stabilizing agents for synthesizing Pd NPs with size range of 3–5 nm and good dispersity at 70 °C. The catalytic test of the antioxidant-stabilized Pd NPs showed a conversion of 100% under conditions of 5 MPa, 150 °C for 2 h. The selectivity of *p*-methyl-cyclohexylamine achieved 26.3%. Recently, it was reported Pd NPs could be produced in *Arabidopsis*. Heating the plant-embedded Pd NPs at 300 °C or 800 °C led to the Pd-P-300 and Pd-P-800 catalysts, respectively. And the carbonized Pd-P-300 can act as an efficient catalyst for Suzuki–Miyaura reactions involving I, Br and Cl leaving groups, which outperformed the commercial catalysts Pd on carbon 10% (Pd/C) and $Pd(OAc)_2$.[42] Compared with the Pd-P-300 catalyst, a marked increase of diameter and size distribution of Pd NPs was found in the Pd-P-800 catalyst, which was detrimental to the catalytic activity.

*(d) Protein-supported metal catalysts.* Proteins have been recently recognized as a new class of supports for stabilizing and protecting NPs. Protein matrices had been shown to be especially effective in gaining narrow size distributions and maintaining long-term dispersion stability of metal NPs. In view of this, a highly catalytic efficiency came up by using protein-templated MNMs as catalysts. For instance, the polyphenol-grafted collagen fiber-templated Au NPs with different sizes were active heterogeneous catalysts for the reduction of 4-nitrophenol to 4-aminophenol in aqueous phase.[293] The catalytic behaviors of as-prepared Au NPs depended on the particle size and the grafting degree of polyphenol. It was found that the smaller size Au NP would significantly promote the accessibility of reactants to the active center of catalyst and thus enhance the catalytic reduction rate. However, a high grafting degree of polyphenol with abundant phenolic hydroxyls would hinder the diffusion of reactant toward the active sites of catalyst and eventually lead to its deactivation. A distinct advantage of collagen-templated Au nanocatalysts is that they can be easily recovered and reused at least twenty times, because of the high stability completed by biomolecules.

Quite recently, ultra-small metal clusters stabilized by proteins show superior catalytic activity due to their high surface energy that makes the surface atoms fairly active. They are widely used as catalysts and enzyme mimics. For example, Kanbak-Aksu *et al.* prepared the Pd-NPs of uniform size ($5 \pm 1$ nm) using the ferritin cage from *P. furiosus*.[294] The high thermal stability of PfFerritin makes it an attractive alternative to the commonly used mesophilic analogs. The resulting Pd–ferritin nanohybrids showed high purity and high robustness, which were used for highly specific aerobic oxidation of alcohols in water. As a matter of fact, the catalytic activity of protein–metal NPs can be further enhanced through formation of the alloy NMs. For example, Suzuki *et al.*[209] reported that apo-ferritin templated Au/Pd bimetallic NPs had the improved catalytic reactivity for olefin hydrogenations compared with Pd NPs alone used. Therefore, in order to obtain the optimal catalyst, an alternative way is to fabricate the different types of bimetallic NPs in protein templates.

Enzymes are a kind of important proteins that can catalyze a wide range of reactions. They have been involved as templates for the synthesis of metal NPs with enhanced activity. Interestingly, many manmade nanostructures have enzyme-like activities, which can replace the natural enzymes. Compared with the native enzymes, the nanomaterial-based enzyme mimics have the advantages of low cost and greater resistance to extremes of pH and temperature and lower sensitivity to proteases, which can be potentially used in the fields of food processing, agriculture, chemical industry and medicine. Protein-templated metal NPs have been considered as one of the most important nanoenzymes due to their highly chemical stability, enhanced catalytic ability, easy preparation, as well as excellent biocompatibility.

For example, Jiang *et al.*[295] synthesized paired Au clusters could efficiently catalyze oxidation of 3,3,5,5-teramethylbenzidine (TMB) in the presence of $H_2O_2$ to produce a color change. This can be developed for the colorimetic sensor of glucose. Compared to the natural horseradish peroxidase (HRP), it was found that the Au–Ft clusters had a much higher catalytic activity to TMB. The kinetic parameters exhibited a lower $K_m$ value and a higher $K_{cat}$ value for TMB than that of horseradish peroxidase (HRP). The catalytic mechanism is a ping-pong mechanism. The Au–Ft was reacted with $H_2O_2$ to release the hydroxyl radical ($HO^{\bullet}$). The generated $HO^{\bullet}$ would efficiently attack TMB to become oxidized TMB.

BSA-templated Pt NPs with peroxidase-like activity can catalyze the oxidation of various chromogenic, fluorogenic, and chemiluminescent substrates in the presence of $H_2O_2$. Kinetic studies indicate that BSA-templated Pt NPs have a much higher affinity for $H_2O_2$ than the other Pt NPs.[296] The BSA shell plays an important role in maintaining the robust stability of Pt NPs. Even in a high ionic strength environment (2 M NaCl), the catalytic activity can be completely preserved. Meanwhile, the short-term stability of BSA-templated Pt NPs was compared with that of HRP. HRP lost its catalytic stability dramatically in a short time and most of the activity after 24 h. However, the catalytic activity of BSA-templated Pt NPs remained unchanged in the time periods. The good biocompatibility, easy modification either chemically or biologically, these excellent properties make the BSA-templated NPs an ideal candidate for a wide range of potential applications as peroxidase mimics.

San *et al.*[297] employed peptidases (PepA) as templates to synthesize ultrasmall Pt NPs (0.9–3.2 nm) as a multifunctional nanocatalyst. The resulting composites (denoted as bioinorganic nanohybrid catalyst) kept the catalytic activities of both the proteins and metal NPs. They could combine to carry out the multistep synthesis of the desired compounds. PepA could be an excellent component of robust biomaterial, as it not only performed the enzymatic function but also stabilized the performance of inorganic NPs, meanwhile, largely reduced the cytoxicity of Pt NPs. In a similar way, various inorganic NMs could be combined with enzymes to catalyze the synthesis of chemical compounds.

Although the existence of protein shells can keep the catalyst stability, they also made an impact on the catalytic activities of NPs at the same time. Kim *et al.* used three proteins (aminopeptidase PepA, serine endoprotease DegP and Clp protease) to synthesize Pt NPs and compared their catalytic activities as scavengers of reactive oxygen species (ROS).[298] Of the three synthesized protein–Pt NPs, PepA–Pt NPs was found to be the most effective ROS quencher, indicating that the catalytic activity of protein-shelled Pt NPs is largely affected by the physicochemical properties of their protein shells. This means that in designing protein–metal catalysts, it is necessary to screen proteins to optimize the functionality of the resulting materials.

*(e) DNA-supported metal catalysts.* As an important biopolymer, DNA can be used as a template to synthesize many metal NPs and the as-synthesized DNA–metal NPs complex has been considered to be a heterogeneous catalyst in many organic reactions. For example, Kundu *et al.*[253] reported the synthesis of organized assemblies of Au NPs on a DNA template through a simple photochemical route, which can be used to catalyze the reduction of 4-nitroaniline. The DNA–Au NWs exhibited a

higher activity than other methods using either spherical or anisotropic Au NPs due to the high surface-to-volume ratio and the widely exposed active surface of the NWs.[253] The non-uniform structure containing some edges and corners was an important additional factor, leading to the increase of the catalytic reaction rates.[253] Very recently, Auyeung *et al.*[299] explored a strategy for the synthesis of catalytically active supported Au NP superlattices. DNA was introduced to direct the assembly of NPs into well-defined architectures. Then the as-synthesized superlattices were embedded in silica and calcined to provide access to the catalytic NP surface sites. The calcined superlattices showed good catalytic activity towards the oxidation of 4-hydroxybenzyl alcohol, which was in sharp contrast to the DNA-functionalized Au NPs (unsupported) as well as the uncalcined superlattice.

The structure of DNA has a great influence on the properties of metal NPs, which in turn affects the catalytic performance. In addition to the typical Watson–Crick duplex conformation, there were a variety of structures like G-quadruplex, I-motif, and other DNA assembled superstructures *via* base pairing interactions. Zheng *et al.*[236] prepared well dispersed Ag NPs with very small size using three different DNA templates with polymorphic structures. Using the reduction of 4-NP as a model reaction, the I-motif DNA-templated Ag NPs showed the highest rate constant, followed by the G-quadruplex DNA-templated Ag and the duplex DNA-templated Ag. Results suggested that the conformation of DNA is closely associated with the catalytic performance, which can provide some guidance to the design of multi-site metal nanocatalysts.

However, most of the synthetic DNA molecules were expensive and usually required harsh reaction conditions, thus limiting the mass production and its development in catalytic application to a large extent. Using natural DNA as the template to synthesize metal NPs has gained more and more attention due to the low cost and its abundant storage in nature. Fish sperm DNA was usually considered as a building block to synthesize DNA-templated metal catalysts. Wang *et al.*[300] prepared several kinds of metal–DNA nanohybrids (including Au, Pd, Ag and Pt) by natural fish sperm in a large scale and employed them as the catalysts for the corresponding organic reactions. For the hydrogenation of nitrophenyl compounds to aniline derivatives, the prepared Pd–DNA nanohybrid exhibited higher catalytic performance than the Au–DNA and Ag–DNA nanohydrids. But towards the aerobic oxidation of 1-phenylethynol to acetophenone, the Au–DNA showed the highest catalytic reactivity. Furthermore, these metal–DNA nanohybrids can be well reused with combined unique features of DNA and metal NPs.[300] Qu *et al.*[301] applied the natural calf thymus DNA as a mediator to construct modified DNA–graphene–Pd hybrid materials in which well dispersed Pd NPs with *ca.* 4.8 nm were densely assembled on the graphene surface. The DNA–graphene–Pd catalyst showed the best activity and durability for formic acid electro-oxidation compared with the commercial Pd/C catalyst and PVP-mediated graphene–Pd NPs.[301] It also can be used as an efficient and recyclable catalyst for the organic Suzuki reaction in aqueous solution under aerobic conditions. DNA was regarded as an important factor for the high catalytic activity because DNA can not only interact strongly with graphene sheets through π–π stacking but also chelate Pd *via* dative bonding.

#### 4.1.2 Interfacing bio-metal and conventional supports

*(1) Monometallic catalysts.* Among precious metals, Au has long thought to be chemically inert as it is very stable. Au catalysts for CO oxidation, selective oxidation of olefins and alcohols have attracted increasing attention in recent years.[302] In a very early report, based on non-enzymatic reduction by bacteria, a highly dispersive Au/α-$Fe_2O_3$ catalyst was prepared by *in situ* reduction of the Au(III) ions impregnated on an α-$Fe_2O_3$ support to Au particles with a mean size of 5 nm.[303] The catalyst showed good catalytic properties for CO oxidation. However, there have been few reports on the fabrication of supported metal catalysts by loading microorganism-mediated metal NPs onto a conventional support. Instead, well-dispersed metal NPs that are synthesized by reduction with plant extract have been further loaded on the conventional support to fabricate active metal catalysts in recent years. Basically, two specific procedures were provided, namely, the sol-immobilization (SI) method and adsorption–reduction (AR) method.[304] For the former method, the catalysts are prepared *via* immobilization of plant-mediated metal NPs on the support. For the latter method, it is designed *via* pre-adsorption of metal ions on the support followed by *in situ* reduction of metal ions with plant extract.

As far as plant-mediated Au catalysts are concerned, a successful example is the fabrication of efficient Au/TS-1 catalysts for gas-phase epoxidation of propylene, liquid-phase oxidation of benzyl alcohol and liquid-phase epoxidation of styrene. Au/TS-1 catalysts with high propylene oxide yields and remarkable stability could be prepared by immobilizing the biosynthesized Au sol on TS-1 supports for gas phase epoxidation of propylene with $H_2$–$O_2$ mixture.[304] Under optimal conditions (Si/Ti molar ratio of 35, Au loading of 1 wt%, plant extract of 10 g $L^{-1}$, K doping amounts of (K : Au = 0.2 : 1) and immobilization pH of 2, reaction temperature of 573 K and space velocity of 4000 mL $g_{cat}^{-1}$ $h^{-1}$), propylene conversion of 16.7%, selectivity of 65.7% to propylene oxide, $H_2$ efficiency of 24.6% and propylene oxide formation rate of 103.2 $g_{PO}$ $kg_{cat}^{-1}$ $h^{-1}$ were achieved.[305] Furthermore, the plausible reaction routes over the bioreduction catalysts were clarified. Acrolein (apparent formation activation energies: 35 kJ $mol^{-1}$) and propylene oxide (29 kJ $mol^{-1}$) were the major primary products at the initial stage of the reaction, while $CO_2$ (64 kJ $mol^{-1}$), ethanal (58 kJ $mol^{-1}$) and acetone (26 kJ $mol^{-1}$) were mainly formed in further oxidation or isomerization of propylene oxide.[305]

Starting from the above plant-mediated Au NPs, Du *et al.*[306] further proposed an ionic liquid-enhanced immobilization (ILEI) method to prepare highly efficient Au/TS-1 catalysts for the epoxidation of propylene. In the ILEI method, such Au NPs were facilely immobilized onto TS-1 by ionic liquid (IL) 1-butyl-3-methylimidazolium tetrafluoroborate ([BMIM][$BF_4$]). The zeta potentials of the TS-1 hydrosol can be changed by cations of [BMIM][$BF_4$] because of the special adsorption, which results in positive charges on the support surface, attracting the Au NPs

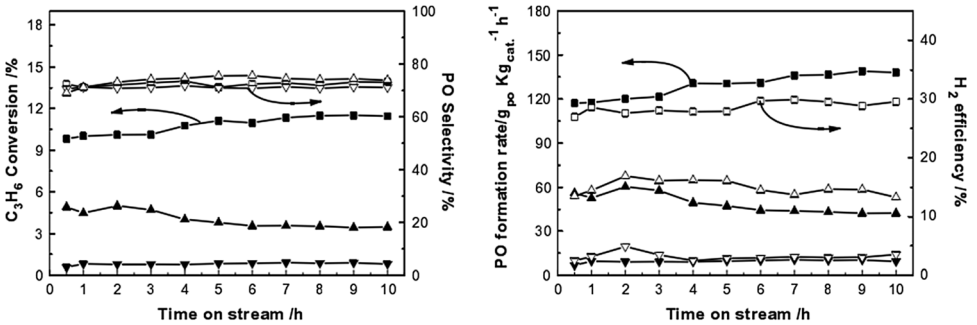


Fig. 19 Epoxidation of propylene over Au/TS-1; ■ □: 0.5Au/TS-1(35)-IL, ▲△: 0.5Au/TS-1(35)-pH, ▼▽: 0.5Au/TS-1(35). Reprinted with permission from ref. 306. Copyright © 2011, Academic Press Inc. Elsevier Science.

with negative charges.[306] The isoelectric point (IEP) of TS-1(35) was shifted from the pH value of 2.6 to 8.0.[306] Therefore, the Au NPs with negative charges can be fully adsorbed on the TS-1 support by the electrostatic attractive forces. And the interaction between Au NPs and TS-1 supports by the ILEI method was stronger than that by acidifying the colloid solution.[306] Compared to the Au/TS-1 catalysts without IL, the Au/TS-1-IL catalysts showed enhancement of catalytic performance, as shown in Fig. 19. Based on the plant-mediated Au/TS-1-IL catalysts, the propylene conversion of 14.6% and PO formation rate of 164.4 $g_{po}$ $kg_{cat}^{-1}$ $h^{-1}$ were higher than those in any other report[307,308] in which some traditional methods were adopted to prepare the catalysts.

Moreover, the Au/TS-1 catalysts can also be used to catalyze liquid-phase oxidation of benzyl alcohol or epoxidation of styrene with $H_2O_2$ as the oxidant.[309,310] Based on optimized parameters for catalyst preparation (AR method, Au loading of 0.3 wt%, and support Si/Ti molar ratio of 35), benzyl alcohol conversion of 67% and benzaldehyde selectivity of 84% were achieved. The kinetics and mechanism of oxidation of benzyl alcohol with $H_2O_2$ over the plant-mediated Au/TS-1 catalysts have been reported after eliminating mass transfer resistances.[311] By fitting the kinetic data using the power-rate law model, the orders of the reaction with respect to benzyl alcohol, $H_2O_2$, benzaldehyde and catalyst were found to be 0.55, 0.22, −0.35 and 1.06, respectively, with an activation energy of 38.2 kJ $mol^{-1}$ from an Arrhenius plot. These fractional orders indicate that the species were adsorbed on the catalyst surface leading to the product, benzaldehyde. In the case of epoxidation of styrene, styrene conversion of 92.7% and selectivity to styrene oxide of 90.4% were achieved, which were comparable or even superior to those reported in the literature.[310] An appropriate size of Au NPs was essential for the excellent catalytic performance while the interaction between the Au NPs and the TS-1 support should be tuned by adjusting the calcination temperature.[310] Recycling tests of the plant-mediated Au/TS-1 catalysts manifested their durability and reusability for the two reactions.

CO oxidation has been usually used as a classical model reaction to study supported Au catalysts. In a earlier report, Vilchis-Nestor *et al.*[312] demonstrated the "one-step" plant-mediated synthesis method (using sinensis extract) for the preparation of Au and AgAu catalysts supported on a $SiO_2$–$Al_2O_3$ (SA) material and their catalytic activity in the oxidation and hydrogenation of CO. The bimetallic AgAu/SA sample showed better behavior in the CO oxidation while the Au/SA monometallic sample showed superior catalytic performance in hydrogenation of CO.[312] Recently, Du *et al.*[313] investigated the effect of Au particle size on Au/$TiO_2$ catalysts for CO oxidation based on the biosynthesis with *C. camphora* extract. The mean size of the Au NPs on the $TiO_2$ surfaces ranging from 2.9 to 5.1 nm was obtained by changing the calcination temperatures and the extract concentration. It can be seen from Fig. 20 that the catalytic activity decreased with increasing Au NP particle size from 3.8 ± 0.6 to 5.1 ± 0.9 nm or decreasing Au NP size from 3.8 ± 0.6 to 2.9 ± 0.6 nm. The catalyst with 3.8 ± 0.6 nm Au NPs showed the best catalytic performance. The dramatic difference in the catalyst activity due to the variation in the size of Au particle further validates the size-dependent effect of Au NPs. The different size of the Au NPs produced various contact boundaries between the Au NPs and the $TiO_2$ support. For the most active catalysts, hemispherical Au NPs (3.8 ± 0.6 nm) had the best contact boundary with the $TiO_2$ support, yielding the longest perimeter interface (Fig. 21), suggesting that the contact boundary was the most critical factor for the CO oxidation. Recently, Yang *et al.*[314] reported

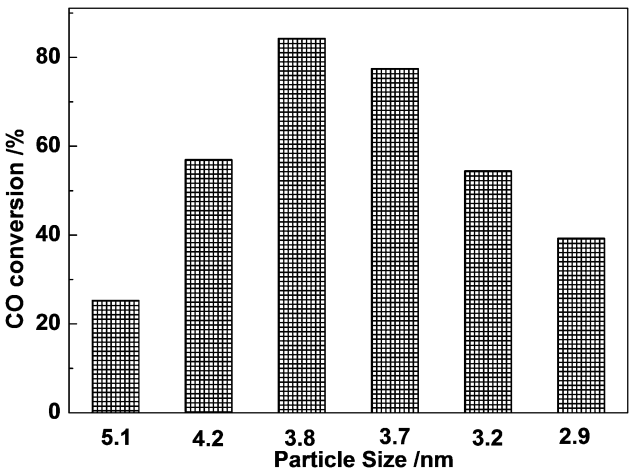


Fig. 20 CO conversion based on Au/$TiO_2$ catalysts with different Au NPs sizes. Reprinted with permission from ref. 313. Copyright © 2014, American Chemical Society.

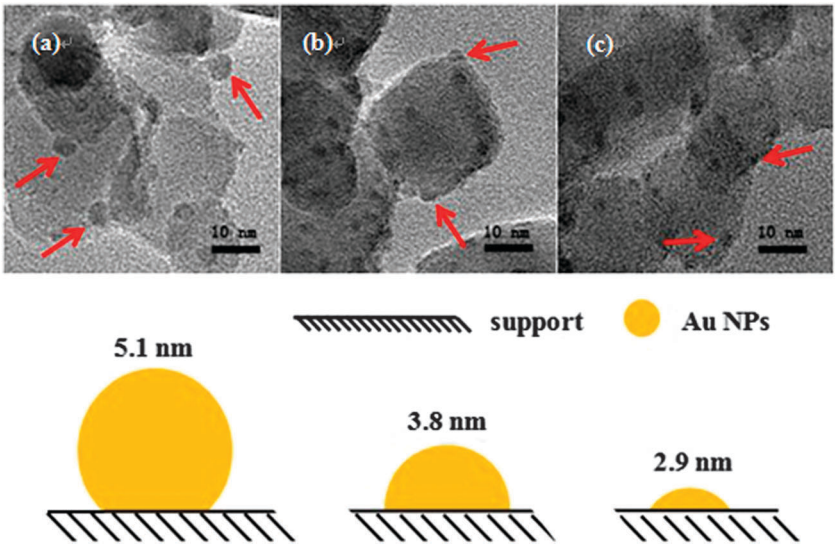


Fig. 21 TEM images of Au/$TiO_2$ catalysts with different Au NPs sizes, (a) 5.1 ± 0.9 nm, (b) 3.8 ± 0.6 nm (c) 2.9 ± 0.6 nm. Reprinted with permission from ref. 313. Copyright © 2014, American Chemical Society.

green and rapid microwave-assisted and plant-mediated Ag NPs with *C. camphora* leaf extract, and their immobilization onto $CeO_2$ towards efficient catalyst for CO oxidization. The catalyst prepared by the bioreduction method had a satisfactory activity with regard to the lower Ag loading, low-oxygen conditions and higher space velocity, compared with those reported in other literature.[314] They also demonstrated that the microwave-assisted biosynthesis of Ag NPs with plant extract could be extended to fabrication of efficient Ag/$ZrO_2$ for selective oxidation of 1,2-propanediol.[315]

Ag/α-$Al_2O_3$ catalysts were also prepared for epoxidation of ethylene by the AR method with *C. camphora* extract. For the influence of Ag precursors, the catalyst prepared from Ag–ethylenediamine complex exhibited better activity compared to the catalysts from the Ag–ammonia complex and $AgNO_3$.[316] Ag/α-$Al_2O_3$ catalysts could also be prepared through the thermal decomposition method assisted by *C. camphora* extract.[317] The calcination temperature and *C. camphora* extract amount in the preparation process were critical to catalysts with higher activities. It was found that 600 °C was the best calcination temperature, below the temperature Ag(I) from the $AgNO_3$ precursor was still detected and above the temperature Ag NPs started to agglomerate. With the increase of *C. camphora* extract concentration, the sizes of the resulting Ag particles decreased. Compared with the traditional thermolysis method, the sintering and aggregation behaviors of Ag NPs were alleviated with the assistance of plant extract.

Active hydrogenation catalysts could be also obtained with the assistance of plant-mediated synthesis of MNMs. Recently, green and reusable Pd/γ-$Al_2O_3$ catalysts for 2-ethyl-9,10-anthraquinone hydrogenation were fabricated by the AR method with *C. Platycladi* extract as both a reductive and a protective agent.[318] The maximum $H_2O_2$ yield of 96.4% could be achieved at lower reaction temperature (40 °C) than those in the literature.[318] Following synthesis of Pt NPs with *C. Platycladi* extract,[45] the plant-mediated Pt/$TiO_2$ catalyst was fabricated for the hydrogenation of cinnamaldehyde to cinnamyl alcohol.[319] In addition to Pd and Pt catalysts, Ru-based catalysts have been applied to hydrogenation processes. Ma *et al.*[320] reported colloidal Ru NPs were prepared by the reduction with *C. Platycladi* extract and then immobilized onto carbon nanotubes (CNTs) and activated carbon (AC). Ru/CNTs was successfully applied to the hydrogenation of benzene to cyclohexane under mild conditions without using any solvents.[320] Under optimized conditions, such as a Ru loading of 2 wt%, preparation temperature of 60 °C, calcination temperature of 500 °C, reaction temperature of 80 °C, pressure of 4 MPa, and the time length of 0.5 h, almost 100% yield of cyclohexane could be obtained. Similarly, the Ru/AC catalyst could be also used for selective hydrogenation of maleic anhydride with both C=C and C=O bonds.[321,322] Results showed that the monometallic Ru was effective in the hydrogenation of C=C bond to the saturated succinic anhydride, since the hydrogenation of C=C bond was promoted. A maximum yield of 99.2% was obtained over 2.0% Ru/AC.[321]

Efficient photocatalysts assisted by bio-inspired synthesis with plant extract were also reported. For example, Tian *et al.*[323] demonstrated a bio-Ag–$TiO_2$ composite (with Ag NPs of 4.0 ± 0.7 nm, 1.3 wt%Ag) as a photoanode for enhanced photocurrent in dye-sensitized solar cells. The best performance was achieved with a short-circuit current of 11.8 mA $cm^{-2}$ corresponding to a photoelectric conversion efficiency of 5.12%, higher than the glucose-Ag–$TiO_2$ and UV-Ag–$TiO_2$ DSSCs. The effective dye absorption phenomenon (residual hydroxyl group), high optical absorption phenomenon (because of the Ag plasmon effect) and electron injection efficiency (N719 dye) synergistically enhanced the performance of the DSSC system.[323] Very recently, it was reported that a bio-Au–$SrTiO_3$ composite (with Au NPs of 8.8 ± 3.2 nm, 3 wt%Au) was prepared by syzygium extract and used for $H_2$ evolution from formaldehyde aqueous solution without any additives at low temperature.[324] The high activity of the bio-Au–$SrTiO_3$ catalyst could be ascribed to the interaction

between hydroxyls (from biomass) and Au–$SrTiO_3$ which resulted in the formation of the Au(I)/Au species.[324] Also, the oxygen vacancies and organic biomass groups on the support may promote the activation of formaldehyde.[324]

*(2) Bimetallic catalysts.* Bimetallic NPs with alloy or core–shell structures are of great interest in catalysis due to their synergetic effect. The SI and AR methods can be adopted to prepare plant-mediated bimetallic nanocatalysts. For example, plant-mediated AuPd/MgO bimetallic catalysts were successfully fabricated and applied to the liquid phase oxidation of benzyl alcohol to benzaldehyde with molecular oxygen as the oxidant.[325] Optimization of catalyst preparation parameters manifested that the SI method (as compared with the AR method), MgO as the support (as compared with several other supports), the Au/Pd molar ratio of 1 : 1, and without calcination treatments were optimum. Optimization of reaction conditions manifested that the reaction temperature of 353 K and oxygen flow rate of 90 mL $min^{-1}$ were optimum. Under optimal conditions, the maximum benzyl alcohol conversion of 52.8% and benzaldehyde selectivity of 99.2% were achieved. Again, the recycling tests indicate a high durability and reusability of these bioreduction catalysts. Recently, Lu *et al.*[190] reported that the plant-mediated AgPd alloy NPs were supported on $\gamma$-$Al_2O_3$ for 1,3-butadiene hydrogenation. The conversion of 1,3-butadiene using $Ag_1Pd_3/\gamma$-$Al_2O_3$ was up to 100%, which reached the same conversion as Pd/$\gamma$-$Al_2O_3$. The promotional effects of Ag/Pd alloy catalysts might be attributed to the synergetic effect of the alloy in the hydrogenation. The addition of Ag could suppress the excessive hydrogenation and increased selectivity to butane.[190]

### 4.2 Sensing

**4.2.1 Electrochemical sensors.** Bio-inspired MNMs possess satisfactory biocompatibility, good conductivity and extensive surface area, which were inherited from both bio-inspired candidates and metal NPs. For example, the unique properties of protein-stabilized MNMs to provide a suitable microenvironment for biomolecule immobilization retaining their biological activity, and to facilitate electron transfer between the immobilized proteins and electrode surfaces, have led to the intensive use of this kind of NMs for the construction of electrochemical biosensors with enhanced analytical performance. Due to their unique optical, electrical, thermal and catalytic properties, metal NPs have attracted considerable interest and have been employed for construction of various electrochemical sensors. Metal NPs as sensing elements could be immobilized on the working electrode surface *via* different methods including physical adsorption, chemical covalent bonding, electrodeposition and so on. Recently, the BSA-templated noble metal microspheres (Au, Ag and Pt) have been employed for developing different kinds of electrochemical biosensor and nanodevices. The as-prepared electrochemical sensors have many special functions and could be applied to the related biological/medical research field, covering cancer cell sensing, protein analysis, small molecule determination, and so on. For example, Ag@BSA microspheres were used as an electrochemical sensing interface for the sensitive detection of urinary retinal-binding protein.[225]

On the one hand, the large surface area of Ag@BSA and the outside biocompatible BSA molecules can increase the amount of targeting molecules immobilized on the electrode surface, meanwhile keep the stability and bioactivity of the immobilized biomolecules. On the other hand, the inside Ag NPs could act as a good electric conductor to improve the electrochemical sensing ability. The immunsensor had a broader detection range and lower detection limit of RBP, revealing significant potential in clinical diagnosis. Besides fabricating the electrochemical immunsensor, the BSA-templated Au microspheres (Au@BSA) were also used as the sensing layer for the preparation of electrochemical cytosensor based on electrochemical impedance spectroscopy (EIS) changes, as shown in Fig. 22.[221] The prepared Au@BSA microspheres exhibited satisfactory biocompatibility for cell proliferation, providing a suitable platform for study of cell adhesion and detection. The unique 3D architecture and high hydrophilicity of Au@BSA could strengthen the adhesive force between biomolecules and nanostructured substrates. The outside BSA layer can not only serve as a multifunctional interface to be easily functionalized with targeting molecules, but also maintain the bioactivity of immune substances and improve the water-solubility of the synthesized nanocomposites. Due to the excellent electro-conductivity of Au NPs, amplified electrochemical signals could be obtained and resulted in the greatly enhanced detection sensitivity. The Au@BSA composite microspheres are regarded as excellent electrochemical sensing materials, revealing a promising technique for early monitoring of tumor cells at a lower level.

Enzyme immobilization is very important in biosensor development. The kinetics, stability and specificity of immobilized enzyme might differ from that of the enzyme in homogeneous solution due to the structural change in immobilization. Therefore, the construction of the immobilized enzyme layer which can retain the enzyme's specific biological function is highly desired. In one of our recent studies, Pt–BSA microspheres are applied as a film forming material to construct a biosensing interface with glucose oxidase (GOx), as shown in Fig. 23.[222] The electrocatalytic activity toward oxygen reduction was significantly enhanced due to the excellent bioactivity of the anchored GOx and superior catalytic performance of interior Pt NPs. Furthermore, this as-proposed electrochemical sensor also revealed qualified storage stability, excellent fabrication reproducibility, as well as good selectivity, indicating a feasible strategy for a glucose level assay in practical applications.

Electrochemiluminescence (ECL) is a kind of chemiluminescence triggered due to the high-energy electron transfer reaction between electro-generated species. BSA-templated Au fluorescent NCs have been used for the ECL detection of small molecules. For example, Li *et al.* reported ECL based on BSA-stabilized Au NCs on a modified indium tin oxide (ITO) surface using $K_2S_2O_8$ as the co-reactant[326] for the detection of dopamine. During the cathodic ECL process, the excited electrons were injected into the conduction band of ITO and then transferred to LUMO of BSA-stabilized $Au_{25}$, resulting in the generation of $Au_{25}^{\bullet -}$.

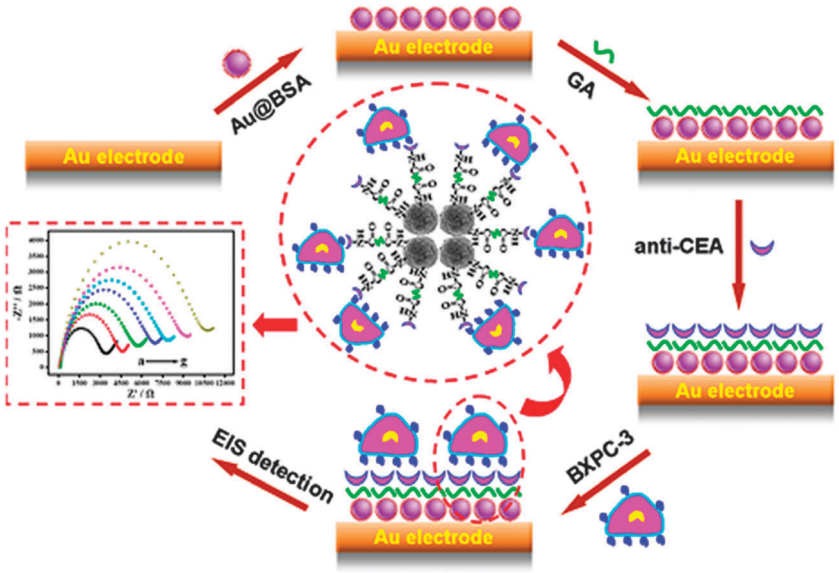


Fig. 22 Schematic representation of the Au–BSA-based cytosensing strategy for CEA-positive tumor cell detection *via* EIS. Reprinted with permission from ref. 221. Copyright © 2014, American Chemical Society.

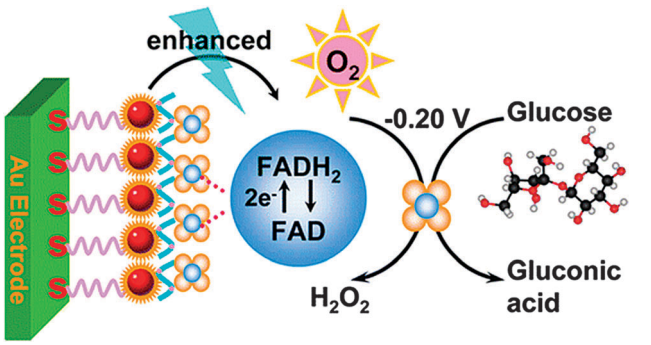


Fig. 23 Schematic illustration of the fabrication process and sensing mechanism of the Pt@BSA–GOx based electrochemical glucose biosensor. Reprinted with permission from ref. 222. Copyright © 2014, American Chemical Society.

The luminophore was oxidized by the same cathodically produced oxidizing radical, $SO_4^{\bullet -}$. When dopamine was added into the electrolyte, it was adsorbed on the surface of $TiO_2$, forming a charge transfer complex. In this way, electrons can transfer from the dopamine ligands directly to the conduction band of $TiO_2$, thus accelerating the electron injection into the conduction-band of ITO.

Considering the fascinating features of good water solubility, low toxicity, ease of labeling and excellent stability, the BSA-templated Au NC could become an efficient candidate for novel ECL biosensor development.

**4.2.2 Fluorescent sensors.** The remarkable photoluminescence properties and excellent photo-stability of metal NCs have lead to their wide application in the analytical and biochemical fields. Protein- and DNA-templated metal NCs have been extensively explored for the fluorescence detection of biomolecules compounds and metal ions.

Hydrogen peroxide ($H_2O_2$) is a kind of important analyte in the field of chemical, biological, pharmaceutical and environmental sciences. Particularly, it is one of the main products of enzymatic reactions by almost all oxidases, thus enabling quantitative enzyme activity as well as various enzyme substrates. Protein-templated fluorescent noble metal NCs have been widely used for the $H_2O_2$ detection. For example, Zhang *et al.* utilized horseradish peroxidase (HRP) enzyme to construct a dual functional Au NC possessing both catalytic and fluorescent properties for the detection of $H_2O_2$.[327] The HRP shell possesses intrinsic catalytic activity, which enables catalytic reaction of HRP–Au itself, and $H_2O_2$, resulting the quenching of fluorescence properties of the core Au NC. Upon the addition of $H_2O_2$ under optimal conditions, the fluorescence intensity was quenched linearly with high sensitivity (LOD = 30 nM).

Hg(II) ions are a highly toxic contaminant that exists in the environment. Protein- and DNA-templated noble metal NCs have been actively explored for the detection of Hg(II) ions. For example, Xie *et al.* utilized BSA-templated Au NCs to design a simple label-free method for the highly selective and ultrasensitive detection of Hg(II) ions.[328] The surface of as-prepared Au cluster is stabilized by a small amount of Au(I), which has a strong and specific interaction with Hg(II) ions. Based on the high-affinity metallophilic Hg(II)–Au(I) interactions, the red fluorescence of BSA-templated $Au_{25}$ NCs could be effectively quenched (Fig. 24). The fluorescence intensity of BSA-templated $Au_{25}$ NCs decreased linearly over the Hg(II) concentration range of 1–20 nM. Additionally, it had a remarkably high selectivity for Hg(II) over other metal ions and a low LOD value (0.5 nM), which could be further developed as a paper test strip for Hg(II) monitoring. Similarly, BSA-templated Ag NCs were also used for Hg(II) detection.[216] Hg(II) ions can also be easily detected by the DNA-templated noble metal NCs.[329,330] Zhu *et al.* synthesized DNA-templated Au NCs and introduced it as a probe for the detections of Hg(II) ions.[329] The formation of thymidine–Hg(II)–thymidine duplexes between DNA-templated Au NCs and Hg(II)

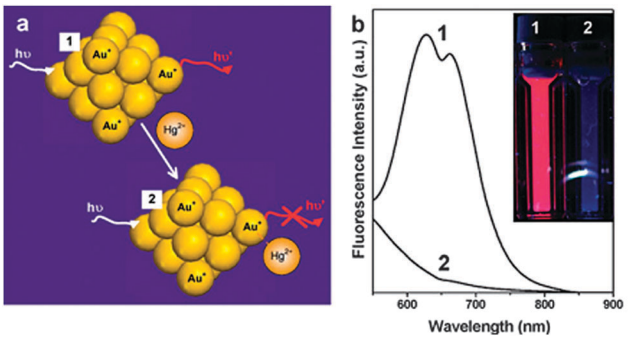


Fig. 24 (a) Schematic illustration of the Hg(II) sensing mechanism based on BSA-templated Au NCs. (b) Photoemission spectra and (inset) photographs of Au NCs under UV light in the absence and presence of Hg(II) ions. Reprinted with permission from ref. 328. Copyright © 2010, Royal Society of Chemistry.

ions resulted in the aggregation of Au NCs and thus facilitated the fluorescence quenching.

Pb(II) detection was also explored by using BSA-templated fluorescent Cu quantum clusters. However, the quenching mechanism is totally different from the above-mentioned metallophilic interactions. It was attributed to the quantum clusters aggregation induced by the complexation between BSA and Pb(II) ions, which was evidenced by dynamic light scattering (DLS) measurements.

BSA-templated noble metal NCs can also be used for toxic anion detection. For example, Lu *et al.* utilized BSA-templated Au NCs for cyanide detection in water. Cyanide is one of the most toxic anions in the environment.[331] It can directly cause the death of human beings in a short time by depressing the central nervous system. Cyanide is able to form a very-stable $Au(CN)_2^-$ complex with Au(0) *via* strong covalent bonding (etching process), thus, leading to the fluorescence quenching of Au NCs. Moreover, the BSA-templated Au sensor has a highly specificity towards cyanide over other anions, which is due to the unique Elsner reaction between cyanide and Au atoms. The simple, ''green'' sensing system has a great potential for the reliable detection of cyanide in water, food, soil as well as some biological samples.

DNA-templated noble metal NCs have also found their application in the detection of other metal ions such as K(I)[332] and Cu(II)[333] ions, and many biomolecules including thiols compounds,[334,335] DNA/RNA[336,337] and proteins.[338,339] In addition to the above ''turn-off'' pattern, a ''turn-on'' pattern was also developed. For example, Lan *et al.*[333] found that the fluorescence intensity of the DNA-templated Cu/Ag NCs was enhanced when Cu(II) ions were introduced into a solution containing the DNA and Ag(I). Increasing the Cu(II) concentration up to 250 nM would lead to continued fluorescence enhancement. Huang *et al.*[334] employed a series of DNA templates to fabricate Ag NCs and then studied the effect of DNA length and base composition on the fluorescent responses of DNA-templated Ag NCs. The results demonstrated that the fluorescent response patterns toward thiol compounds was template-dependent and the fluorescence intensities could be enhanced when using a series of polycytosine DNA as the template. This turn-on assay can be applied for the sensitive and specific detection of thiol compounds.

**4.2.3 Colorimetric sensors.** In recent years, colorimetric nanosensors have become popular because they provide several practical advantages, including the ability for naked-eye visualization, cost effectiveness, simplicity, portability and a low detection limit.[340] Of all the NMs, Au NPs are widely used for the colorimetric assays. The sensing mechanism is due to the color changes of Au NPs, which are sensitive to the size, shape, capping agents, medium refractive index and the aggregation state of Au NPs. Since there have been many reviews that have extensively described the Au NPs-based colorimetric assays, herein, we mainly introduce the emerging metal nanoenzyme-based colorimetric assays. As mentioned above, protein-templated NMs possess enzyme-like activities, which can catalyze substrate molecules to give rise to color changes. When exotic metal ions or organic molecules are added into the metal nanoenzymes aqueous solution, the metallophilic interaction occurs, leading to nanoenzyme inactivity and color changes. For example, Li *et al.*[341] reported the BSA-stabilized Pt NPs with 57% Pt(0) and 43% Pt(II) composition possessing a high peroxidase-like activity, which can catalyze the substrates of TMB (3,3′,5,5′-tetramethylbenzidine) and $H_2O_2$. The colorimetric sensing mechanism of Hg(II) ions is based on the metallophilic interaction (Hg(II)–Pt(0)), which down-regulate the peroxidase activity of Pt NPs. The deactivated Pt nanoenzyme failed to convert a multitude of substrate molecules into colored products. To a Pt nanoenzyme–TMB–$H_2O_2$ system, increasing the concentration of Hg(II) ions results in a color progression from dark blue to colorless, revealing the Hg(II) ions induced decrease of active Pt(0) species. The detection limit is 7.2 nM with a linear response range of 0–120 nM. The as-prepared senor can be potentially applicable for the quantitative determination of Hg(II) ions in a real water sample.

The detection of glucose concentration in blood is an especially important part of monitoring the health of an individual. Nanoenzyme is becoming a novel tool for glucose detection due to its low cost, high chemical stability, simplicity, as well as excellent biocompatibility. Based on the intrinsic peroxidase catalytic activity of apoferritin paired Au clusters (Au–Ft),[295] a colorimetric detection system has been developed for glucose detection. The linear range of glucose concentrations is from 2.0 mM to 10 mM, which is fit for the practical application. In addition, other saccharides will not interfere with the detection of glucose, revealing the good selectivity. Thus, the protein–Au NMs can be regarded as a new future candidate for glucose sensor development.

**4.2.4 Gas or humidity sensors.** Bio-inspired MNMs have also been used for gas sensing. An earlier report was demonstrated by Ankamwar *et al.*,[163] who showed the electrical response of Au films comprising plant-mediated Au nanoplates during exposure to different organic solvent vapors. Results indicated that the film resistance was a strong function of the polarity of the vapor molecules (*e.g.* acetone and methanol).[163] Recently, Moon *et al.*[342] showed highly sensitive $H_2$ sensors based on Pd

NWs through straightforward templated assembly by the M13 bacteriophage. Furthermore, Moon *et al.*[343] demonstrated a facile, site-specific virus-templated assembly method for the fabrication of sensitive hydrogen sulfide ($H_2S$) gas sensors at room temperature. The M13 bacteriophage served to organize Au NPs into linear arrays which were used as seeds for subsequent nanowire formation through electroless deposition.[343]

Based on cationic genetically engineered M13 viral particles and anionic spherical Au NPs, Mao *et al.*[344,345] reported the integration of LBL assembly and virus-templated nanoparticle assembly to fabricate virus-based nanocomposite films. It was interesting that the virus-based nanocomposite films were successfully used for humidity sensing, which was little reported previously.[344] Specifically, the longitudinal band of the SPR spectra of the Au nanorods exhibited a large red-shift upon increasing the water content in the organic-solvent–water mixture.[344]

**4.2.5 Surface-enhanced Raman scattering.** SERS can provide ultrasensitive and non-destructive detection of chemical molecules on metal substrates.[346] Some researchers have explored the SERS applications of bio-inspired MNMs in recent years. Table 6 presents some examples of SERS applications of bio-inspired MNMs in recent years. As shown, Ag and Au NMs with various shapes (*e.g.* microspheres, NFs, NWs, nanohorns, ''meatball'', sea urchin, *etc.*) as well as bimetallic AuPd NPs (alloy and core–shell structure) were employed. And a satisfactory SERS enhancement towards a series of probe molecules can be achieved by the bio-inspired MNMs, which is comparable or superior to those MNMs prepared using chemical methods.[347–349]

An excellent example was reported by Yang *et al.*,[350] who synthesized hollow Ag microspheres with a huge and rough surface area assisted using a surfactant-free bacteria-templated method. The large and rough surface as well as nanoporous structures confers the advantage of much higher absorption of 4-mercaptopyridine molecules and abundant ''hot spots'' between ''Ag islands''.[350,351] It was also reported that, through the aforementioned MSD approach, closely packed and polycrystalline Au NWs and nanohorns exhibited excellent Raman enhancement.[98,99,101,103] Interestingly, chemically difficult-to-synthesize Au nanohorns possessed nanopores in their walls, which favored entrapping of probe molecules for effective SERS detection.[101]

As discussed above, combining plant-mediated synthesis and other reagents/methods can give rise to complicated and hierarchical metal nanostructures. Such MNMs should be excellent options for SERS enhancement. For example, 3D Ag NFs by trisodium citrate-assisted biosynthesis could be employed as a SERS-sensitive platform for R6G detection at $10^{-6}$ M. The densely packed petals offered confined space for excited hot spots.[182] Recently, interesting reports were demonstrated by Sun *et al.*,[192,193] who showed that biogenic flower-shaped alloy AuPd and core–shell Au@Pd NPs could serve as SERS-active substrates for the detection of R6G at $10^{-8}$ M. The hierarchical and polycrystalline structures might provide some defects as a ''hot spot'' for Raman enhancement.[354]

As far as the SERS enhancement with protein-templated MNMs was concerned, two earlier reports were demonstrated by a research group in the Chinese Academy of Sciences.[352,353] They showed that 4-aminothiophenol could be tested on films of Au and Ag NPs through type I collagen-mediated synthesis and assembly.[352,353] Later, Wang *et al.* reported interesting Au architectures that were very similar to sea urchin. Results showed that the Au urchin-like architectures possessed much higher SERS activity than the Au microspheres, using 4-mercaptopyridine as the probe molecule.[224]

However, except the other bio-inspired MNMs, SERS application of virus-templated MNMs has been little reported. Much work has been focused on SERS detection of viruses[355] rather than SERS enhancement with virus-templated MNMs.

### 4.3 Antimicrobial

The microbial infections constitute a serious concern to public health, where the appearance and development of resistance to antibiotics are a challenging issue to modern medicine. Although NMs are considered as a ''rising star'' for the development of antimicrobial agents,[356] the poor dispersibility and thermal instability make them difficult for practical applications. Among metal NMs, Ag NPs have been considered as a new generation broad-spectrum antimicrobial agent. They display a low level of cytotoxicity to mammalian cells. The antimicrobial properties of Ag NPs depend on sizes, shape, surface oxidation or charge, and dispersion degree in medium.

Table 6 Some recent examples of SERS applications of bio-inspired MNMs

| Bio-inspired candidates | MNMs | Probe molecules (detection limit) |
|---|---|---|
| *P. pastoris* | Densely packed Au NWs[98] | Rhodamine 6G (R6G) ($10^{-6}$ M) |
| *E. coli* | 3D Au nanohorns[101] | 4-Mercaptobenzoic acid ($10^{-6}$ M) |
| *cocci* | Ag microspheres[350] | 4-Mercaptopyridine ($10^{-15}$ M) |
| *Canarium album Foliar* extract | 3D Ag NFs[182] | R6G ($10^{-6}$ M) |
| *C. Platycladi* extract | Flower-shaped AuPd NPs[192] | R6G ($10^{-8}$ M) |
| *C. Platycladi* extract | Flower-like Au@Pd NPs[193] | R6G ($10^{-8}$ M) |
| *Neurospora crassa* extract | Au NPs[351] | Methylene blue (—[a]) |
| Green tea extract | ''meatball''-like Au NPs[184] | 4-Mercaptopyridine ($10^{-4}$ M) |
| Collagen | Au NPs[352] | 4-Aminothiophenol ($10^{-5}$ M) |
| Collagen | Ag NPs[353] | 4-Aminothiophenol ($10^{-7}$ M) |
| BSA | Sea urchin-like Au architectures[224] | 4-Mercaptopyridine ($10^{-6}$ M) |
| DNA | Au NWs[253] | R6G ($10^{-6}$ M) |
| DNA | Ag NCs[245] | Methylene blue ($10^{-12}$ M) |

[a] The minimum concentration was not mentioned in the literature.

 

However, the chemical synthesis of Ag NMs often suffers from the agglomeration and oxidation, hindering its further use in medical fields.

Microorganism-mediated synthesized Ag NPs have been explored as antimicrobial materials. Microorganisms can also be used as supports for Ag NPs. For example, Thomas *et al.*[357] demonstrated the synergistic effect of biosynthesized Ag NPs with antibiotics against multidrug-resistant biofilm-forming coagulase-negative *Staphylococci* isolated from clinical samples. The highest synergistic effect of the Ag NPs was observed with chloramphenicol against *Salmonella typhi* was validated.[357] Alternatively, microorganism-mediated synthesized Ag NPs can be further loaded onto inorganic supports. For example, Chen *et al.*[358] demonstrated Ag NPs (18.0 ± 5.6 nm) were rapidly synthesized by non-enzymatic reduction and loaded onto $\alpha$-$Al_2O_3$ through heat treatment at 200 °C. The 1%wtAg/$\alpha$-$Al_2O_3$ composites killed 100% of *E. coli* and *Staphylococcus aureus* (*S. aureus*) after contact times of 30 s and 5 min, respectively.[358]

As a facile approach to Ag NPs, plant-mediated synthesis has been adopted to produce antibacterial Ag NPs.[44,359–361] However, Ag ions are also toxic to tested strains. Therefore, incomplete reduction of Ag ions should be taken into account and the antibacterial effect of Ag ions should be ruled out.[44] Complete reduction of Ag ions with *C. Platycladi* extract at 90 °C led to the formation of Ag NPs of 18.4 ± 4.6 nm, which exhibited excellent antibacterial activity against *E. coli* and *S. aureus* at the Ag concentration of 50 ppm.[44] Vijayakumar *et al.*[362] investigated the antibacterial effect of plant-mediated Ag NPs (70–90 nm) using *Artemisia nilagirica*. The Ag NPs exhibited exhibited excellent potent inhibitory activity against *S. aureus*, *Bacillus subtilis*, *E. coli*, and *Proteus subtilis.*[362] Very recently, Muthukrishnan *et al.*[363] studied the antibacterial effect of *ca.* 100 nm Ag NPs synthesized by reduction with *Ceropegia thwaitesii*. The antimicrobial activity of Ag NPs shows highly potent inhibitory activity against *S. typhi* and *B. subtilis.*[363]

Proteins are often employed as templates and stabilizers to prepare MNMs, providing excellent stability and desirable properties for various applications. Of all the proteins, lysozyme has attracted vast attention due to its antibacterial activity. Lysozyme is a nearly spherical protein (belonging to glycoside hydrolase) and has the antibacterial property primarily against bacteria *via* enzymatic hydrolysis of the peptidoglycian layer surrounding the cell membrane. Utilizing lysozyme as the template and stabilizer, some novel antimicrobial metal NMs and devices with enhanced activities have been synthesized. For example, Eby *et al.*[364] utilized hen egg white lysozyme acting as the reducing and stabilizing agent to catalyze the formation of Ag NPs in the presence of light. The use of lysozyme during the synthesis of Ag NPs is advantageous because it combines two different biocidal mechanisms into one composite: lysozyme mainly inhibits the growth of the Gram-type positive strains through its muramidase activity, while Ag NPs inhibited the growth of both Gram-type positive and negative strains by inhibiting membrane function and enzyme activity. The antimicrobial results showed that the lysozyme–Ag nanocomposites exhibited efficient antimicrobial activity against three representative bacterial strains (*E. coli*, *Staphylococcus aureus*, *Bacillus anthracis*) and one fungal strain (*Candida albicans*). What is more, a strong antimicrobial effect against Ag-resistant *Proteus mirabilis* strains and a recombinant *E. coli* strain was observed. In addition, the toxicological studies showed that the lysozyme–Ag was nontoxic to human epidermal keratinocytes at concentrations sufficient to inhibit microbial growth. This is significant to develop a potent and safe biological reagent replacing the conventional antibiotics for aseptic and therapeutic use in the future.

Spherical Ag NPs (3.5 nm in diameter) stabilized in collagen protein were prepared using a photochemical method.[229] The biocompatibility and cytotoxicity were evaluated *in vitro* on two primary cell lines: dermal fibroblast and epidermal keratinocytes. The results showed that both cell lines were not affected by Ag-NP@collagen NPs, revealing an excellent biocompatibility. Three bacterial species including *B.megaterium*, *S.epidermidis* and *E.coli* were selected to assess the antibacterial activity of Ag-NP@collagen NPs. The proposed system was found to have bactericidal properties against *B.megaterium* and *E. colin* but only bacteriostatic properties against *S.epidermidis*. Compared with Ag ions, the Ag@collagen NPs are about four times more active in equimolar concentrations of Ag content. The excellent antibacterial performance can be partially attributed to the stability of the Ag@collagen particle itself.

Gelatin-templated Cu NPs were also reported for the antimicrobial studies. For example, Chatterjee *et al.* synthesized metallic Cu NPs using gelatin as the template.[365] The as-prepared Cu NPs are about 50–60 nm in size and have a high stability. They can be stored for at least one month in an air-tight container without considerable oxidation. A series of experiments were carried out to demonstrate its antibacterial activity. The gelatin-templated Cu NPs showed a highly effective antibacterial ability against *E. coli* with a minimum inhibitory concentration of 3.0 μg $mL^{-1}$ and a minimum bactericidal concentration of 7.5 μg $mL^{-1}$. Besides *E. coli*, the antibacterial effect of gelatin-templated Cu NPs was also observed in Gram-positive *Bacillus subtilis* and *Staphylococcus aureus*, revealing a potential antibacterial agent instead of antibiotics.

Silk fibroin was used as a biotemplate to produce Ag NPs *in situ* under both incandescent light and sunlight at room temperature for antibacterial applications.[366] The whole reaction process is rather environment-friendly and energy-saving, because it does not need any chemicals and only uses light as the power source. Tyr residues in silk fibroin backbone are thought to act in reducing roles. The as-prepared fibroin–Ag nanocomposites showed an effective antibacterial activity against the methicillin-resistant *Staphylcoccus aureus* (*S. aureus*) and inhibited its biofilm formation. The minimum inhibitory concentration (MIC) and minimum bactericidal concentration (MBC) are 19.2 mg $L^{-1}$ and 76.8 mg $L^{-1}$, respectively. What is more, the silk fibroin–Ag nanocomposites could further destroy the maturely biofilm created by methicillin-resistant *S. aureus*, which can be developed as an efficient antibacterial and biofilm-disrupting agent to satisfy the clinical requirements.

There are few reports on antibacterial application of virus-templated or DNA-templated Ag MNMs. Recently, the only report was demonstrated by Yang *et al.*,[121] who demonstrated

a high antibacterial activity of TMV-biomediated Ag NPs against *E. coli* cells, where 2 nm Ag NPs showed better performance than 9 nm ones.

### 4.4 Imaging

Protein-templated noble metal NCs typically possessing sizes below 2 nm are highly attractive fluorescence contrast agents probes for cancer imaging applications due to their low toxicity, bright fluorescence properties, strong stability, as well as the ultrasmall sizes. Many proteins have been employed for preparing metal–protein NCs that maintain the biological function of protein itself, and then they can be used to target specific cells *in vitro via* conjugation of cancer cell recognized molecules (*e.g.*, folic acid and herceptin). For instance, Retnakumari *et al.* have successfully used the BSA-templated $Au_{25}$ NCs for the oral carcinoma cells and breast adenocarcinoma cell MCF-7 imaging through folic acid receptor targeting.[367] The folic acid conjugated nanocomposites demonstrated no toxicity to the cells and were internalized in a time-dependent manner. It was also found that the internalized Au clusters maintained their bright fluorescence properties in cytosol. The study showed for the first time that the BSA–Au NCs could be used for molecular-receptor-specific detection of cancer, at the single cell level, by fluorescence imaging.

Choosing available carriers to develop nuclear delivery and targeting therapeutics strategy is a challenging task in current nanomedicine. BSA-templated Au NCs (2 nm size) are excellent bioimaging agents for nuclear nanomedicine. For instance, Herceptin was conjugated onto BSA-templated Au NCs to form a fluorescence contrast through the EDC linkage (Fig. 25, left) for simultaneous fluorescence imaging and cancer therapy.[368] Single point fluorescence correlation spectroscopy (FCS) measurements confirmed the presence of Au-NCs–Her in the nucleus of live SK-BR3 cells (Fig. 25, right). BSA-templated Au NCs conjugated with Herceptin possessed high targeting specificity and nuclear localization ability, with the potential to become an excellent drug carrier to achieve nuclear targeting imaging and therapy of tumor cells.

Very recently, Chen *et al.* adopted a one-pot synthetic method to prepare BSA–Ce/Au-NCs with dual-emission fluorescence.[369] Interestingly, two fluorescence emission bands at 410 and 650 nm are present under the same excitation wavelength (325 nm), which are pH dependent and independent, respectively. The fluorescence emission band at 410 nm (pH dependent) is due to BSA–Ce complexes, while that at 650 nm (pH independent) could be assigned to Au NCs. The stable and biocompatible BSA–Ce/Au-NCs could be used as ratiometric probes for monitoring local pH values inside cancer cells. The blue fluorescence at 410 nm became weaker upon decreasing pH values from basic to acidic conditions during incubation with HeLa cells, while the red fluorescence at 650 nm stayed almost unchanged. The dual-emission features of BSA–Ce/Au-NCs enabled the detection of highly reactive oxygen species (ROS) through live cell fluorescence imaging.

Besides the fluorescence imaging *in vitro*, protein-templated NMs are extremely useful when applied to therapeutics and medical imaging *in vivo* due to their possibilities for being well-dispersed in bodies without aggregation. For example, BAS-templated Au NCs were selected for *in vivo* tumor imaging research.[370] Studies indicated a high tumor uptake of Au–BSA NCs with excellent contrast from surrounding tissues (Fig. 26). BSA-templated Au NCs could also be regarded as a very promising contrast imaging agent for *in vivo* fluorescence tumor imaging.

Protein-templated metal NCs were also used as multimodal imaging contrast agents to enhance accuracy in diagnosis. For example, Cai *et al.* utilized BSA and metal ions to prepare hybrid BSA–Au–gadolinium NCs for triple-modal imaging (near-infrared fluorescence (NIRF), X-ray computed tomography (CT), and magnetic resonance imaging (MRI)) probes for *in vivo* tumor-bearing mice.[371] The resulting NCs exhibited ultrasmall particle size, high stability and good biocompatibility. Upon being intravenously injected, the fluorescence, CT, and T1-weighted MRI signal derived from the NCs were all very distinguishable in the tumor region from other tissues, indicating an outstanding targeting ability through the enhanced permeation and retention effect and reduced clearance from

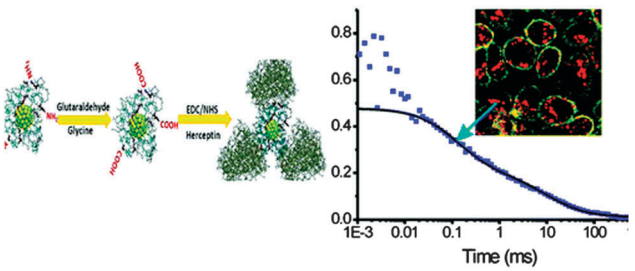


Fig. 25 Left: schematic illustration of BSA-templated Au NCs conjugated with Herceptin (Au-NCs–Her); right: typical autocorrelation curve (solid squares) of Au-NCs–Her diffusing inside the nucleus fitted with two components (black solid line). Inset is the image of SK-BR3 cells incubated with Au-NCs–Her-Alexa647 for 4 h. Reprinted with permission from ref. 368. Copyright © 2011, American Chemical Society.

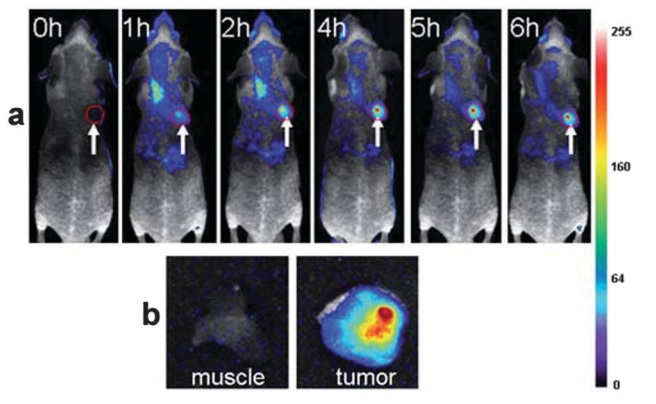


Fig. 26 (a) Fluorescence images of mice bearing an MDA-MB-45 tumor. Strong signal from BSA–Au NCs was observed in the tumor (marked by the red circle). The arrowheads indicated the tumor. (b) *Ex vivo* fluorescence image of the tumor tissue and the muscle tissue around the tumor from the mice used in a. Reprinted with permission from ref. 370. Copyright © 2010, Royal Society of Chemistry.

the tumor. Such prepared ultrasmall NCs are a versatile imaging nanoprobe for tumor diagnosis.

### 4.5 Therapy

Chemotherapy, radiotherapy and surgery are the main therapeutic modes in clinic. Although these measures can prolong patient lifetime, the effectiveness is still limited in handling cancer metastasis. Since protein-templated MNMs show some unique optical and magnetic properties as well as good biocompatibility, they are regarded as promising candidates for cancer therapy applications.

Photothermal therapy (PTT) is a novel cancer therapeutic strategy that normally uses near-infrared (NIR) light absorbing agents to kill cancer cells. PTT exhibited the merits of minimal invasiveness, high specificity and high efficiency as compared to current cancer treatments. Human serum albumin (HAS) covalently linked with diethylenetriamine pentaacetic acid (DTPA) molecules were utilised to chelate Gd(III) ions and then complexed with IR825 (a near-infrared dye) to form HAS–Gd–IR825 nanocomposites.[369] As-prepared products exhibited a strong fluorescence together with high near-infrared (NIR) absorbance and high photothermal conversion efficiency at 808 nm laser irradiation. Meanwhile, it could act as both a fluorescence and magnetic resonance (MT) imaging agent to carry out dual-modal imaging guided PPT. Prior to PTT, the standard methyl thiazolyltetrazolium (MTT) assay based on 4T1 cancer cells was tested, indicating no obvious dark cytotoxicity of HSA–Gd–IR825 even at high protein concentrations (up to 30 mM). The temperatures of their sentinel lymph node (SLNs) reaches up 55 °C for mice with HAS–Gd–IR825 injection *in vivo* for 10 min (0.8 W $cm^{-2}$), which is high enough to carry out efficient photothermal ablation of cancer cells inside.

The increased photon absorption of high atomic number ($Z$) materials at kilovoltage ($kV_p$) could augment the efficacy of current radiotherapy. Due to the high atomic number and excellent biocompatibility, protein-templated Ag ($Z$ = 47) and Au ($Z$ = 79) MNMs may become promising radiosensitising agents for cancer treatment. For example, Huang *et al.* synthesized BSA-conjugated Ag microspheres (*ca.* 200 nm in diameter) *via* one-pot reaction in the aqueous phase at room temperature.[223] As-prepared products exhibited good stability and biocompatibility. To gastric cancer cells (MGC803 cells), MTT assays exhibited no cytoxicity in the concentration range of 0–50 μg $mL^{-1}$ BSA–Ag microspheres. Radio sensitization assay showed that BSA-conjugated Ag microspheres could enhance the radiosensitivity of gastric cancer cells, presenting a dose-dependent cytotoxicity. The protein-templated MNMs might be employed as a novel type of sensitizers when combined with anticancer drugs to play a synergistic killing effect of cancer cells, further improving the healing outcomes of radio-based cancer therapy.

Nanoparticulate delivery systems are also being actively investigated as a novel drug delivery strategy in pharmaceutic research. Protein-templated MNMs can serve as potent and versatile carriers for drug targeting therapy and improving pharmacokinetic profiles. Yao *et al. in situ* prepared Au NPs-loaded lysozyme–dextran nanogels having a size of *ca.* 200 nm and a structure comprising of a lysozyme core and dextran shell.[372] Au NPs (*ca.* 8 nm) were embedded in the nanogels and stable under physiological conditions. The hybrid materials exhibited almost no inhibition effect on cell proliferation (two cancer cell lines and one normal cell line) after 72 h of incubation, with Au NP concentrations ranging from 1 to 50 μg $mL^{-1}$ which revealed a good biocompatibility. Doxorubicin was loaded into the nanogels, accumulated in the tumor *via* EPR effect to reduce the toxic effects and was released inside the cells to enhance the antitumor activity. Such prepared hybrid nanogels may be a promising system for simultaneous drug delivery and imaging applications.

BSA has long been used for improving the stability, non-immunogenicity, biocompability, biodegradability and pharmacokinetic profile of many therapeutic drugs. BSA-templated MNMs have been used as a multifunctional drug carrier for cancer therapy. For example, Prasad *et al. in situ* synthesized BSA-capped Au NPs to carry anticancer drug methotrexate (MTX) for breast cancer cell (MCF-7) therapy. BSA capped Au NPs (Au–BSA) possessed superior stability against varying pH and salt concentrations, providing a robust and monodisperse vehicle to load large quantities of MTX. In addition, BSA also afforded abundant functional groups to bind drug molecules, as well as high delivery abilities into cancerous cells. MTT assays and Ki-67 proliferation studies indicated that bare Au–BSA had no effect on cell viability at increasing concentration even after 72 h of incubation. However, Au–BSA–MTX composites showed a higher cytotoxicity on MCF-7 cells at the same dose as compared to free MTX, revealing their excellent anticancer effect.[373]

### 4.6 Others

Bio-inspired MNMs have interesting properties and may find myriad potential applications. Due to limited page space, some recent examples are given in this subsection to elucidate other applications of bio-inspired MNMs. For instance, bio-inspired 1D assemblies of MNMs may act as excellent conductive materials. Bio-inspired MNMs can therefore find application as conductive materials in electronic devices, *e.g.* the conductive hybrid nanobiomaterials derived from viral assemblies[374] and DNA-templated NWs from metals.[375] Another interesting application is related to microwave absorption, demonstrated by size-controllable Ag NPs synthesized using bayberry application of tannin (BT) grafted collagen fiber (CF).[376] The weight of Ag-NPs–BT@CF composites was only 1/10–1/5 as compared to those inorganic wave-absorbing materials with similar thickness.[376] All in all, there are many other applications that have emerged or are going to emerge with the rapid development of bio-inspired synthesis in the near future. We envisage that an increasing number of efforts will be devoted to applications of bio-inspired MNMs.

## 5. Conclusions and prospects

This contribution was aimed to provide a comprehensive overview on the possibilities, potential and exciting applications of

bio-inspired MNMs synthesized using various methods. Recent advances in the bio-inspired synthesis of metal NMs pointed out that a good number of bio-candidates (microorganisms, viruses, plants, proteins and DNA) could provide a unique versatility with a wide range of bio-templating systems and innovative protocols aimed to a careful control of critical parameters in NP growth such as morphology, size and assembly of bio-MNMs and derived super-structures. Important advantages of these protocols include the use of mild synthetic conditions, environmentally friendly and biocompatible substrates, avoidance of any auxiliary capping agents and/or in certain cases minor quantities of reducing agents, offering an attractive and increasingly sustainable alternative to NP syntheses using pure physical/chemical synthesis. In some cases, innovative MNMs with interesting shapes and assembled structures can be simply synthesized under bio-inspired conditions, which are challenging/not possible to obtain *via* conventional physical and chemical methods. The applications of various MNMs were also discussed in detail in this contribution, illustrated in a number of key examples in different areas including catalysis, sensing, imaging, antimicrobial, therapy and many others. As alternatives to conventional inorganic supports, bio-inspired candidates are also able to support highly dispersed metal NPs through bio-inspired synthesis, resulting in useful bio-metal nanocomposites. On the one hand, bio-metal nanocomposites possess easy separation and recovery, which may be reusable in some applications especially in catalysis. Particularly, a strong interaction exists between bio-support and metal NPs which can provide access to highly active and durable metal catalysts. In some other cases, the biocompatibility of bio-templated MNMs can offer interesting applications in biomedicine and related fields in which the utilization of designer nanoentities prepared under physico-chemical methods is restricted. Furthermore, innovative protocols for the design of MNMs can lead to an increasing number of possibilities due to the excellent properties of NPs (*e.g.* plasmon resonance) and bio-derived origin (*i.e.* cancer treatment, tissue engineering, *etc.*).

On the basis of the above premises, bio-inspired synthetic protocols have a significant potential to be extended to the preparation of related NMs (even oxides) from a fundamental understanding of the synthetic methodologies and properties of as-obtained MNMs. A number of opportunities and challenges are present in both fundamental and applied frontiers of MNMs bio-inspired syntheses waiting for further development in the field. Various possibilities lie ahead for the different types of bio-templating systems. As far as microorganisms are concerned, the most important challenge relates to the complex and yet not well understood enzymatic reduction to NPs as compared to the more simple and generally agreed mechanism of non-enzymatic reduction. Pure microbial syntheses (without auxiliary reductants and electron donors) to design bimetallic or trimetallic NMs as well as hybrid NMs comprising metal and metal oxides/sulfides also remain a significant challenge in the area that requires further investigation. Of interest is also the versatile and flexible nature of cell-free extracts in MNM synthesis, with a remarkable potential in appropriate combination with conventional or new techniques to provide access to interesting and novel MNMs and applications.

Virus-templated synthesis can also offer relevant possibilities for designing advanced MNMs. The use of several types of WT viruses and modifications in capsids were sound approaches to improve metallization efficiencies. In this way, particle sizes, patterns, metal loadings as well as the development of metal–virus superstructures could be effectively controlled. Simpler approaches to genetic and chemical modification of WT viruses as well as hierarchical assembly of viruses (followed by *in situ* metallization) are envisaged as key areas for further research endeavours in order to provide an effective metallization as well as advanced and innovative nano-biocomposites for various applications. Live plants have been the subject of scientific studies to be employed in the preparation of matrix-embedded MNMs with potential applications. The identification of complex biomolecules, *i.e.* reductive and protecting agents, and their roles in shaping MNMs with different morphologies are essential to better understand the formation mechanism of MNMs. Furthermore, a better understanding of the roles of biological residues in processes (*i.e.* catalytic reaction) and interaction between metal NPs and support can facilitate the design of increasingly efficient bio-MNM materials in the future. Catalytic applications of well-dispersed MNMs prepared *via* reduction with plant extracts were extensively discussed in this contribution. For some catalytic reactions (*e.g.* epoxidation of propene, solvent-free oxidation of benzyl alcohol), the catalysts show excellent catalytic performance superior to those prepared by conventional chemical reduction. Plant-matrix-embedded MNMs have a remarkable potential in environmental treatment and fine chemical synthesis and consequently more research efforts should continue in this area. However, there is plenty of room for further investigation and advances in the field related to the effect of catalyst post-treatment, phases and impurities, *etc.*, considering the trade-off between catalytic activity and stability. Furthermore, the illustrated continuous-flow biosynthesis of MNMs clearly exemplifies the versatility in uses of plant extracts and possibilities for being combined with other techniques for innovation in the preparation of MNMs.

Protein-templated MNMs (*e.g.* BSA as the model protein) were also discussed as an interesting alternative for the facile ''bottom-up'' synthesis of MNMs with tunable sizes and shapes. More proteins are expected to be able to continue and further expand the functions of BSA in the future, offering binding, catalytic or therapeutic properties due to their different functions. Alternatively, proteins can also be only passively utilized as inert coating or scaffolding material to design innovative MNMs and/or assemblies. Despite the significant potential in this area, a major concern of protein-templated MNMs relates to potential losses of activities due to chelation, reduction, unfolding, denaturation or blocking of an active site with the protein being initially attached to MNMs. Properties of MNMs (*i.e.* optical, magnetic, catalytic and electrochemical) may also be affected by the presence of such proteins. The design and preparation of multifunctional MNMs based on proteins as templates consequently require a careful control and consideration of reaction conditions including temperature, pH, stoichiometry and time for a rational system design. In any

 

case, working with proteins requires a significant body of work (currently insufficient) to systematically investigate and elucidate the interactions between metal ions and proteins, conformational and functional changes of proteins, *etc.* Furthermore, the relationship between protein structure and MNM structure need to be thoroughly clarified. In addition, *in vivo* toxicity assays are still deficient although the majority of protein-templated MNMs exhibit excellent biocompatibility *in vitro* various cellular models. Long-term exposure effects on experimental animals and environment microorganisms, an accurate tissue localization and bio-distribution, as well as a detailed pharmacokinetics need to be further investigated as nanotoxicology is closely related to sizes, shapes, surface charges, and coatings of protein-templated MNMs. Future work may also be directed towards the rational design and precise control of compositions and structures of MNMs *via* protein engineering and computer simulation.

Last but not least, the inherent physico-chemical properties of DNA make it an excellent biotemplate for NP self-assembly. DNA-conjugated metal NPs with different sizes and well-organized architectures were reported to exhibit promising application in SERS, catalysis and sensors. Further research can predictably be directed towards the design of MNMs with more diversified and specific structures based on the rapid developments in DNA technology. Currently, one of the main problems for the synthesis of DNA-templated MNMs is the low yield of synthesized nanostructures, also requiring complex protocols and work-up which involve high costs. These issues deeply influenced DNA-templated NMs production and subsequent applications. Yield improvements and simplification of synthetic protocols will be key research aspects for further advances in the future.

In spite of the challenges and current shortcomings of some bio-inpired protocols for the design and development of MNMs, this contribution clearly illustrates the potential and identified a number of research avenues for conducting further research to advance the field in the coming years which will certainly contribute to position some of the discussed bio-synthetic protocols as suitable practical alternatives to current physico-chemical methods for MNM preparation for a more sustainable future. Research efforts must be redoubled to better understand the essential interactions, mechanisms and procedures in the bio-design of MNMs which we hope can lead us to the next generation of bio-compatible NMs for advanced applications.

## Acknowledgements

This work was supported by the National Natural Science Foundation of China (NSFC Project No. 21036004, 21106117, 31400851, 21206140 and 81472001). J. H. is grateful to the Fujuan Provincial Department of Education for the Breeding Plan for Outstanding Young Investigators of Universities in Fujian Province. L. L. and D. Y. were supported by a startup fund from Quanzhou Normal University.

## References

1 C. Joachim, *Nat. Mater.*, 2005, **4**, 107–109.
2 Y. Xia, Y. J. Xiong, B. Lim and S. E. Skrabalak, *Angew. Chem., Int. Ed.*, 2009, **48**, 60–103.
3 Z. Y. Zhou, N. Tian, J. T. Li, I. Broadwell and S. G. Sun, *Chem. Soc. Rev.*, 2011, **40**, 4167–4185.
4 Y. N. Xia, P. D. Yang, Y. G. Sun, Y. Y. Wu, B. Mayers, B. Gates, Y. D. Yin, F. Kim and Y. Q. Yan, *Adv. Mater.*, 2003, **15**, 353–389.
5 G. Chen, Y. Zhao, G. Fu, P. N. Duchesne, L. Gu, Y. Zheng, X. Weng, M. Chen, P. Zhang and C.-W. Pao, *Science*, 2014, **344**, 495–499.
6 B. H. Wu and N. F. Zheng, *Nano Today*, 2013, **8**, 168–197.
7 R. J. White, R. Luque, V. L. Budarin, J. H. Clark and D. J. Macquarrie, *Chem. Soc. Rev.*, 2009, **38**, 481–494.
8 J. R. Heath, *Acc. Chem. Res.*, 1999, **32**, 388.
9 Y. Xia, X. Xia, Y. Wang and S. Xie, *MRS Bull.*, 2013, **38**, 335–344.
10 T. Klaus, R. Joerger, E. Olsson and C. G. Granqvist, *Proc. Natl. Acad. Sci. U. S. A.*, 1999, **96**, 13611–13614.
11 J. Gardea-Torresdey, K. Tiemann, G. Gamez, K. Dokken, S. Tehuacanero and M. Jose-Yacaman, *J. Nanopart. Res.*, 1999, **1**, 397–404.
12 E. Dujardin, C. Peet, G. Stubbs, J. N. Culver and S. Mann, *Nano Lett.*, 2003, **3**, 413–417.
13 J. Xie, Y. Zheng and J. Y. Ying, *J. Am. Chem. Soc.*, 2009, **131**, 888–889.
14 M. Mertig, L. Colombi Ciacchi, R. Seidel, W. Pompe and A. De Vita, *Nano Lett.*, 2002, **2**, 841–844.
15 E. Dujardin and S. Mann, *Adv. Mater*, 2002, **14**, 1–14.
16 A.-W. Xu, Y. Ma and H. Cölfen, *J. Mater. Chem.*, 2007, **17**, 415–449.
17 F. C. Meldrum and H. Cölfen, *Chem. Rev.*, 2008, **108**, 4332–4432.
18 S. Mann, *Biomineralization*, Oxford University Press, Oxford, 2001.
19 F. J. Eber, S. Eiben, H. Jeske and C. Wege, *Angew. Chem., Int. Ed.*, 2013, **52**, 7203–7207.
20 B. Cao, Y. Zhu, L. Wang and C. Mao, *Angew. Chem., Int. Ed.*, 2013, **52**, 11750–11754.
21 F. Wang, S. L. Nimmo, B. Cao and C. Mao, *Chem. Sci.*, 2012, **3**, 2639–2645.
22 C. Mao, F. Wang and B. Cao, *Angew. Chem., Int. Ed.*, 2012, **51**, 6411–6415.
23 B. Cao, H. Xu and C. Mao, *Angew. Chem., Int. Ed.*, 2011, **50**, 6264–6268.
24 F. Wang, B. Cao and C. Mao, *Chem. Mater.*, 2010, **22**, 3630–3636.
25 F. Wang, D. Li and C. Mao, *Adv. Funct. Mater.*, 2008, **18**, 4007–4013.
26 W. J. Crookes-Goodson, J. M. Slocik and R. R. Naik, *Chem. Soc. Rev.*, 2008, **37**, 2403–2412.
27 T. X. Fan, S. K. Chow and Z. Di, *Prog. Mater. Sci.*, 2009, **54**, 542–659.
28 R. K. Das and S. K. Brar, *Nanoscale*, 2013, **5**, 10155–10162.

29 A. K. Mittal, Y. Chisti and U. C. Banerjee, *Biotechnol. Adv.*, 2013, **31**, 346–356.
30 M. N. Alam, N. Roy, D. Mandal and N. A. Begum, *RSC Adv.*, 2013, **3**, 11935–11956.
31 M. S. Akhtar, J. Panwar and Y.-S. Yun, *ACS Sustainable Chem. Eng.*, 2013, **1**, 591–602.
32 J. Mittal, A. Batra, A. Singh and M. M. Sharma, *Adv. Nat. Sci.: Nanosci. Nanotechnol.*, 2014, **5**, 043002.
33 K. P. Talaro, A. Talaro, G. Delisle and L. Tomalty, *Foundations in microbiology*, McGraw-Hill Higher Education, Burr Ridge, 1996.
34 B. Nair and T. Pradeep, *Cryst. Growth Des.*, 2002, **2**, 293–298.
35 R. Y. Parikh, S. Singh, B. L. V. Prasad, M. S. Patole, M. Sastry and Y. S. Shouche, *ChemBioChem*, 2008, **9**, 1415–1422.
36 D. Mandal, M. E. Bolander, D. Mukhopadhyay, G. Sarkar and P. Mukherjee, *Appl. Microbiol. Biotechnol.*, 2006, **69**, 485–492.
37 L. Q. Lin, W. W. Wu, J. L. Huang, D. H. Sun, N. M. Waithera, Y. Zhou, H. T. Wang and Q. B. Li, *Chem. Eng. J.*, 2013, **225**, 857–864.
38 C. Yang, C.-H. Choi, C.-S. Lee and H. Yi, *ACS Nano*, 2013, **7**, 5032–5044.
39 A. K. Manocchi, N. E. Horelik, B. Lee and H. Yi, *Langmuir*, 2010, **26**, 3670–3677.
40 W. Ernst, *Appl. Geochem.*, 1996, **11**, 163–167.
41 J. Gardea-Torresdey, J. Parsons, E. Gomez, J. Peralta-Videa, H. Troiani, P. Santiago and M. J. Yacaman, *Nano Lett.*, 2002, **2**, 397–401.
42 H. L. Parker, E. L. Rylott, A. J. Hunt, J. R. Dodson, A. F. Taylor, N. C. Bruce and J. H. Clark, *PLoS One*, 2014, **9**, e87192.
43 S. S. Shankar, A. Rai, B. Ankamwar, A. Singh, A. Ahmad and M. Sastry, *Nat. Mater.*, 2004, **3**, 482–488.
44 J. L. Huang, G. W. Zhan, B. Y. Zheng, D. H. Sun, F. F. Lu, Y. Lin, H. M. Chen, Z. D. Zheng, Y. M. Zheng and Q. B. Li, *Ind. Eng. Chem. Res.*, 2011, **50**, 9095–9106.
45 B. Zheng, T. Kong, X. Jing, T. Odoom-Wubah, X. Li, D. Sun, F. Lu, Y. Zheng, J. Huang and Q. Li, *J. Colloid Interface Sci.*, 2013, **396**, 138–145.
46 J. M. Galloway and S. S. Staniland, *J. Mater. Chem.*, 2012, **22**, 12423–12434.
47 R. M. Choueiri, A. Klinkova, H. Thérien-Aubin, M. Rubinstein and E. Kumacheva, *J. Am. Chem. Soc.*, 2013, **135**, 10262–10265.
48 L. Au, B. Lim, P. Colletti, Y.-S. Jun and Y. Xia, *Chem. – Asian J.*, 2010, **5**, 123–129.
49 A. V. Singh, B. M. Bandgar, M. Kasture, B. Prasad and M. Sastry, *J. Mater. Chem.*, 2005, **15**, 5115–5121.
50 H. R. Zhang, Q. B. Li, Y. H. Lu, D. H. Sun, X. P. Lin, X. Deng, N. He and S. Z. Zheng, *J. Chem. Technol. Biotechnol.*, 2005, **80**, 285–290.
51 J. R. Lloyd, *FEMS Microbiol. Rev.*, 2003, **27**, 411–425.
52 P. Mukherjee, A. Ahmad, D. Mandal, S. Senapati, S. R. Sainkar, M. I. Khan, R. Parishcha, P. V. Ajaykumar, M. Alam, R. Kumar and M. Sastry, *Nano Lett.*, 2001, **1**, 515–519.
53 R. Ramanathan, A. P. O'Mullane, R. Y. Parikh, P. M. Smooker, S. K. Bhargava and V. Bansal, *Langmuir*, 2011, **27**, 714–719.
54 I. W.-S. Lin, C.-N. Lok and C.-M. Che, *Chem. Sci.*, 2014, **5**, 3144–3150.
55 S. K. Das, J. Liang, M. Schmidt, F. Laffir and E. Marsili, *ACS Nano*, 2012, **6**, 6165–6173.
56 L. M. Rösken, S. Körsten, C. B. Fischer, A. Schönleber, S. van Smaalen, S. Geimer and S. Wehner, *J. Nanopart. Res.*, 2014, **16**, 2370.
57 Y. Konishi, T. Tsukiyama, T. Tachimi, N. Saitoh, T. Nomura and S. Nagamine, *Electrochim. Acta*, 2007, **53**, 186–192.
58 Y. Konishi, T. Tsukiyama, K. Ohno, N. Saitoh, T. Nomura and S. Nagamine, *Hydrometallurgy*, 2006, **81**, 24–29.
59 P. Yong, N. A. Rowson, J. P. G. Farr, I. R. Harris and L. E. Macaskie, *Biotechnol. Bioeng.*, 2002, **80**, 369–379.
60 P. Yong, M. Paterson-Beedle, I. P. Mikheenko and L. E. Macaskie, *Biotechnol. Lett.*, 2007, **29**, 539–544.
61 Y. Konishi, K. Ohno, N. Saitoh, T. Nomura, S. Nagamine, H. Hishida, Y. Takahashi and T. Uruga, *J. Biotechnol.*, 2007, **128**, 648–653.
62 G. Attard, M. Casadesús, L. E. Macaskie and K. Deplanche, *Langmuir*, 2012, **28**, 5267–5274.
63 M. D. Yates, R. D. Cusick and B. E. Logan, *ACS Sustainable Chem. Eng.*, 2013, **1**, 1165–1171.
64 R. Ramanathan, M. R. Field, A. P. O'Mullane, P. M. Smooker, S. K. Bhargava and V. Bansal, *Nanoscale*, 2013, **5**, 2300–2306.
65 P. Mukherjee, A. Ahmad, D. Mandal, S. Senapati, S. R. Sainkar, M. I. Khan, R. Ramani, R. Parischa, P. V. Ajayakumar, M. Alam, M. Sastry and R. Kumar, *Angew. Chem., Int. Ed.*, 2001, **40**, 3585–3588.
66 A. Ahmad, S. Senapati, M. I. Khan, R. Kumar and M. Sastry, *Langmuir*, 2003, **19**, 3550–3553.
67 A. N. Mabbett, P. Yong, J. P. G. Farr and L. E. Macaskie, *Biotechnol. Bioeng.*, 2004, **87**, 104–109.
68 M. Oves, M. S. Khan, A. Zaidi, A. S. Ahmed, F. Ahmed, E. Ahmad, A. Sherwani, M. Owais and A. Azam, *PLoS One*, 2013, **8**, e59140.
69 C. K. Ng, K. Sivakumar, X. Liu, M. Madhaiyan, L. Ji, L. Yang, C. Tang, H. Song, S. Kjelleberg and B. Cao, *Biotechnol. Bioeng.*, 2013, **110**, 1831–1837.
70 P. Mukherjee, S. Senapati, D. Mandal, A. Ahmad, M. I. Khan, R. Kumar and M. Sastry, *ChemBioChem*, 2002, **3**, 461–463.
71 E. P. Vetchinkina, E. A. Loshchinina, A. M. Burov, L. A. Dykman and V. E. Nikitina, *J. Biotechnol.*, 2014, **182**, 37–45.
72 S. Talekar, G. Joshi, R. Chougle, B. Nainegali, S. Desai, A. Joshi, S. Kambale, P. Kamat, R. Haripurkar and S. Jadhav, *Catal. Commun.*, 2014, **53**, 62–66.
73 S. A. Khan and A. Ahmad, *RSC Adv.*, 2014, **4**, 7729–7734.
74 M. Gholami-Shabani, A. Akbarzadeh, D. Norouzian, A. Amini, Z. Gholami-Shabani, A. Imani, M. Chiani, G. Riazi,

M. Shams-Ghahfarokhi and M. Razzaghi-Abyaneh, *Appl. Biochem. Biotechnol.*, 2014, **172**, 4084–4098.
75 A. Ahmad, P. Mukherjee, S. Senapati, D. Mandal, M. I. Khan, R. Kumar and M. Sastry, *Colloids Surf., B*, 2003, **28**, 313–318.
76 S. Senapati, A. Ahmad, M. I. Khan, M. Sastry and R. Kumar, *Small*, 2005, **1**, 517–520.
77 J. L. Huang, W. T. Wang, L. Q. Lin, Q. B. Li, W. S. Lin, M. Li and S. Mann, *Chem. – Asian J.*, 2009, **4**, 1050–1054.
78 M. Gericke and A. Pinches, *Gold Bull.*, 2006, **39**, 22–28.
79 M. Gericke and A. Pinches, *Hydrometallurgy*, 2006, **83**, 132–140.
80 Y. Liu, J. Fu, H. Hu, D. Tang, Z. Ni and X. Yu, *Chin. Sci. Bull.*, 2001, **46**, 1709–1712.
81 J. K. Fu, Y. Y. Liu, P. Y. Gu, D. L. Tang, Z. Y. Lin, B. X. Yao and S. Z. Weng, *Acta Phys.-Chim. Sin.*, 2000, **16**, 779–782.
82 Z. Lin, C. Zhou, J. Wu, H. Cheng, B. Liu, Z. Ni, J. Zhou and J. Fu, *Chin. Sci. Bull.*, 2002, **47**, 1262–1266.
83 H. R. Zhang, Q. B. Li, H. X. Wang, D. H. Sun, Y. H. Lu and N. He, *Appl. Biochem. Biotechnol.*, 2007, **143**, 54–62.
84 S. De Corte, T. Hennebel, S. Verschuere, C. Cuvelier, W. Verstraete and N. Boon, *J. Chem. Technol. Biotechnol.*, 2011, **86**, 547–553.
85 H. Chen, D. Huang, L. Lin, T. Odoom-Wubah, J. Huang, D. Sun and Q. Li, *J. Colloid Interface Sci.*, 2014, **433**, 204–210.
86 Z. Lin, R. Xue, Y. Ye, J. Zheng and Z. Xu, *BMC Biotechnol.*, 2009, **9**, 62.
87 M. X. Fu, Q. B. Li, D. H. Sun, Y. H. Lu, N. He, X. Deng, H. X. Wang and J. L. Huang, *Chin. J. Chem. Eng.*, 2006, **14**, 114–117.
88 H. X. Wang, H. M. Chen, Y. Z. Wang, J. L. Huang, T. Kong, W. S. Lin, Y. Zhou, L. Q. Lin, D. H. Sun and Q. B. Li, *Curr. Nanosci.*, 2012, **8**, 838–846.
89 D. H. Sun, Q. B. Li, N. He, J. L. Huang and H. X. Wang, *Rare Met. Mater. Eng.*, 2011, **40**, 148–151.
90 Z. Y. Lin, J. M. Wu, R. Xue and Y. Yang, *Spectrochim. Acta, Part A*, 2005, **61**, 761–765.
91 Z. Lin, Y. Ye, Q. Li, Z. Xu and M. Wang, *BMC Biotechnol.*, 2011, **11**, 98.
92 M. R. Salvadori, R. A. Ando, C. A. O. do Nascimento and B. Corrêa, *PLoS One*, 2014, **9**, e87968.
93 S. Y. He, Y. Zhang, Z. R. Guo and N. Go, *Biotechnol. Prog.*, 2008, **24**, 476–480.
94 S. A. Wadhwani, U. U. Shedbalkar, R. Singh, M. S. Karve and B. A. Chopade, *World J. Microbiol. Biotechnol.*, 2014, **30**, 2723–2731.
95 K. G. Lee, J. Hong, K. W. Wang, N. S. Heo, D. H. Kim, S. Y. Lee, S. J. Lee and T. J. Park, *ACS Nano*, 2012, **6**, 6998–7008.
96 P. Velmurugan, M. Iydroose, M. H. A. K. Mohideen, T. S. Mohan, M. Cho and B.-T. Oh, *Bioprocess Biosyst. Eng.*, 2014, 1–8.
97 N. R. Jana, L. Gearheart and C. J. Murphy, *J. Phys. Chem. B*, 2001, **105**, 4065–4067.
98 M. Wang, T. Kong, X. L. Jing, Y. K. Hung, D. H. Sun, L. Q. Lin, Y. M. Zheng, J. L. Huang and Q. B. Li, *Ind. Eng. Chem. Res.*, 2012, **51**, 16651–16659.
99 M. Wang, T. Odoom-Wubah, H. M. Chen, X. L. Jing, T. Kong, D. H. Sun, J. L. Huang and Q. B. Li, *Nanoscale*, 2013, **5**, 6599–6606.
100 H. X. Yang, M. M. Du, T. Odoom-Wubah, J. Wang, D. H. Sun, J. L. Huang and Q. B. Li, *J. Chem. Technol. Biotechnol.*, 2014, **89**, 1410–1418.
101 X. L. Jing, D. P. Huang, H. M. Chen, T. Odoom-Wubah, D. H. Sun, J. L. Huang and Q. B. Li, *J. Chem. Technol. Biotechnol.*, 2015, **90**, 678–685.
102 H. Yang, L. Lin, T. Odoom-Wubah, D. Huang, D. Sun, J. Huang and Q. Li, *Sep. Purif. Technol.*, 2014, **133**, 380–387.
103 J. L. Huang, D. P. Huang, Y. Liu, H. M. Chen, X. L. Jing, D. H. Sun and Q. B. Li, *Chem. Eng. J.*, 2015, **267**, 43–50.
104 N. Garg, C. Scholl, A. Mohanty and R. C. Jin, *Langmuir*, 2010, **26**, 10271–10276.
105 H. M. Chen, D. H. Sun, X. L. Jing, F. F. Lu, T. Odoom-Wubah, Y. M. Zheng, J. L. Huang and Q. B. Li, *RSC Adv.*, 2013, **3**, 15389–15395.
106 H. M. Chen, J. L. Huang, D. P. Huang, M. H. Shao, D. H. Sun and Q. B. Li, *J. Mater. Chem. A*, 2015, **3**, 4846–4854.
107 W. X. Jia, *Medical microbiology*, People's Medical Publishing House, Beijing, 2005.
108 L. A. Lee, H. G. Nguyen and Q. Wang, *Org. Biomol. Chem.*, 2011, **9**, 6189–6195.
109 K. N. Avery, J. E. Schaak and R. E. Schaak, *Chem. Mater.*, 2009, **21**, 2176–2178.
110 A. S. Blum, C. M. Soto, C. D. Wilson, J. D. Cole, M. Kim, B. Gnade, A. Chatterji, W. F. Ochoa, T. Lin and J. E. Johnson, *Nano Lett.*, 2004, **4**, 867–870.
111 J. C. Zhou, C. M. Soto, M. S. Chen, M. A. Bruckman, M. H. Moore, E. Barry, B. R. Ratna, P. E. Pehrsson, B. R. Spies and T. S. Confer, *J. Nanobiotechnol.*, 2012, **10**, 18.
112 L. Hou, F. M. Gao and N. Li, *Chem. – Eur. J.*, 2010, **16**, 14397–14403.
113 K. T. Nam, D.-W. Kim, P. J. Yoo, C.-Y. Chiang, N. Meethong, P. T. Hammond, Y.-M. Chiang and A. M. Belcher, *Science*, 2006, **312**, 885–888.
114 A. A. Aljabali, J. E. Barclay, G. P. Lomonossoff and D. J. Evans, *Nanoscale*, 2010, **2**, 2596–2600.
115 L. Hou, D. Tong, Y. Jiang and F. Gao, *Nano*, 2014, **9**, 1450058.
116 M. Knez, A. M. Bittner, F. Boes, C. Wege, H. Jeske, E. Maiβ and K. Kern, *Nano Lett.*, 2003, **3**, 1079–1082.
117 S. Balci, K. Hahn, P. Kopold, A. Kadri, C. Wege, K. Kern and A. M. Bittner, *Nanotechnology*, 2012, **23**, 045603.
118 M. Wnęk, M. Ł. Górzny, M. Ward, C. Wälti, A. Davies, R. Brydson, S. Evans and P. Stockley, *Nanotechnology*, 2013, **24**, 025605.
119 C. Yang, J. H. Meldon, B. Lee and H. Yi, *Catal. Today*, 2014, **233**, 108–116.
120 J.-S. Lim, S.-M. Kim, S.-Y. Lee, E. A. Stach, J. N. Culver and M. T. Harris, *J. Nanomater.*, 2010, **2010**, 4.
121 C. X. Yang, S. Jung and H. M. Yi, *Biochem. Eng. J.*, 2014, **89**, 10–20.
122 S.-Y. Lee, E. Royston, J. N. Culver and M. T. Harris, *Nanotechnology*, 2005, **16**, S435.

123 J. S. Lim, S. M. Kim, S. Y. Lee, E. A. Stach, J. N. Culver and M. T. Harris, *Nano Lett.*, 2010, **10**, 3863–3867.
124 Y. Lee, J. Kim, D. S. Yun, Y. S. Nam, Y. Shao-Horn and A. M. Belcher, *Energy Environ. Sci.*, 2012, **5**, 8328–8334.
125 A. A. Aljabali, G. P. Lomonossoff and D. J. Evans, *Biomacromolecules*, 2011, **12**, 2723–2728.
126 A. A. Aljabali, J. E. Barclay, O. Cespedes, A. Rashid, S. S. Staniland, G. P. Lomonossoff and D. J. Evans, *Adv. Funct. Mater.*, 2011, **21**, 4137–4142.
127 M. Knez, M. Sumser, A. Bittner, C. Wege, H. Jeske, S. Kooi, M. Burghard and K. Kern, *J. Electroanal. Chem.*, 2002, **522**, 70–74.
128 M. Knez, M. Sumser, A. M. Bittner, C. Wege, H. Jeske, T. P. Martin and K. Kern, *Adv. Funct. Mater.*, 2004, **14**, 116–124.
129 A. A. Aljabali, F. Sainsbury, G. P. Lomonossoff and D. J. Evans, *Small*, 2010, **6**, 818–821.
130 H. Yi, S. Nisar, S.-Y. Lee, M. A. Powers, W. E. Bentley, G. F. Payne, R. Ghodssi, G. W. Rubloff, M. T. Harris and J. N. Culver, *Nano Lett.*, 2005, **5**, 1931–1936.
131 S.-Y. Lee, J. Choi, E. Royston, D. B. Janes, J. N. Culver and M. T. Harris, *J. Nanosci. Nanotechnol.*, 2006, **6**, 974–981.
132 J. S. Lim, S. M. Kim, S. Y. Lee, E. A. Stach, J. N. Culver and M. T. Harris, *J. Colloid Interface Sci.*, 2010, **342**, 455–461.
133 A. K. Manocchi, S. Seifert, B. Lee and H. Yi, *Langmuir*, 2011, **27**, 7052–7058.
134 A. K. Manocchi, S. Seifert, B. Lee and H. M. Yi, *Langmuir*, 2010, **26**, 7516–7522.
135 A. A. Aljabali, S. N. Shah, R. Evans-Gowing, G. P. Lomonossoff and D. J. Evans, *Integr. Biol.*, 2011, **3**, 119–125.
136 E. S. Royston, A. D. Brown, M. T. Harris and J. N. Culver, *J. Colloid Interface Sci.*, 2009, **332**, 402–407.
137 K. M. Bromley, A. J. Patil, A. W. Perriman, G. Stubbs and S. Mann, *J. Mater. Chem.*, 2008, **18**, 4796–4801.
138 A. A. Khan, E. K. Fox, M. Ł. Górzny, E. Nikulina, D. F. Brougham, C. Wege and A. M. Bittner, *Langmuir*, 2013, **29**, 2094–2098.
139 C. Mao, D. J. Solis, B. D. Reiss, S. T. Kottmann, R. Y. Sweeney, A. Hayhurst, G. Georgiou, B. Iverson and A. M. Belcher, *Science*, 2004, **303**, 213–217.
140 J. Fontana, W. J. Dressick, J. Phelps, J. E. Johnson, R. W. Rendell, T. Sampson, B. R. Ratna and C. M. Soto, *Small*, 2014, **10**, 3058–3063.
141 C. Yang and H. Yi, *Biochem. Eng. J.*, 2010, **52**, 160–167.
142 K. Gerasopoulos, M. McCarthy, P. Banerjee, X. Fan, J. Culver and R. Ghodssi, *Nanotechnology*, 2010, **21**, 055304.
143 C. L. Lewis, Y. Lin, C. Yang, A. K. Manocchi, K. P. Yuet, P. S. Doyle and H. Yi, *Langmuir*, 2010, **26**, 13436–13441.
144 Z. Niu, M. Bruckman, V. S. Kotakadi, J. He, T. Emrick, T. P. Russell, L. Yang and Q. Wang, *Chem. Commun.*, 2006, 3019–3021.
145 T. Sawada, S. Kang, J. Watanabe, H. Mihara and T. Serizawa, *ACS Macro Lett.*, 2014, **3**, 341–345.
146 N. M. D. Courchesne, M. T. Klug, P. Y. Chen, S. E. Kooi, D. S. Yun, N. Hong, N. X. Fang, A. M. Belcher and P. T. Hammond, *Adv. Mater.*, 2014, **26**, 3398–3404.
147 J. L. Gardea-Torresdey, E. Gomez, J. R. Peralta-Videa, J. G. Parsons, H. Troiani and M. Jose-Yacaman, *Langmuir*, 2003, **19**, 1357–1361.
148 R. Bali, R. Siegele and A. T. Harris, *J. Nanopart. Res.*, 2010, **12**, 3087–3095.
149 C. W. Anderson, S. M. Bhatti, J. Gardea-Torresdey and J. Parsons, *ACS Sustainable Chem. Eng.*, 2013, **1**, 640–648.
150 N. C. Sharma, S. V. Sahi, S. Nath, J. G. Parsons, J. L. Gardea-Torresdey and T. Pal, *Environ. Sci. Technol.*, 2007, **41**, 5137–5142.
151 R. Haverkamp and A. Marshall, *J. Nanopart. Res.*, 2009, **11**, 1453–1463.
152 G. Zhai, K. S. Walters, D. W. Peate, P. J. Alvarez and J. L. Schnoor, *Environ. Sci. Technol. Lett.*, 2014, **1**, 146–151.
153 A. F. Taylor, E. L. Rylott, C. W. Anderson and N. C. Bruce, *PLoS One*, 2014, **9**, e93793.
154 Y. Zhou, W. Lin, J. Huang, W. Wang, Y. Gao, L. Lin, Q. Li, L. Lin and M. Du, *Nanoscale Res. Lett.*, 2010, **5**, 1351–1359.
155 P. Mohanpuria, N. K. Rana and S. K. Yadav, *J. Nanopart. Res.*, 2008, **10**, 507–517.
156 V. Kumar and S. K. Yadav, *J. Chem. Technol. Biotechnol.*, 2009, **84**, 151–157.
157 D. Bhattacharya and R. K. Gupta, *Crit. Rev. Biotechnol.*, 2005, **25**, 199–204.
158 J. Huang, Q. Li, D. Sun, Y. Lu, Y. Su, X. Yang, H. Wang, Y. Wang, W. Shao and N. He, *Nanotechnology*, 2007, **18**, 105104.
159 S. S. Shankar, A. Ahmad and M. Sastry, *Biotechnol. Prog.*, 2003, **19**, 1627–1631.
160 S. S. Shankar, A. Ahmad, R. Pasricha and M. Sastry, *J. Mater. Chem.*, 2003, **13**, 1822–1826.
161 S. S. Shankar, A. Rai, A. Ahmad and M. Sastry, *J. Colloid Interface Sci.*, 2004, **275**, 496–502.
162 S. S. Shankar, A. Rai, A. Ahmad and M. Sastry, *Chem. Mater.*, 2005, **17**, 566–572.
163 B. Ankamwar, M. Chaudhary and M. Sastry, *Synth. React. Inorg., Met.-Org., Nano-Met. Chem.*, 2005, **35**, 19–26.
164 B. Ankamwar, C. Damle, A. Ahmad and M. Sastry, *J. Nanosci. Nanotechnol.*, 2005, **5**, 1665–1671.
165 S. Prathap Chandran, M. Chaudhary, R. Pasricha, A. Ahmad and M. Sastry, *Biotechnol. Prog.*, 2006, **22**, 577–583.
166 B. Liu, J. Xie, J. Y. Lee, Y. P. Ting and J. P. Chen, *J. Phys. Chem. B*, 2005, **109**, 15256–15263.
167 D. Philip, *Spectrochim. Acta, Part A*, 2009, **73**, 374–381.
168 J. Kasthuri, S. Veerapandian and N. Rajendiran, *Colloids Surf., B*, 2009, **68**, 55–60.
169 J. Y. Song and B. S. Kim, *Korean J. Chem. Eng.*, 2008, **25**, 808–811.
170 M. Iosin, F. Toderas, P. Baldeck and S. Astilean, *J. Optoelectron. Adv. Mater.*, 2008, **10**, 2285–2288.
171 K. B. Narayanan and N. Sakthivel, *Mater. Lett.*, 2008, **62**, 4588–4590.
172 A. T. Harris and R. Bali, *J. Nanopart. Res.*, 2008, **10**, 691–695.
173 R. Shukla, S. K. Nune, N. Chanda, K. Katti, S. Mekapothula, R. R. Kulkami, W. V. Welshons, R. Kannan and K. V. Katti, *Small*, 2008, **4**, 1425–1436.

174 K. Govindaraju, S. K. Basha, V. G. Kumar and G. Singaravelu, *J. Mater. Sci.*, 2008, **43**, 5115–5122.
175 M. N. Nadagouda and R. S. Varma, *Green Chem.*, 2008, **10**, 859–862.
176 A. R. Vilchis-Nestor, V. Sanchez-Mendieta, M. A. Carnacho-Lopez, R. M. Gomez-Espinosa, M. A. Camacho-Lopez and J. A. Arenas-Alatorre, *Mater. Lett.*, 2008, **62**, 3103–3105.
177 R. G. Haverkamp, A. T. Marshall and D. van Agterveld, *J. Nanopart. Res.*, 2007, **9**, 697–700.
178 S. K. Li, Y. H. Shen, A. J. Xie, X. R. Yu, L. G. Qiu, L. Zhang and Q. F. Zhang, *Green Chem.*, 2007, **9**, 852–858.
179 J. P. Xie, J. Y. Lee, D. I. C. Wang and Y. P. Ting, *Small*, 2007, **3**, 672–682.
180 G. Zhan, L. Ke, Q. Li, J. Huang, D. Hua, A.-R. Ibrahim and D. Sun, *Ind. Eng. Chem. Res.*, 2012, **51**, 15753–15762.
181 W. W. Wu, J. L. Huang, L. F. Wu, D. H. Sun, L. Q. Lin, Y. Zhou, H. T. Wang and Q. B. Li, *Sep. Purif. Technol.*, 2013, **106**, 117–122.
182 L. Wu, W. Wu, X. Jing, J. Huang, D. Sun, T. Odoom-Wubah, H. Liu, H. Wang and Q. Li, *Ind. Eng. Chem. Res.*, 2013, **52**, 5085–5094.
183 J. P. Xie, J. Y. Lee, D. I. C. Wang and Y. P. Ting, *ACS Nano*, 2007, **1**, 429–439.
184 S. Wu, X. Zhou, X. Yang, Z. Hou, Y. Shi, L. Zhong, Q. Jiang and Q. Zhang, *J. Nanopart. Res.*, 2014, **16**, 1–13.
185 J. L. Huang, L. Q. Lin, Q. B. Li, D. H. Sun, Y. P. Wang, Y. H. Lu, N. He, K. Yang, X. Yang, H. X. Wang, W. T. Wang and W. S. Lin, *Ind. Eng. Chem. Res.*, 2008, **47**, 6081–6090.
186 H. Y. Liu, J. L. Huang, D. H. Sun, L. Q. Lin, W. S. Lin, J. Li, X. D. Jiang, W. W. Wu and Q. B. Li, *Chem. Eng. J.*, 2012, **209**, 568–576.
187 H. Liu, J. Li, D. Sun, T. Odoom-Wubah, J. Huang and Q. Li, *Ind. Eng. Chem. Res.*, 2014, **53**, 4263–4270.
188 H. Liu, J. Huang, D. Sun, T. Odoom-Wubah, J. Li and Q. Li, *J. Nanopart. Res.*, 2014, **16**, 1–9.
189 G. Zhan, J. Huang, M. Du, I. Abdul-Rauf, Y. Ma and Q. Li, *Mater. Lett.*, 2011, **65**, 2989–2991.
190 F. Lu, D. Sun, J. Huang, M. Du, F. Yang, H. Chen, Y. Hong and Q. Li, *ACS Sustainable Chem. Eng.*, 2014, **2**, 1212–1218.
191 G. L. Zhang, M. M. Du, Q. B. Li, X. L. Li, J. L. Huang, X. D. Jiang and D. H. Sun, *RSC Adv.*, 2013, **3**, 1878–1884.
192 D. Sun, G. Zhang, X. Jiang, J. Huang, X. Jing, Y. Zheng, J. He and Q. Li, *J. Mater. Chem. A*, 2014, **2**, 1767–1773.
193 D. Sun, G. Zhang, J. Huang, H. Wang and Q. Li, *Materials*, 2014, **7**, 1360–1369.
194 G. Zhan, J. Huang, L. Lin, W. Lin, K. Emmanuel and Q. Li, *J. Nanopart. Res.*, 2011, **13**, 4957–4968.
195 X. Jiang, D. Sun, G. Zhang, N. He, H. Liu, J. Huang, T. Odoom-Wubah and Q. Li, *J. Nanopart. Res.*, 2013, **15**, 1–11.
196 F. Lu, Y. Gao, J. Huang, D. Sun and Q. Li, *Chin. J. Chem. Eng.*, 2014, **22**, 706–712.
197 H. Chen, J. Wang, D. Huang, X. Chen, J. Zhu, D. Sun, J. Huang and Q. Li, *Mater. Lett.*, 2014, **122**, 166–169.
198 Y. Zhou, H. Wang, W. Lin, L. Lin, Y. Gao, F. Yang, M. Du, W. Fang, J. Huang and D. Sun, *J. Colloid Interface Sci.*, 2013, **407**, 8–16.
199 Y. Zhou, W. Lin, F. Yang, W. Fang, J. Huang and Q. Li, *Chem. Phys.*, 2014, **441**, 23–29.
200 H. A. Lowenstam and S. Weiner, *On biomineralization*, Oxford University Press, New York, 1989.
201 L. Addadi and S. Weiner, *Proc. Natl. Acad. Sci. U. S. A.*, 1985, **82**, 4110–4114.
202 M. B. Dickerson, K. H. Sandhage and R. R. Naik, *Chem. Rev.*, 2008, **108**, 4935–4978.
203 R. K. Watt, O. D. Petrucci and T. Smith, *Catal. Sci. Technol.*, 2013, **3**, 3103–3110.
204 M. Uchida, M. T. Klem, M. Allen, P. Suci, M. Flenniken, E. Gillitzer, Z. Varpness, L. O. Liepold, M. Young and T. Douglas, *Adv. Mater.*, 2007, **19**, 1025–1042.
205 N. D. Chasteen and P. M. Harrison, *J. Struct. Biol.*, 1999, **126**, 182–194.
206 K. K. Wong and S. Mann, *Adv. Mater.*, 1996, **8**, 928–932.
207 C. Sun, H. Yang, Y. Yuan, X. Tian, L. Wang, Y. Guo, L. Xu, J. Lei, N. Gao and G. J. Anderson, *J. Am. Chem. Soc.*, 2011, **133**, 8617–8624.
208 J. Fan, J.-J. Yin, B. Ning, X. Wu, Y. Hu, M. Ferrari, G. J. Anderson, J. Wei, Y. Zhao and G. Nie, *Biomaterials*, 2011, **32**, 1611–1618.
209 M. Suzuki, M. Abe, T. Ueno, S. Abe, T. Goto, Y. Toda, T. Akita, Y. Yamada and Y. Watanabe, *Chem. Commun.*, 2009, 4871–4873.
210 T. Peters, *Adv. Protein Chem.*, 1985, **37**, 161–245.
211 P. L. Xavier, K. Chaudhari, A. Baksi and T. Pradeep, *Nano Rev.*, 2012, **3**, 14767.
212 J. Xie, J. Y. Lee and D. I. Wang, *J. Phys. Chem. C*, 2007, **111**, 10226–10232.
213 M. S. Bakshi, H. Kaur, P. Khullar, T. S. Banipal, G. Kaur and N. Singh, *J. Phys. Chem. C*, 2011, **115**, 2982–2992.
214 X. Le Guével, B. Hötzer, G. Jung, K. Hollemeyer, V. Trouillet and M. Schneider, *J. Phys. Chem. C*, 2011, **115**, 10955–10963.
215 N. Goswami, A. Giri, M. Bootharaju, P. L. Xavier, T. Pradeep and S. K. Pal, *Anal. Chem.*, 2011, **83**, 9676–9680.
216 C. Guo and J. Irudayaraj, *Anal. Chem.*, 2011, **83**, 2883–2889.
217 M. Li, D.-P. Yang, X. Wang, J. Lu and D. Cui, *Nanoscale Res. Lett.*, 2013, **8**, 1–5.
218 J. S. Mohanty, P. L. Xavier, K. Chaudhari, M. Bootharaju, N. Goswami, S. Pal and T. Pradeep, *Nanoscale*, 2012, **4**, 4255–4262.
219 H. Cao, D.-P. Yang, D. Ye, X. Zhang, X. Fang, S. Zhang, B. Liu and J. Kong, *Biosens. Bioelectron.*, 2015, **68**, 329–335.
220 C. Hu, D.-P. Yang, Z. Wang, P. Huang, X. Wang, D. Chen, D. Cui, M. Yang and N. Jia, *Biosens. Bioelectron.*, 2013, **41**, 656–662.
221 C. Hu, D.-P. Yang, Z. Wang, L. Yu, J. Zhang and N. Jia, *Anal. Chem.*, 2013, **85**, 5200–5206.
222 C. Hu, D.-P. Yang, F. Zhu, F. Jiang, S. Shen and J. Zhang, *ACS Appl. Mater. Interfaces*, 2014, **6**, 4170–4178.
223 P. Huang, D.-P. Yang, C. Zhang, J. Lin, M. He, L. Bao and D. Cui, *Nanoscale*, 2011, **3**, 3623–3626.
224 X. Wang, D.-P. Yang, P. Huang, M. Li, C. Li, D. Chen and D. Cui, *Nanoscale*, 2012, **4**, 7766–7772.

225 C. Hu, D.-P. Yang, K. Xu, H. Cao, B. Wu, D. Cui and N. Jia, *Anal. Chem.*, 2012, **84**, 10324–10331.
226 L. Zhuang, W. Wang, F. Hong, S. Yang, H. You, J. Fang and B. Ding, *J. Solid State Chem.*, 2012, **191**, 239–245.
227 C. Hou, D. Yang, B. Liang and A. Liu, *Anal. Chem.*, 2014, **86**, 6057–6063.
228 Q. Liu, X. Jiang, S. Gao, H. Xu and L. Sun, *Mater. Lett.*, 2014, **128**, 322–324.
229 E. I. Alarcon, K. Udekwu, M. Skog, N. L. Pacioni, K. G. Stamplecoskie, M. González-Béjar, N. Polisetti, A. Wickham, A. Richter-Dahlfors and M. Griffith, *Biomaterials*, 2012, **33**, 4947–4956.
230 H. Wu, C. Wu, Q. He, X. Liao and B. Shi, *Mater. Sci. Eng., C*, 2010, **30**, 770–776.
231 X. Huang, H. Wu, S. Pu, W. Zhang, X. Liao and B. Shi, *Green Chem.*, 2011, **13**, 950–957.
232 P. Zhang, J. Lan, Y. Wang and C. Z. Huang, *Biomaterials*, 2015, **36**, 26–32.
233 T. Cohen-Karni, K. J. Jeong, J. H. Tsui, G. Reznor, M. Mustata, M. Wanunu, A. Graham, C. Marks, D. C. Bell and R. Langer, *Nano Lett.*, 2012, **12**, 5403–5406.
234 M. G. Warner and J. E. Hutchison, *Nat. Mater.*, 2003, **2**, 272–277.
235 H. J. Kim, Y. Roh, S. K. Kim and B. Hong, *J. Appl. Phys.*, 2009, **105**, 074302.
236 L. Zheng, R. Zhang, Y. Ni, Q. Du, X. Wang, J. Zhang and W. Li, *Catal. Lett.*, 2010, **139**, 145–150.
237 A. Thomas, *Chem. Commun.*, 2012, **48**, 6845–6847.
238 J. Park, J. Song, J. Park, N. Park and S. Kim, *Bull. Korean Chem. Soc.*, 2014, **35**, 1105–1109.
239 W.-Y. Chen, G.-Y. Lan and H.-T. Chang, *Anal. Chem.*, 2011, **83**, 9450–9455.
240 X. Jia, J. Li, L. Han, J. Ren, X. Yang and E. Wang, *ACS Nano*, 2012, **6**, 3311–3317.
241 A. Zinchenko, Y. Miwa, L. I. Lopatina, V. G. Sergeyev and S. Murata, *ACS Appl. Mater. Interfaces*, 2014, **6**, 3226–3232.
242 J. Leng, W.-M. Wang, L.-M. Lu, L. Bai and X.-L. Qiu, *Nanoscale Res. Lett.*, 2014, **9**, 1–8.
243 M. N. Al-Hinai, R. Hassanien, N. G. Wright, A. B. Horsfall, A. Houlton and B. R. Horrocks, *Faraday Discuss.*, 2013, **164**, 71–91.
244 S. Helmi, C. Ziegler, D. J. Kauert and R. Seidel, *Nano Lett.*, 2014, **14**, 6693–6698.
245 D. Majumdar, A. Singha, P. K. Mondal and S. Kundu, *ACS Appl. Mater. Interfaces*, 2013, **5**, 7798–7807.
246 S.-y. Pu, A. Zinchenko, L.-l. Qin, C.-w. Ye, M. Xu and S. Murata, *Mater. Lett.*, 2014, **130**, 168–171.
247 H. Xu and K. S. Suslick, *Adv. Mater.*, 2010, **22**, 1078–1082.
248 B. Sengupta, C. M. Ritchie, J. G. Buckman, K. R. Johnsen, P. M. Goodwin and J. T. Petty, *J. Phys. Chem. C*, 2008, **112**, 18776–18782.
249 C. A. Mirkin, R. L. Letsinger, R. C. Mucic and J. J. Storhoff, *Nature*, 1996, 607–609.
250 Y. Li, Y. Zheng, M. Gong and Z. Deng, *Chem. Commun.*, 2012, **48**, 3727–3729.
251 B. Ding, Z. Deng, H. Yan, S. Cabrini, R. N. Zuckermann and J. Bokor, *J. Am. Chem. Soc.*, 2010, **132**, 3248–3249.
252 S. Pal, Z. T. Deng, B. Q. Ding, H. Yan and Y. Liu, *Angew. Chem., Int. Ed.*, 2010, **49**, 2700–2704.
253 S. Kundu and M. Jayachandran, *RSC Adv.*, 2013, **3**, 16486–16498.
254 J. Richter, R. Seidel, R. Kirsch, M. Mertig, W. Pompe, J. Plaschke and H. K. Schackert, *Adv. Mater.*, 2000, **12**, 507–510.
255 Z. Deng and C. Mao, *Nano Lett.*, 2003, **3**, 1545–1548.
256 C. F. Monson and A. T. Woolley, *Nano Lett.*, 2003, **3**, 359–363.
257 H. J. Kim, Y. Roh and B. Hong, *IEEE Trans. Nanotechnol.*, 2010, **9**, 254–257.
258 S. J. Barrow, A. M. Funston, D. E. Gómez, T. J. Davis and P. Mulvaney, *Nano Lett.*, 2011, **11**, 4180–4187.
259 Y. Geng, A. C. Pearson, E. P. Gates, B. Uprety, R. C. Davis, J. N. Harb and A. T. Woolley, *Langmuir*, 2013, **29**, 3482–3490.
260 M. Pilo-Pais, A. Watson, S. Demers, T. H. LaBean and G. Finkelstein, *Nano Lett.*, 2014, **14**, 2099–2104.
261 J. Sharma, R. Chhabra, A. Cheng, J. Brownell, Y. Liu and H. Yan, *Science*, 2009, **323**, 112–116.
262 X. Shen, A. Asenjo-Garcia, Q. Liu, Q. Jiang, F. J. García de Abajo, N. Liu and B. Ding, *Nano Lett.*, 2013, **13**, 2128–2133.
263 Y. Hatakeyama, M. Umetsu, S. Ohara, F. Kawadai, S. Takami, T. Naka and T. Adschiri, *Adv. Mater.*, 2008, **20**, 1122–1128.
264 A. Rotaru, S. Dutta, E. Jentzsch, K. Gothelf and A. Mokhir, *Angew. Chem., Int. Ed.*, 2010, **49**, 5665–5667.
265 J.-Y. Kim and J.-S. Lee, *Nano Lett.*, 2009, **9**, 4564–4569.
266 N. Duran, P. D. Marcato, M. Duran, A. Yadav, A. Gade and M. Rai, *Appl. Microbiol. Biotechnol.*, 2011, **90**, 1609–1624.
267 V. Baxter-Plant, I. P. Mikheenko and L. E. Macaskie, *Biodegradation*, 2003, **14**, 83–90.
268 V. S. Baxter-Plant, I. P. Mikheenko, M. Robson, S. J. Harrad and L. E. Macaskie, *Biotechnol. Lett.*, 2004, **26**, 1885–1890.
269 N. J. Creamer, V. S. Baxter-Plant, J. Henderson, M. Potter and L. E. Macaskie, *Biotechnol. Lett.*, 2006, **28**, 1475–1484.
270 S. Harrad, M. Robson, S. Hazrati, V. S. Baxter-Plant, K. Deplanche, M. D. Redwood and L. E. Macaskie, *J. Environ. Monit.*, 2007, **9**, 314–318.
271 L. E. Macaskie, V. S. Baxter-Plant, N. J. Creamer, A. C. Humphries, I. P. Mikheenko, P. M. Mikheenko, D. W. Penfold and P. Yong, *Biochem. Soc. Trans.*, 2005, **33**, 76–79.
272 M. D. Redwood, K. Deplanche, V. S. Baxter-Plant and L. E. Macaskie, *Biotechnol. Bioeng.*, 2008, **99**, 1045–1054.
273 A. N. Mabbett, D. Sanyahumbi, P. Yong and L. E. Macaskie, *Environ. Sci. Technol.*, 2006, **40**, 1015–1021.
274 N. J. Creamer, I. P. Mikheenko, P. Yong, K. Deplanche, D. Sanyahumbi, J. Wood, K. Pollmann, M. Merroun, S. Selenska-Pobell and L. E. Macaskie, *Catal. Today*, 2007, **128**, 80–87.
275 J. Wood, L. Bodenes, J. Bennett, K. Deplanche and L. E. Macaskie, *Ind. Eng. Chem. Res.*, 2010, **49**, 980–988.

 

276 W. De Windt, P. Aelterman and W. Verstraete, *Environ. Microbiol.*, 2005, **7**, 314–325.
277 L. S. Sobjerg, D. Gauthier, A. T. Lindhardt, M. Bunge, K. Finster, R. L. Meyer and T. Skrydstrup, *Green Chem.*, 2009, **11**, 2041–2046.
278 L. S. Søbjerg, A. T. Lindhardt, T. Skrydstrup, K. Finster and R. L. Meyer, *Colloids Surf., B*, 2011, **85**, 373–378.
279 J. M. Foulkes, K. J. Malone, V. S. Coker, N. J. Turner and J. R. Lloyd, *ACS Catal.*, 2011, **1**, 1589–1594.
280 T. Hennebel, S. Van Nevel, S. Verschuere, S. De Corte, B. De Gusseme, C. Cuvelier, J. P. Fitts, D. van der Lelie, N. Boon and W. Verstraete, *Appl. Microbiol. Biotechnol.*, 2011, 1–11.
281 S. De Corte, T. Hennebel, J. P. Fitts, T. Sabbe, V. Bliznuk, S. Verschuere, D. van der Lelie, W. Verstraete and N. Boon, *Environ. Sci. Technol.*, 2011, **45**, 8506–8513.
282 K. Deplanche, M. L. Merroun, M. Casadesus, D. T. Tran, I. P. Mikheenko, J. A. Bennett, J. Zhu, I. P. Jones, G. A. Attard and J. Wood, *J. R. Soc., Interface*, 2012, **9**, 1705–1712.
283 B. Hosseinkhani, L. S. Søbjerg, A. E. Rotaru, G. Emtiazi, T. Skrydstrup and R. L. Meyer, *Biotechnol. Bioeng.*, 2012, **109**, 45–52.
284 F. Lakaye and W. W. De, *Geneva, Switzerland Pat.*, WO2011141418A1, 2011.
285 E. Castro-Longoria, A. R. Vilchis-Nestor and M. Avalos-Borja, *Colloids Surf., B*, 2011, **83**, 42–48.
286 K. Deplanche, M. L. Merroun, M. Casadesus, D. T. Tran, I. P. Mikheenko, J. A. Bennett, J. Zhu, I. P. Jones, G. A. Attard, J. Wood, S. Selenska-Pobell and L. E. Macaskie, *J. R. Soc., Interface*, 2012, **9**, 1705–1712.
287 K. Deplanche, I. P. Mikheenko, J. A. Bennett, M. Merroun, H. Mounzer, J. Wood and L. E. Macaskie, *Top. Catal.*, 2011, **54**, 1110–1114.
288 T. S. A. Heugebaert, C. S. De, T. Sabbe, T. Hennebel, W. Verstraete, N. Boon and C. V. Stevens, *Tetrahedron Lett.*, 2012, **53**, 1410–1412.
289 C. Yang, A. K. Manocchi, B. Lee and H. Yi, *Appl. Catal., B*, 2010, **93**, 282–291.
290 C. Yang, A. K. Manocchi, B. Lee and H. Yi, *J. Mater. Chem.*, 2011, **21**, 187–194.
291 Y. S. Nam, H. Park, A. P. Magyar, D. S. Yun, T. S. Pollom and A. M. Belcher, *Nanoscale*, 2012, **4**, 3405–3409.
292 L. S. Jia, Q. Zhang, Q. B. Li and H. Song, *Nanotechnology*, 2009, **20**, 385601.
293 H. Wu, X. Huang, M. Gao, X. Liao and B. Shi, *Green Chem.*, 2011, **13**, 651–658.
294 S. Kanbak-Aksu, M. N. Hasan, W. Hagen, F. Hollmann, D. Sordi, R. Sheldon and I. Arends, *Chem. Commun.*, 2012, **48**, 5745–5747.
295 X. Jiang, C. Sun, Y. Guo, G. Nie and L. Xu, *Biosens. Bioelectron.*, 2015, **64**, 165–170.
296 S. B. He, H. H. Deng, A. L. Liu, G. W. Li, X. H. Lin, W. Chen and X. H. Xia, *ChemCatChem*, 2014, **6**, 1543–1548.
297 B. H. San, S. Kim, S. H. Moh, H. Lee, D. Y. Jung and K. K. Kim, *Angew. Chem.*, 2011, **123**, 12130–12135.
298 B. H. San, S. H. Moh and K. K. Kim, *J. Mater. Chem.*, 2012, **22**, 1774–1780.
299 E. Auyeung, W. Morris, J. E. Mondloch, J. T. Hupp, O. K. Farha and C. A. Mirkin, *J. Am. Chem. Soc.*, 2015, **137**, 1658–1662.
300 Y. Wang, G. Ouyang, J. Zhang and Z. Wang, *Chem. Commun.*, 2010, **46**, 7912–7914.
301 K. Qu, L. Wu, J. Ren and X. Qu, *ACS Appl. Mater. Interfaces*, 2012, **4**, 5001–5009.
302 Y. Zhang, X. Cui, F. Shi and Y. Deng, *Chem. Rev.*, 2011, **112**, 2467–2505.
303 J. K. Fu, Y. Y. Liu, R. Z. Hu, J. L. Zegn, P. P. Xu, Z. Y. Lin, B. X. Yao and S. Z. Weng, *Acta Phys.-Chim. Sin.*, 1998, **14**, 769–771.
304 G. W. Zhan, M. M. Du, J. L. Huang and Q. B. Li, *Catal. Commun.*, 2011, **12**, 830–833.
305 G. W. Zhan, M. M. Du, D. H. Sun, J. L. Huang, X. Yang, Y. Ma, A. R. Ibrahim and Q. B. Li, *Ind. Eng. Chem. Res.*, 2011, **50**, 9019–9026.
306 M. Du, G. Zhan, X. Yang, H. Wang, W. Lin, Y. Zhou, J. Zhu, L. Lin, J. Huang, D. Sun, L. Jia and Q. Li, *J. Catal.*, 2011, **283**, 192–201.
307 W.-S. Lee, M. Cem Akatay, E. A. Stach, F. H. Ribeiro and W. Nicholas Delgass, *J. Catal.*, 2012, **287**, 178–189.
308 X. Feng, X. Duan, G. Qian, X. Zhou, D. Chen and W. Yuan, *Appl. Catal., B*, 2014, **150–151**, 396–401.
309 G. Zhan, J. Huang, M. Du, D. Sun, I. Abdul-Rauf, W. Lin, Y. Hong and Q. Li, *Chem. Eng. J.*, 2012, **187**, 232–238.
310 J. Huang, C. Liu, D. Sun, Y. Hong, M. Du, T. Odoom-Wubah, W. Fang and Q. Li, *Chem. Eng. J.*, 2014, **235**, 215–223.
311 G. Zhan, Y. Hong, F. Lu, A.-R. Ibrahim, M. Du, D. Sun, J. Huang, Q. Li and J. Li, *J. Mol. Catal. A: Chem.*, 2013, **366**, 215–221.
312 A. Vilchis-Nestor, M. Avalos-Borja, S. Gómez, J. A. Hernández, A. Olivas and T. Zepeda, *Appl. Catal., B*, 2009, **90**, 64–73.
313 M. Du, D. Sun, H. Yang, J. Huang, X. Jing, T. Odoom-Wubah, H. Wang, L. Jia and Q. Li, *J. Phys. Chem. C*, 2014, **118**, 19150–19157.
314 F. Yang, J. L. Huang, T. Odoom-Wubah, Y. L. Hong, M. M. Du, D. H. Sun, L. S. Jia and Q. B. Li, *Chem. Eng. J.*, 2015, **269**, 105–112.
315 F. Yang, X. Jing, J. Huang, D. Sun and Q. Li, *Ind. Eng. Chem. Res.*, 2015, **54**, 5373–5380.
316 X. Jing, H. Wang, H. Chen, J. Huang, Q. Li and D. Sun, *RSC Adv.*, 2014, **4**, 27597–27603.
317 D. Sun, H. Wang, G. Zhang, J. Huang and Q. Li, *RSC Adv.*, 2013, **3**, 20732–20737.
318 H. Chen, D. Huang, X. Su, J. Huang, X. Jing, M. Du, D. Sun, L. Jia and Q. Li, *Chem. Eng. J.*, 2015, **262**, 356–363.
319 B. Zheng, X. Jing, T. Odoom-Wubah, T. Kong, H. Chen, D. Sun, J. Huang and Q. Li, *Synth. React. Inorg., Met.-Org., Nano-Met. Chem.*, 2015, **45**, 967–973.
320 Y. Ma, Y. Huang, Y. Cheng, L. Wang and X. Li, *Appl. Catal., A*, 2014, **484**, 154–160.
321 Y. Ma, Y. Huang, Y. Cheng, L. Wang and X. Li, *Catal. Commun.*, 2014, **57**, 40–44.
322 Y. Huang, Y. Ma, Y. Cheng, L. Wang and X. Li, *Appl. Catal., A*, 2015, **495**, 124–130.

323 Z. Tian, L. Wang, L. Jia, Q. Li, Q. Song, S. Su and H. Yang, *RSC Adv.*, 2013, **3**, 6369–6376.
324 X. Pan, L. Wang, F. Ling, Y. Li, D. Han, Q. Pang and L. Jia, *Int. J. Hydrogen Energy*, 2015, **40**, 1752–1759.
325 G. Zhan, Y. Hong, V. Mbah, J. Huang, A.-R. Ibrahim, M. Du and Q. Li, *Appl. Catal., A*, 2012, **439**, 179–186.
326 L. Li, H. Liu, Y. Shen, J. Zhang and J.-J. Zhu, *Anal. Chem.*, 2011, **83**, 661–665.
327 F. Wen, Y. Dong, L. Feng, S. Wang, S. Zhang and X. Zhang, *Anal. Chem.*, 2011, **83**, 1193–1196.
328 J. Xie, Y. Zheng and J. Y. Ying, *Chem. Commun.*, 2010, **46**, 961–963.
329 S. Zhu, Y. Zhuo, H. Miao, D. Zhong and X. Yang, *Luminescence*, 2015, DOI: 10.1002/bio.2797.
330 J. Yin, X. He, X. Jia, K. Wang and F. Xu, *Analyst*, 2013, **138**, 2350–2356.
331 Y. Liu, K. Ai, X. Cheng, L. Huo and L. Lu, *Adv. Funct. Mater.*, 2010, **20**, 951–956.
332 J. Lee, J. Park, H. H. Lee, H. I. Kim and W. J. Kim, *J. Mater. Chem. B*, 2014, **2**, 2616–2621.
333 G. Y. Lan, C. C. Huang and H. T. Chang, *Chem. Commun.*, 2010, **46**, 1257–1259.
334 Z. Huang, F. Pu, Y. Lin, J. Ren and X. Qu, *Chem. Commun.*, 2011, **47**, 3487–3489.
335 Y. Lin, Y. Tao, J. Ren, F. Pu and X. Qu, *Biosens. Bioelectron.*, 2011, **28**, 339–343.
336 J. M. Obliosca, C. Liu and H.-C. Yeh, *Nanoscale*, 2013, **5**, 8443–8461.
337 M. Zhang, Y.-Q. Liu, C.-Y. Yu, B.-C. Yin and B.-C. Ye, *Analyst*, 2013, **138**, 4812–4817.
338 M. Zhang, S.-M. Guo, Y.-R. Li, P. Zuo and B.-C. Ye, *Chem. Commun.*, 2012, **48**, 5488–5490.
339 Y. Zhang, Y. Cai, Z. Qi, L. Lu and Y. Qian, *Anal. Chem.*, 2013, **85**, 8455–8461.
340 D. Liu, Z. Wang and X. Jiang, *Nanoscale*, 2011, **3**, 1421–1433.
341 W. Li, B. Chen, H. Zhang, Y. Sun, J. Wang, J. Zhang and Y. Fu, *Biosens. Bioelectron.*, 2015, **66**, 251–258.
342 C. H. Moon, Y. Yan, M. Zhang, N. V. Myung and E. D. Haberer, *SPIE NanoSci. Eng.*, 2014, **9171**, 91710U.
343 C. H. Moon, M. Zhang, N. V. Myung and E. D. Haberer, *Nanotechnology*, 2014, **25**, 135205.
344 A. Liu, G. Abbineni and C. Mao, *Adv. Mater.*, 2009, **21**, 1001–1005.
345 B. Cao, H. Xu and C. B. Mao, *Microsc. Res. Tech.*, 2011, **74**, 627–635.
346 J. F. Li, Y. F. Huang, Y. Ding, Z. L. Yang, S. B. Li, X. S. Zhou, F. R. Fan, W. Zhang, Z. Y. Zhou, D. Y. Wu, B. Ren, Z. L. Wang and Z. Q. Tian, *Nature*, 2010, **464**, 392–395.
347 A. Michota and J. Bukowska, *J. Raman Spectrosc.*, 2003, **34**, 21–25.
348 L. Wang, C.-H. Liu, Y. Nemoto, N. Fukata, K. C.-W. Wu and Y. Yamauchi, *RSC Adv.*, 2012, **2**, 4608–4611.
349 J. A. Baldwin, B. Vlčková, M. P. Andrews and I. S. Butler, *Langmuir*, 1997, **13**, 3744–3751.
350 D.-P. Yang, S. Chen, P. Huang, X. Wang, W. Jiang, O. Pandoli and D. Cui, *Green Chem.*, 2010, **12**, 2038–2042.
351 K. Quester, M. Avalos-Borja, A. R. Vilchis-Nestor, M. A. Camacho-López and E. Castro-Longoria, *PLoS One*, 2013, **8**, e77486.
352 G. Wei, L. Wang, L. Sun, Y. Song, Y. Sun, C. Guo, T. Yang and Z. Li, *J. Phys. Chem. C*, 2007, **111**, 1976–1982.
353 Y. Sun, G. Wei, Y. Song, L. Wang, L. Sun, C. Guo, T. Yang and Z. Li, *Nanotechnology*, 2008, **19**, 115604.
354 L. Guerrini, J. V. Garcia-Ramos, C. Domingo and S. Sanchez-Cortes, *J. Phys. Chem. C*, 2008, **112**, 7527–7530.
355 T. Vo-Dinh, Y. Liu, A. M. Fales, H. Ngo, H. N. Wang, J. K. Register, H. Yuan, S. J. Norton and G. D. Griffin, *Wiley Interdiscip. Rev.: Nanomed. Nanobiotechnol.*, 2015, **7**, 17–33.
356 M. Rai, A. Yadav and A. Gade, *Biotechnol. Adv.*, 2009, **27**, 76–83.
357 R. Thomas, A. P. Nair, K. Soumya, J. Mathew and E. Radhakrishnan, *Appl. Biochem. Biotechnol.*, 2014, **173**, 449–460.
358 H. Chen, L. Zhang, O.-W. Tareque, J. Huang, H. Wang, M. Fu, D. Sun and Q. Li, *Curr. Nanosci.*, 2014, **10**, 271–276.
359 M. Sathishkumar, K. Sneha, S. Won, C.-W. Cho, S. Kim and Y.-S. Yun, *Colloids Surf., B*, 2009, **73**, 332–338.
360 C. Krishnaraj, E. Jagan, S. Rajasekar, P. Selvakumar, P. Kalaichelvan and N. Mohan, *Colloids Surf., B*, 2010, **76**, 50–56.
361 A. Nabikhan, K. Kandasamy, A. Raj and N. M. Alikunhi, *Colloids Surf., B*, 2010, **79**, 488–493.
362 M. Vijayakumar, K. Priya, F. Nancy, A. Noorlidah and A. Ahmed, *Ind. Crops Prod.*, 2013, **41**, 235–240.
363 S. Muthukrishnan, S. Bhakya, T. S. Kumar and M. Rao, *Ind. Crops Prod.*, 2015, **63**, 119–124.
364 D. M. Eby, N. M. Schaeublin, K. E. Farrington, S. M. Hussain and G. R. Johnson, *ACS Nano*, 2009, **3**, 984–994.
365 A. K. Chatterjee, R. K. Sarkar, A. P. Chattopadhyay, P. Aich, R. Chakraborty and T. Basu, *Nanotechnology*, 2012, **23**, 085103.
366 X. Fei, M. Jia, X. Du, Y. Yang, R. Zhang, Z. Shao, X. Zhao and X. Chen, *Biomacromolecules*, 2013, **14**, 4483–4488.
367 A. Retnakumari, S. Setua, D. Menon, P. Ravindran, H. Muhammed, T. Pradeep, S. Nair and M. Koyakutty, *Nanotechnology*, 2010, **21**, 055103.
368 Y. Wang, J. Chen and J. Irudayaraj, *ACS Nano*, 2011, **5**, 9718–9725.
369 Y. Chen, P. Chen, C. Wang, Y. Lin, C. Ou, L. Ho and H. Chang, *Chem. Commun.*, 2014, **50**, 8571–8574.
370 X. Wu, X. He, K. Wang, C. Xie, B. Zhou and Z. Qing, *Nanoscale*, 2010, **2**, 2244–2249.
371 D.-H. Hu, Z.-H. Sheng, P.-F. Zhang, D.-Z. Yang, S.-H. Liu, P. Gong, D.-Y. Gao, S.-T. Fang, Y.-F. Ma and L.-T. Cai, *Nanoscale*, 2013, **5**, 1624–1628.
372 H. Cai and P. Yao, *Nanoscale*, 2013, **5**, 2892–2900.
373 P. Murawala, A. Tirmale, A. Shiras and B. Prasad, *Mater. Sci. Eng., C*, 2014, **34**, 158–167.
374 G. Plascencia-Villa, L. Carreño-Fuentes, D. Bahena, M. José-Yacamán, L. A. Palomares and O. T. Ramírez, *Nanotechnology*, 2014, **25**, 385706.
375 S. M. Watson, A. R. Pike, J. Pate, A. Houlton and B. R. Horrocks, *Nanoscale*, 2014, **6**, 4027–4037.
376 J. Guo, H. Wu, X. Liao and B. Shi, *J. Phys. Chem. C*, 2011, **115**, 23688–23694.